

國立交通大學
電機與控制工程學系

碩士論文

利用腦波之獨立成份分析結合虛擬實境動態
模擬系統開發駕駛員瞌睡偵測技術

EEG-Based Drowsiness Estimation Using Independent
Component Analysis in Virtual-Reality
Dynamic Driving Simulator

研究生： 陳 俞 傑
指導教授： 林 進 燈 教授

中華民國九十四年七月

利用腦波之獨立成分分析結合虛擬實境動態
模擬系統開發駕駛員瞌睡偵測技術

EEG-Based Drowsiness Estimation Using Independent Component
Analysis in Virtual-Reality Dynamic Driving Simulator

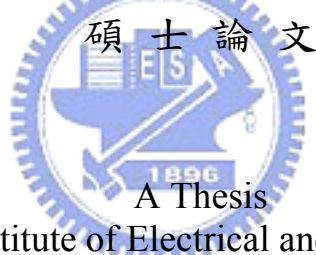
研究生：陳 俞 傑

Student : Yu-Jie, Chen

指導教授：林 進 燈 教授

Advisor : Prof. Chin-Teng, Lin

國立交通大學
電機與控制工程學系



A Thesis

Submitted to Institute of Electrical and Control Engineering
College of Electrical Engineering and Computer Science
National Chiao Tung University
in partial Fulfillment of the Requirements
for the Degree of
Master
in

Electrical and Control Engineering

July 2005

Hsinchu, Taiwan, Republic of China

中華民國九十四年七月

EEG-Based Drowsiness Estimation Using Independent Component Analysis in Virtual-Reality Dynamic Driving Simulator

Student : Yu-Jie, Chen

Advisor : Prof. Chin-Teng, Lin

Institute of Electrical and Control Engineering
National Chiao Tung University

ABSTRACT

Preventing accidents caused by drowsiness has become a major focus of active safety driving in recent years. It requires an optimal estimation system to online continuously detect drivers' cognitive state related to abilities in perception, recognition and vehicle control. The propose of this thesis is to develop an adaptive drowsiness estimation system based on electroencephalogram (EEG) by combining with independent component analysis (ICA), time-frequency spectral analysis, correlation analysis and fuzzy neural network model to estimate a driver's cognitive state in Virtual-Reality (VR) dynamic driving simulator. Moreover, the VR-based motion platform with EEG measured system is the innovation of brain and cognitive engineering researches.

Firstly, there is good evidence to show that the necessary of VR-based motion platform for brain research in driving simulation. This is an important fact to stress that the kinesthetic stimuli obviously influence the cognitive states and the phenomenon can be indicated by the EEG signals. Secondly, a single-trial event-related potential (ERP) is applied to recognize different brain potentials by the five degrees of drowsiness in driving. And we demonstrate a close relationship between the fluctuations in driving performance and the EEG signal log bandpower spectrum. Our Experimental results show that it is feasible to accurately estimate the driving performance. Then we observe that the brain source related to drowsiness is on cerebral cortex. Finally, the spiked dry electrodes and the corresponding movement artifact removal technology were designed to replace the regular wet electrode for the purpose of applications in the realistic driving or working environments.

Keyword : Drowsiness, Electroencephalogram, Virtual Reality, Dynamic Platform, Cognitive State, Event-Related Potential, Kinesthetic Stimulus, Independent Component Analysis, Dry Electrode.

利用腦波之獨立成分分析結合虛擬實境動態 模擬系統開發駕駛員瞌睡偵測技術

研究生：陳 俞 傑

指導教授：林 進 燈 教授

國立交通大學電機與控制工程學系碩士班

摘 要

近年來，預防瞌睡所導致的交通意外，已經成為交通安全研究的重要課題，我們需要一個最理想的估測系統，可以即時連續的偵測駕駛員的精神認知狀態、知覺以及控制車輛的能力。本論文的目的是發展一套有效的駕駛精神認知狀態估測系統，利用腦電波訊號結合頻譜分析、獨立成分分析演算法、相關係數分析以及類神經網路模型，結合虛擬實境動態模擬駕駛系統，開發駕駛員的瞌睡偵測技術；此外在虛擬實境的環境中，結合腦波量測系統與動感平台，進行神經認知系統研究，在腦科學與認知工程領域上都是一項創新。

首先我們證明利用虛擬實境結合動感平台，以進行實用之認知工程研究是必要的，動態刺激會明顯的影響腦波訊號認知狀態。我們亦利用單一試驗的事件相關腦電位分析，去識別開車時不同瞌睡程度的腦電位變化，並且證明人類腦波特定的頻帶活動與開車行為表現之間的關係非常密切，並經由實驗結果顯示，利用腦波訊號分析以估測駕駛員行為表現是可行的。我們亦研究在大腦皮層上與發生瞌睡相關的區域，最後為了實際應用的可行性，我們利用乾式電極結合獨特之雜訊消除技術取代傳統電極，以期將本論文所開發的技術，未來應用於實際駕駛與工作環境中。

關鍵字：瞌睡偵測，腦電波，虛擬實境，動態平台，認知狀態，事件相關電位，動覺刺激，獨立成分分析，乾式電極。

誌 謝

本論文的完成，首先要感謝我的指導教授 林進燈博士在過去兩年研究期間，提供豐富的研究資源和實驗環境，並從旁指導協助，使得本文得以順利完成。

其次，我要感謝我的父母對我的照顧與栽培，教導我做人品德為最，強調人格健全之發展與學習生活之態度，由於他們辛勞的付出和細心的照顧，才有今天的我；亦感謝我哥哥在我研究的路上隨時給予指導與協助，豐富的經驗減少我許多錯誤的發生。

特別感謝美國加州聖地牙哥大學的 鐘子平教授、 段正仁教授及 黃瑞松學長，給予我研究上最大的協助，從實驗設計、實驗分析、實驗結果討論到論文撰寫，給我最專業的意見跟看法。

另外，我要感謝腦科學研究實驗室的全體成員，沒有他們也就沒有我個人的成就。特別感謝 梁勝富教授給予我在各方面的指導，無論是研究上疑難的解答、研究方法、寫作方式、經驗分享以及生活上壓力調適等惠我良多。另外要感謝士政、行偉以及欣泓同學，在過去兩年研究生活中同甘共苦，相互扶持。此外，我也要感謝陳玉潔學姊與黃騰毅學長在研究上的幫助，還有感謝力碩、宗哲以及弘義學弟，在過去這一年中的相伴。同樣地也感謝實驗室助理在許多事務上的幫忙。

最後，我要感謝我的女朋友黃莉萍小姐，替我分擔許多研究上的壓力與挫折，也讓我在研究所的生活當中，增添更多色彩。

謹以本文獻給我親愛的家人與親友們，以及關心我的師長，願你們共享這份榮耀與喜悅。

Content

Abstract in English	i
Abstract in Chinese	ii
Acknowledgement	iii
Content	iv
List of Tables	vi
List of Figures	vii
Abbreviation	x
I .Introduction	1
1.1 Current Researches of Drowsiness Estimation.....	2
1.1.1 Detecting Physical Changes	3
1.1.2 Measuring Physiological Changes	5
1.2 Virtual Reality Dynamic Simulator	7
1.3 Organization of This Thesis	10
II . System Architecture	12
2.1 3D Virtual Reality Environment.....	13
2.2 Stewart Motion Platform	15
2.3 EEG Data Acquisition	16
2.4 Subject	17
2.5 Spiked Dry Electrode	18
III .Experimental Design	20
3.1 The Influence of Kinesthetic Stimulus on Cognitive State	21
3.2 Investigation of Drowsiness Event-Related Potentials.....	23
3.3 Adaptive Estimation of Continuous Driving Performance.....	24
3.4 Search for Brain Source of Drowsiness on Cerebral Cortex	25
3.5 Application of Dry Electrodes in the Drowsiness Experiment.....	28
IV .Data Analysis	29
4.1 Event-Related Potential (ERP) Analysis	29
4.2 Analysis of Continuous EEG Data	32
4.3 Independent Component Analysis (ICA)	36
4.4 Time-Frequency Spectral Analysis	40
4.5 Correlation Analysis	42
4.6 Adaptive Feature Selection Mechanism	44
4.7 Self-cOnstructing Neuro-Fuzzy Inference Network (SONFIN)	45

V.Results and Discussions.....	49
5.1 The Influence of the VR-based Motion Platform on Cognitive States.....	49
5.1.1 The Brain Source of Kinesthetic Stimulus on the Cerebral Cortex.....	49
5.1.2 Necessity of VR-based Motion Platform	53
5.2 The Brain Activity of Drowsiness in Different Cognitive States.....	59
5.2.1 The Degree of Cognitive States in Drowsiness.....	59
5.2.2 The Dynamic Platform Influences Drowsiness ERP.....	63
5.3 The Performance of Adaptive Drowsiness Estimation.....	64
5.3.1 Relationship between the ICA/EEG Power Spectrum and Drowsiness...	65
5.3.2 The Dominant ICA Components and EEG Channels for Drowsiness	67
5.3.3 Selection of Frequency Bands Based on Spectral Correlation and AFSM	69
5.3.4 Drowsiness Estimation based on ICA Components or EEG Channels....	72
5.3.5 Driving Performance Estimation based on AFSM and SONFIN.....	74
5.3.6 Performance Comparison Using Different Moving-Average Window	76
5.4 The Brain Source of Drowsiness on the Cerebral Cortex	77
5.4.1 Comparison with Using Different Number of EEG Channels	77
5.4.2 Comparison of Using Different Region of EEG Channels.....	80
5.5 Actual Application of the Spiked Dry Electrodes	83
Reference	90

List of Tables

Table 1-1 Techniques for Detecting Drowsiness.....	3
Table 5-1 The scalp topographies of two ICA components have different response in the two conditions	52
Table 5-2 Two ICA components and two EEG channels of the five participants with the highest correlation coefficients with the driving deviation are selected for adaptive drowsiness estimation.....	68
Table 5-3 The correlation coefficients between the log subband power spectra and the driving performance of Subject 3 corresponding to the different frequency bands from 8 to 15 Hz of the ICA component 11 and 13 in the training and testing sessions that uses the same ICA weighting matrix obtained from the training session	69
Table 5-4 The correlation coefficients between log subband power spectra and the driving performance of subject 3 using the optimal frequency bands (from 10 to 14 Hz) corresponding to single component.....	70
Table 5-5 The frequency bands for the two ICA components in Table 5-2 selected by manual method and the AFSM technology corresponding to different subjects	71
Table 5-6 Driving performance estimation using the optimal frequency bands and linear regression model of the five participants by two ICA components or two EEG channels	73
Table 5-7 Driving performance estimation using the frequency bands selected by manual method and the AFSM technology based on two dominant ICA components as input features of the linear regression model and SONFIN models for five subjects	75
Table 5-8 Comparison of driving performance estimation obtained from different number EEG channels by using the optimal frequency bands of two EEG channels or ICA components as the features of linear regression model for the five participant	77
Table 5-9 Comparison of driving performance estimation using two EEG channels of the four different regions.....	80
Table 5-10 Driving performance estimation of subject 2 by using two spiked dry electrodes	87

List of Figures

Fig. 1-1: The vestibular system and its measurement principles.	8
Fig. 2-1: The block diagram of the dynamic VR-based driving simulation environment with the EEG-based physiological measurement system.	12
Fig. 2-2: Flowchart of the VR-based highway scene development. The dynamic models and shapes of the 3D objects in the VR scene are created and linked to the WTK library to form a complete interactive VR simulated scene.	13
Fig. 2-3: The VR-based four-lane highway scenes are projected into 360° surround screen with seven projectors. Several photos captured from different view angle at a fixed point are connected to form this wide figure.	14
Fig. 2-4: The Stewart platform. (a) The sketch map for the Stewart platform. (b) The actual Stewart platform. A driving cabin is mounted on this platform in our laboratory.	15
Fig. 2-5: The International 10-20 system of electrode placement. (a) A lateral view, (b) A top view.	16
Fig 2-6: Corresponding equivalent circuit illustrated below shows that spiked dry electrodes can perform a low-impedance interface better than the standard electrodes. (a) Standard wet electrode, (b) Spiked dry electrode.	18
Fig. 2-7: Photographing of fabrication result of spiked dry electrodes using optics microscope.	19
Fig. 3-1: The flowchart of designs and goals of all experiments.	20
Fig. 3-2: The view of the driving cabin forward at rear in VR-based highway scene.	21
Fig. 3-3: Illustration of the design for stop and start experiments.	22
Fig. 3-4: The width of highway is equally divided into 256 units and the width of the car is 32 units.	23
Fig. 3-5: The continuous driving performance of long-term recordings in the driving simulation. (a) The distribution of driving performance, (b) Moving averaged driving error in a 60-minute experiment with at least 2 drowsy periods.	25
Fig. 3-6: Five conditions for different number of EEG channels. (a) 30 channels, (b) 20 channels, (c) 15 channels, (d) 10 channels, (e) 6 channels.	26
Fig. 3-7: Four clusters of electrodes on the scalp. (a) Frontal location, (b) Left temporal location, (c) Right temporal location, (d) Parietal and occipital location.	27
Fig. 4-1: The flowchart of EEG data analysis in the first experiment.	31
Fig. 4-5: Moving-averaged log power spectral analysis for i_{th} ICA component.	40
Fig. 4-6: Canonical correlation spectral matrix of subject 3. Note that the higher correlation coefficients appear at 9 ~ 25 Hz in ICA components 11 and 13, respectively.	43

Fig. 4-7: Example of the adaptive feature selection mechanism for subject 3. Note that the band power of ICA components 11 and 13 at frequency bands 10 ~ 14 Hz are selected as input feature of the estimators.	45
Fig. 4-8: The network structure of SONFIN.	46
Fig. 5-1: The scalp topographies of all ICA components trained by EEG data from Subject 1.	50
Fig. 5-2: Two ICA components have different responses between the two conditions of all events. (a) The source near FC3 location, (b) The source near FC4 location.	50
Fig. 5-3: The ERP and ERSP analyses of component 20 for stop event. (a) The ERP of motion condition, (b) The ERP of motionless condition, (c) Overplot power spectrum of two conditions, (d) The ERSP of motion condition, (e) The ERSP of motionless condition.	54
Fig. 5-4: The ERP and ERSP analyses of component 20 for start event. (a) The ERP of motion condition, (b) The ERP of motionless condition, (c) Overplot power spectrum of two conditions, (d) The ERSP of motion condition, (e) The ERSP of motionless condition.	55
Fig. 5-5: The ERP and ERSP analyses of component 20 for deviation event. (a) The ERP of motion condition, (b) The ERP of motionless condition, (c) Overplot power spectrum of two conditions, (d) The ERSP of motion condition, (e) The ERSP of motionless condition.	56
Fig. 5-6: The ERP analysis of component 20 for deviation event with reaction time. (a) The ERP with reaction time of motion condition, (b) The ERP with reaction time of motionless condition, (c) Aligning onset by reaction time from (a), (d) Aligning onset by reaction time from (b).	57
Fig. 5-7: The trials are sorted according to reaction time and equally divided into five groups of subject 4.	59
Fig. 5-8: One component is related to drowsiness and the ERP analysis with all single-trials.	60
Fig. 5-9: The results of ERSP analysis in five different cognitive states. (a) Drowsiness level from 1 ~ 20 %, (b) Drowsiness level from 21 ~ 40 %, (c) Drowsiness level from 41 ~ 60 %, (d) Drowsiness level from 61 ~ 80 %, (e) Drowsiness level from 81 ~ 100 %.	61
Fig. 5-10: The results of ERSP analysis in five different cognitive states if the dynamic platform is motionless. (a) Drowsiness level from 1 ~ 20 %, (b) Drowsiness level from 21 ~ 40 %, (c) Drowsiness level from 41 ~ 60 %, (d) Drowsiness level from 61 ~ 80 %, (e) Drowsiness level from 81 ~ 100 %.	63
Fig. 5-11: The results of correlation coefficient analysis for Subject 3. (a) The correlation coefficient spectra of ICA components, (b) The correlation coefficient spectra of EEG channels, (c) The ICA component with highest correlation with the driving performance, (d) The EEG channel with highest correlation with the driving performance.	65

Fig. 5-12: Two ICA components and two EEG channels with the highest correlation coefficient with the driving performance index. (a) ICA Component 11, (b) ICA Component 13, (c) EEG Pz channel, (d) EEG P4 channel.....	66
Fig. 5-13: Driving performance estimation of Subject 3 using linear regression model with the optimal frequency bands selected manually. (a) Result of training session by using ICA components, (b) Result of testing session by using ICA components, (c) Result of training session by using EEG channels, (d) Result of testing session by using EEG channels.	72
Fig. 5-14: Correlation coefficients between the driving performance and EEG log power spectrum from 9 ~ 15 Hz in Pz channel of subject 3 by using different moving averaged windows lengths.	76
Fig. 5-15: Comparison of estimating results by using ICA components and EEG channels...	79
Fig. 5-16: The ESEI comparison between dry electrodes and wet electrode with/without skin preparation. (a) Without skin preparation, (b) With/without skin preparation.....	83
Fig. 5-17: The scalp topographies of all ICA components trained by EEG data of Subject 2 using 2 spiked dry electrodes and 30 wet electrodes.....	84
Fig. 5-18: The raw EEG data are measured by placing the spiked dry electrodes at FP1 and FP2 channels using the standard electrodes for the others channels of Subject 2. (a) The EEG signals of FP1 and FP2 channels with movement artifacts, (b) The EEG signals after ICA-based artifact removal.	85
Fig. 5-19: The EEG signals measured by using the spiked dry electrodes before/after artifacts removal using ICA decomposition technology. (a) and (b) EEG power spectra signals of FP1 and FP2 channels before removing all noise components, (c) and (d) EEG power spectra of FP1 and FP2 channels after removing all noise components.	86
Fig. 5-20: Correlation coefficients spectra of all EEG channels after removing all noise components.....	87

Abbreviation

Subject	Be an Abbreviation for
AFSM	Adaptive Feature Selection Mechanism
API	Application Programmer's Interface
DOF	Degree Of Freedom
ECG / EKG	Electrocardiogram
EEG	Electroencephalogram
EMG	Electro Muscle-movement Graph
EOG	Electrooculogram
ERP	Event-Related Potential
ERSP	Event-Related Spectral Perturbation
FNN	Fuzzy Neural Network
GSR	Galvanic Skin Response
HMD	Head Mounted Display
HRV	Heart Rate Variability
ICA	Independent Component Analysis
MEMS	Micro Electro Mechanical Systems
NREM	Non-Rapid Eye Movement
REM	Rapid Eye Movement
SONFIN	Self-cOnstructing Neuro-Fuzzy Inference Network
SVM	Support Vector Machine
VR	Virtual Reality
WTK	WorldToolKit

I .Introduction

During the past few years, driving safely has received extensive attention from the public due to the growing number of traffic accidents. Drivers' fatigue has been a causal factor in many accidents because of the marked decline in the drivers' abilities of perception, recognition and vehicle control abilities while sleepy. In the United States, according to the National Highway Traffic Safety Administration's (NHTSA) conservative estimation, 100,000 police-reported crashes are direct results of driver's fatigue in each year [1], which results in about 1,550 deaths, 71,000 injuries and \$12.5 billion in monetary losses. The National Science Foundation (NSF) also reported that 51% of adult drivers felt drowsy while driving vehicles and 17% actually fall asleep in 2002 [2]. Although many governments and vehicle manufacturers try to make policies, including strategies to address rates of speed, alcohol consumption, promotion of using helmets and seat belts, and enhancements of vehicle structures, etc [3-4], to prevent accidents, it is difficult to avoid disasters resulted from drivers' loss of alertness and lack of attentions.

Driving under drowsiness will cause: (a) longer reaction time, which increases the risk of crash, particularly at high speeds; (b) vigilance reduction, including no or delaying response to emergency; (c) deficits in information processing, which will reduce accuracy in decision-making tasks [5-7]. Many factors, including lack of sleep, long driving hours, use of sedating medications, consumption of alcohol and some driving patterns such as driving at midnight, early morning, or mid-afternoon hours, will cause drowsiness or fatigue in driving. In addition, the nature of the task, such as driving in a monotonous environment, may also cause fatigue. The improvement of vehicles has made drivers more and more effortless to operate their vehicles on the road. An examination of the situations when drowsiness occurred shows that most of the accidents occur on freeways [8]. Hence, accurate and non-intrusive

real-time monitoring of driver's drowsiness would be highly desirable, particularly if this measure could be further used to predict changes in driver's performance capacity.

The purpose of this thesis is to develop an adaptive drowsiness estimation system based on electroencephalogram by using independent component analysis. In the following session, we first survey current researches of drowsiness estimation. Then we emphasize the importance of the Virtual-Reality-based dynamic motion platform to brain research in driving experiments. Finally, the organization of this thesis is summarized in the last section.

1.1 Current Researches of Drowsiness Estimation

Table 1-1 summarizes a number of methods that have been proposed to detect drowsiness [8]. For the sensing approaches of human physiological phenomena, these methods can be categorized into two main fields. For drowsiness estimation, these methods can be further classified in two categories, non-contact and direct-contact. Direct-contact methods require sensors attached to the driver's body. Non-contact methods use optical sensors or video cameras to detect vigilance changes and achieve a satisfactory recognition rate. However, these parameters vary in different environmental situations and driving conditions. It is necessary to devise different detection logic for different types of vehicles.

Table 1-1
Techniques for Detecting Drowsiness

Detection Techniques		Description	Detection Accuracy	Practicality	Extendibility
Sensing of Human	Physiological Signals	Detection by Changes in Brain Waves, Blinking, Heart Rate, Pulse Rate, Skin Electric Potential, etc.	◎	×	△
Physiological Phenomena	Physical Reactions	Detection by Changes in Inclination Driver's Head, Sagging posture, Frequency at Which Eyes Close, Gripping force on Steering Wheel, etc.	◎	○	×
Sensing of Driving Operation		Detection by Changes in Driving Operations (Steering, Accelerator, Braking, Shift Lever, etc.)	○	◎	×
Sensing of Vehicle Behavior		Detection by Changes in Driving Behavior (Speed, Lateral G, Yaw Rate, Lateral Position, etc.)	○	◎	×
Response of Driver		Detection by Periodic Request for Response	△	×	◎
Traveling Conditions		Detection by Measurement of Traveling Time and Conditions (Daytime or Nighttime, Speed, etc.)	×	○	◎

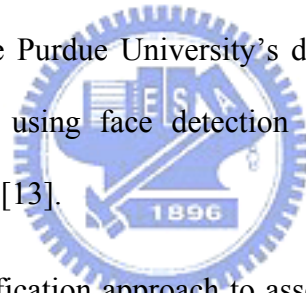
◎ : Very Good ○ : Good △ : Average × : Poor

Reference: Hiroshi Ueno and Masayuki Kaneda and Masataka Tsukino (1994) [8]

1.1.1 Detecting Physical Changes

The physical change during approaches detect of eye-closure over time, eye tracking as quantization of drowsiness level, driver's head movements, and steering wheel angle [8]. In Hamouda's study, all available information was collected by the police and recorded in the accident report. It showed that the presence of driver fatigue relating drowsiness is an important cause of truck accidents. This study also proposed to classify truck accident relating fatigue and non-fatigue by neural network model [9]. Richard Grace, a researcher at the Carnegie Mellon Driving Research Center, developed a driver monitoring system [11]. The

vehicle performance and physiological data were measured when drivers were driving trucks. This research proposed two drowsiness detection methods, including a video-based system that measures drowsiness associated with slow eye closure and the other based on vehicle performance data. The video-based system measured eye closure to obtain the percentage of eye-closure over time (PERCLOS) for detecting driver drowsiness in real time under nighttime driving conditions. A video-based system (CCD), the PERCLOS Camera, successfully measured eye closure and detect drowsiness in heavy vehicle truck operators [12]. Perez developed a non-invasive interface that tracks eye positions using digital image processing techniques. This approach detected eyes positions using image processing algorithms and a non-invasive interface and labeled eye tracking into five stages as a quantization index of driver's drowsiness. Only gray-level images were processed in this research: 102 images from the Purdue University's database and 897 images from a video sequence were pre-processed using face detection algorithm and the results of correct detection rates were very high. [13].



Pilutti proposed an identification approach to assess driver's state in lane-keeping tasks [14]. This approach used a driver model to simulate a real highway driving situation, including the perfectly smooth, asphalt, and concrete road surface. They obtained lateral positions of vehicles to assess drivers' performance, using driver steering wheel as the input of the driver model, and extracted the parameters from the chosen candidate model (ARX model). The model parameters are estimated for driving task and the results are good for model fit with the ARX model to represent the relationship between vehicle lateral position and the driver steering wheel angular position for detecting driving patterns, assessing driver performance, and improving vehicle active safety [14]. Popieul proposed a set of drowsiness indicators using evolution of driver's head movements for monitoring drivers' drowsiness efficiently. They considered variables related to the head position and the driving performance.

The approach developed a driving simulator with basic highway section such as straight line, right line, and left line. The driving performance (steering wheel angle) and physiological signals (driver's head movements) of the subjects participated in a long-term simulated highway trip were measured. [15].

Ji et al. predicted driver's fatigue by a real-time noninvasive monitoring system. They remotely acquired video images of the driver by using charge-coupled-device (CCD) cameras which are equipped with active infrared illuminators. Ji's research team used the Support Vector Machine (SVM) to catch eyes in the facial images and the Kalman filter to track eyes. The approach indicated that the fatigue relating to eyelids' movement of a person can be used as driver's drowsiness index. They quantized the fatigue of the eyelids' movement with two methods percentage of eye-closure over time (PERCLOS) and the average of eye-closure speed (AECS). They used the Bayesian network (BN) to model fatigue index, extract the level of alertness of a person, infer the driver's fatigue level, and systematically display the fatigue level on fatigue evidence window in real-time [16].



1.1.2 Measuring Physiological Changes

The other field focused on measuring drivers' physiological changes such as the heart rate variability (HRV), the galvanic skin response (GSR), and especially the electroencephalogram (EEG), as a means of detecting the human cognitive states [17-21]. Studies show that the human EEG generated by synchronous post-synaptic currents in large populations of neurons in the cortex can reflect brain activities. It has been known that abundant information in EEG recording can be related to drowsiness, arousal, sleep, and attention [22]. Previous psychophysiological studies show that typical sleep rhythm regulated

by the circadian process can be divided into non-rapid-eye-movement (NREM) sleep and rapid-eye-movement (REM) sleep [23-24]. NREM sleep is further subdivided into 4 stages. In the first part of falling into sleep (micro-sleep at NREM), increasing amplitudes of slow alpha waves of the EEG signals are observed with positive correlation at occipital sites (O1 and O2) and negative correlation at central sites (C3 or C4) [25-26]. While the approaches based on EEG signals have the advantages for making accurate and quantitative judgments of alertness levels, relatively little information has been captured in real time until signal processing methods and computer power are fast enough to extract the relevant information from the EEG. Thus, it is practicable and appealing to know what information about human cognitive state and behavior are available through analyzing complex EEG signals.

Roberts developed a tool to characterize the level of the vigilance of vehicle drivers by recording the physiological signals in real-time [19]. This approach builds up a portable device for the alertness detection of vehicle drivers by recording the EEG signals, then, studying the implementation of a decision algorithm based on Kohonen artificial neural networks by the variations of alpha, beta, theta and delta waves of the EEG signals according to a data base of 12 files of 24-hour EEG registered in volunteers. They observed a negative correlation between the score of vigilance and the percentage of the beta band and a positive correlation between the score of vigilance and the percentage of the other EEG (theta, alpha, and beta) spectral bands.

Wilson detected the instance at which a person had lost the level of alertness necessary to assure safe operation of a vehicle or display vigilance. They proposed a neural network to detect the driver's alertness state. The input of the neural network system is a feature vector composed of the Wavelet transforms representations of EEG signals at different scales, and the output of the system is a binary decision to decide the EEG represents either an alert state or a drowsy state [21]. In Parikh's study, the subjects EEG data were recorded while driving a

vehicle simulator and the EEG data was analyzed using the four-ordered Wavelet Transform as an indicator. The subjects were asked to observe their driving in the same position without any movement. In this study, increasing amplitudes of slow alpha waves of the EEG signals were observed during the monotony of the long distance driving because of repeating driving, viewing of the same track, less tension, or the tendency to drowsiness [25].

Some issues remain in practical applications using EEG signals such as the handling of artifacts. While driving, subjects move their hands, torso, head, and eyes, which create huge muscle movements, eye movements, and blink artifacts. Low pass filtering cannot resolve this problem. Another issue is individual difference in EEG dynamics accompanying loss of alertness. It is not easy to accurately estimate or predict individual changes in alertness and performance [27-31].



1.2 Virtual Reality Dynamic Simulator

Virtual reality (VR) technology is gradually being recognized as a useful tool for the study and assessment of normal and abnormal brain function, as well as for cognitive rehabilitation. Virtual Environments (VE) are created by powerful computers that generate realistic animated graphics in three dimensions. The computers are configured with peripheral devices, such as immersible head-mounted displays (HMDs) that allow complex interactions within the VE with a sense of presence. Creating carefully controlled, dynamic, 3D stimulus environments combined with physiological and behavioral response recording can be offer more assessment options that are not available by traditional neuropsychological methods.

The VR technique allows subjects to interact directly with a virtual environment rather than monotonic auditory and visual stimuli. It is an excellent strategy for brain research on

interactive and realistic tasks due to low cost and avoiding risk of operating on the actual machines. In recent years, some researchers designed the VR senses to provide the appropriate environments for brain activity study. In this study, a VR-based dynamic motion platform combined with EEG measured system is an innovation in brain and cognitive engineering researches. Without combining with dynamic motion platform, it is unable to study the influence of kinesthetic stimulus on cognitive state. Human brain can deal with complicated information. An example is the balance between optic scenes and kinesthetic perception. If the simulator environments cannot produce visual and kinesthetic stimuli simultaneously, the subjects may not correctly response in the real world.

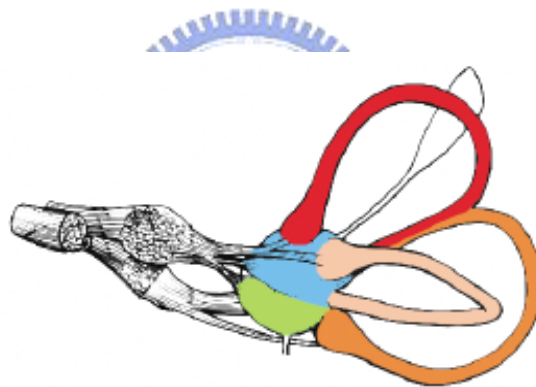


Fig. 1-1: The vestibular system and its measurement principles.

Reference: Andras Kemeny and Francesco Panerai (2003) [32]

The relevant organ system of human body to kinesthetic perception is the vestibular system [32]. The vestibular system is a sensory apparatus located bilaterally in the inner ears. Its function is to detect the motion of the head and body in space [33]. A vestibular system is composed of two functional parts shown as Fig. 1-1: (1) the otolith organs (Fig. 1-1, blue and

green colored areas), and (2) the semicircular canals (Fig. 1-1, red, pink and orange areas), which are selectively sensitive to linear and angular accelerations respectively. There are three semicircular canals filled with a viscous liquid, the endolymph. The pressure on the cupula, a specialized structure at the end of each canal, is increased by the liquid when the head moves. Pressure stimuli are transformed into nerve discharge, encoding the angular acceleration of the head. In the same way, the otolith receptors, composed of a mass of crystals floating in the endolymph, encode both linear acceleration and tilt of the head. [34]. Moreover, the otoliths signal the rotation of the head relative to gravity, that is, head tilt [35], which the nervous system resolves from linear acceleration by means of internal models [36].

In many types of sensori-motor processes such as the postural control, normal functioning of this system is essential. Additionally, vestibular information plays an important role in perceptual tasks such as egomotion estimation [37]. Vestibular information was shown to disambiguate the interpretation of dynamic visual information experienced simultaneously during observer's movement recently [38]. During the simulation process of driving, the absence of vestibular information increases steering reaction times to external movement perturbations [39], and also decreases safety margins in the control of lateral acceleration in curve driving [40]. In real driving, improper signals from disordered vestibular organs are reported to determine inappropriate steering adjustment [41]. Furthermore, the presence of vestibular information in driving simulators seems important because it influences the perception of illusory self-tilt and illusory self-motion [42].

1.3 Organization of This Thesis

The purpose of this study is to develop methods of using EEG signals to accurately and non-intrusively monitor the continuous fluctuations of driver's global level of drowsiness accompanying changes in driver's performance near real-time in a realistic driving task. We first construct a Virtual-Reality interactive driving environment consisting of a highway scene and a six degree-of-freedom (6-DOF) motion platform. By several simple driving actions such as deceleration, acceleration, and deviation, we demonstrate that distinct cognitive state responses are discernible between the dynamic platform which is motion and motionless. This is a good evidence to show that the dynamic motion platform is required for the study of human cognitive state estimation. Secondly, we design a lane-keeping driving experiment to indirectly quantify driver's drowsiness level [43]. It helps to illustrate the changes of drowsy event-related-potential (ERP) between different drowsiness states. After we recognize the feature of brain activities in drowsiness, we develop a novel adaptive feature selection mechanism (AFSM) for EEG spectra. And then we build an individualized fuzzy neural network models to assess the EEG dynamics accompanying loss of alertness for each subject.

Finally we consider the feasibility of the proposed method for practical applications. The main issue is to use less EEG channels to perform satisfactory results. The main purpose of the experiment is to investigate the cortical sources of drowsiness. The driving performance can be estimated according to the analysis of the number of dominated EEG channels and the source regions on the scalp. Finally, we try to use spiked dry electrodes to replace the standard wet electrodes on the prior experiment. The reason is that driver may be difficult to use electrodes cap and electrolytic gel in a realistic driving situation.

This thesis is organized as follows. Section II describes the details the EEG-based drowsiness experimental setup, VR-based dynamic driving environment, EEG data collection,

instructions, and spiked dry electrode. In Section III, we design a series of experiments for drowsiness estimation for EEG processing. We explore the innovative methods by applying ICA, time-frequency spectral analysis, correlation analysis, and fuzzy neural network in Section IV. Detailed discussions of our experimental results are given in section V. Finally, we conclude our findings in Section VI.



II . System Architecture

In this chapter, a VR-based dynamic driving environment is designed and built up for interactive driving experiments. It includes four major parts as shown in Fig. 2-1: (1) the 3D highway driving scene based on the virtual reality technology, (2) the driving cabin simulator mounted on a 6-DOF dynamic Stewart motion platform, (3) the EEG physiological signal measurement system with 36-channel EEG/EOG/ECG sensors, and (4) the proposed signal processing modules including ICA decomposition, power spectral analysis, and fuzzy neural work model. This environment will be presented in details as follows. In addition, the novel spiked dry electrodes used in our experiments for EEG acquisition are also being introduced.



Fig. 2-1: The block diagram of the dynamic VR-based driving simulation environment with the EEG-based physiological measurement system.

2.1 3D Virtual Reality Environment

In this thesis, a VR-based high-fidelity 3D interactive highway scene and its emulation software, WorldToolKit (WTK) library and application programmer's interface (API) are developed [60]. The detailed development diagram of the VR-based scene is shown in Fig. 2-2. Firstly, we create the models of various objects (such as cars, roads, and trees, etc.) for the scene and setup the corresponding positions, attitudes, and other relative parameters. Then we develop the dynamic models among these virtual objects and build a complete highway simulated scene of full functionality with the aid of the high-level C-based API program.

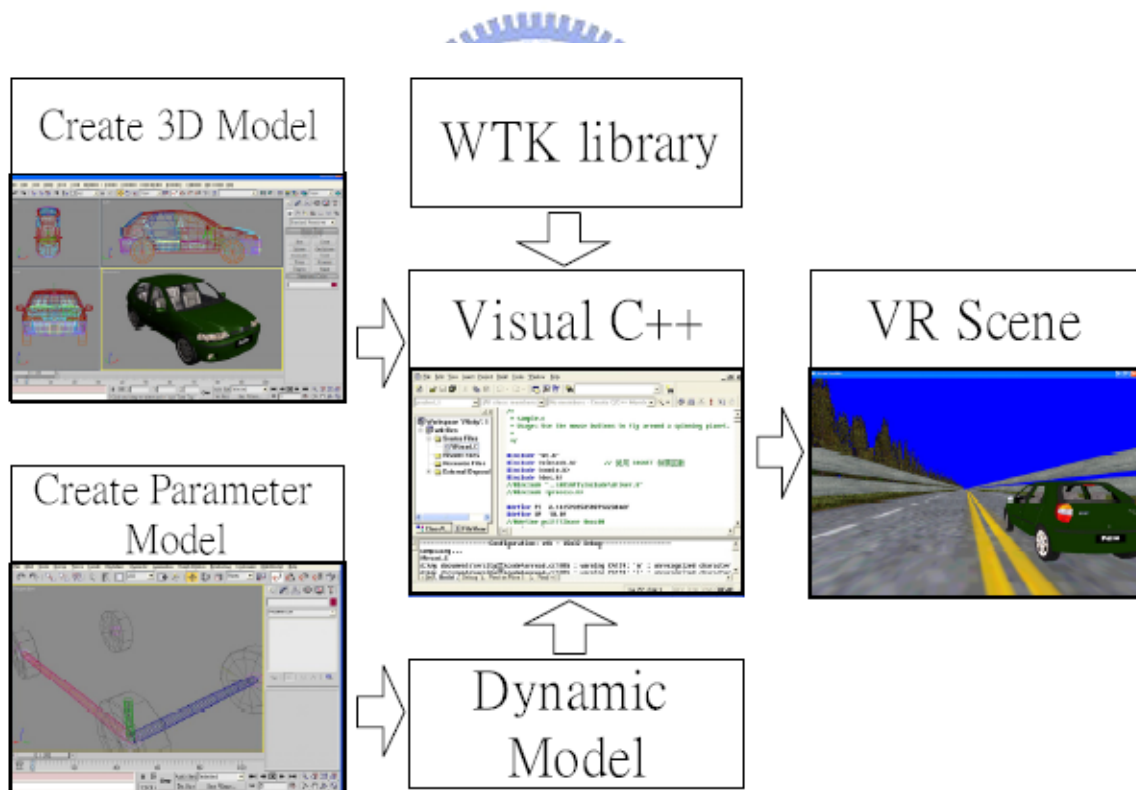


Fig. 2-2: Flowchart of the VR-based highway scene development. The dynamic models and shapes of the 3D objects in the VR scene are created and linked to the WTK library to form a complete interactive VR simulated scene.

Generally, the VR scenes are projected onto a curved screen or one or more flat screens, and some simulators use head-mounted displays (HMDs) to provide stereoscopic viewing. In our laboratory, the VR-based four-lane highway scenes are projected into the 360° surround screen with seven projectors at different positions as shown in Fig. 2-3.

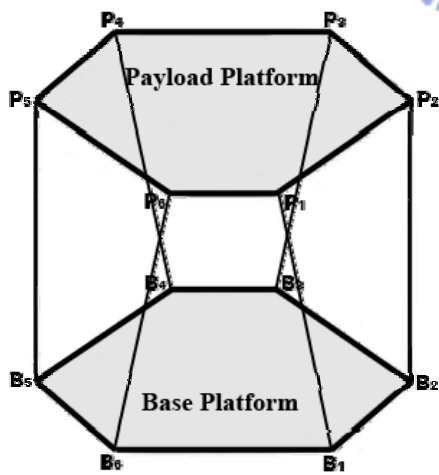


Fig. 2-3: The VR-based four-lane highway scenes are projected into 360° surround screen with seven projectors. Several photos captured from different view angle at a fixed point are connected to form this wide figure.

In order to increase stereoscopic perception and avoid the questions caused by using HMDs such as uncomfortableness, a little oppression, and the overheated instrument, we use two projectors to reach the binocular parallax. The VR scenes for the left and right eyes are projected onto the frontal screen with two projectors, respectively. By wearing the light 3D glasses, such configuration provides more stereoscopic VR scene than using HMDs.

2.2 Stewart Motion Platform

Since Stewart developed a prototype of a six-degree-of-freedom (6-DOF) parallel manipulator in 1953 [61]. It has attracted tremendous attention from researchers for high-precision robotic tasks where the requirements of accuracy and sturdiness are more essential than those of a large workspace and manoeuvrability [62-64]. A typical Stewart platform has a lower base platform and an upper payload platform connected by six extensible legs with ball joints at both ends, as shown in Fig. 2-4. The parallel manipulator has 6-DOF including coordinates of X, Y, Z for position and roll, pitch, yaw for direction in space. In the following, an inverse kinematics analysis of the Stewart platform will first be made. Then a fuzzy control algorithm will be designed for the position control. Lastly, a washout filter is designed for the angular velocity/linear acceleration control of the Stewart platform [65].



(a)



(b)

Fig. 2-4: The Stewart platform. (a) The sketch map for the Stewart platform. (b) The actual Stewart platform. A driving cabin is mounted on this platform in our laboratory.

2.3 EEG Data Acquisition

34 EEG/EOG channels (using sintered Ag/AgCl electrodes with an unipolar reference at right earlobe), 2 ECG channels (bipolar connections between the right clavicle and left rib), and one 8-bit digital signal produced from VR scene are simultaneously recorded by the Scan NuAmps Express system (Compumedics Ltd., VIC, Australia). All EEG/EOG channels were located based on a modified International 10-20 system as shown in Fig. 2-5 [66]. The 10-20 system is based on the relationship between the location of an electrode and the underlying area of cerebral cortex. Before acquiring EEG data, the contact impedance between EEG electrodes and skin was calibrated to be less than $5k\Omega$ by injecting NaCl based conductive gel. The EEG data were recorded with 16-bit quantization levels at a sampling rate of 500 Hz and were down sampled to 250 Hz for the simplicity of data processing. All EEG data were preprocessed using a simple low-pass filter with a cut-off frequency at 60 Hz in order to remove the line noise and other high-frequency noise. Similarly, a high-pass filter with a cut-off frequency at 0.5 Hz was applied to remove baseline drifts for further analysis.

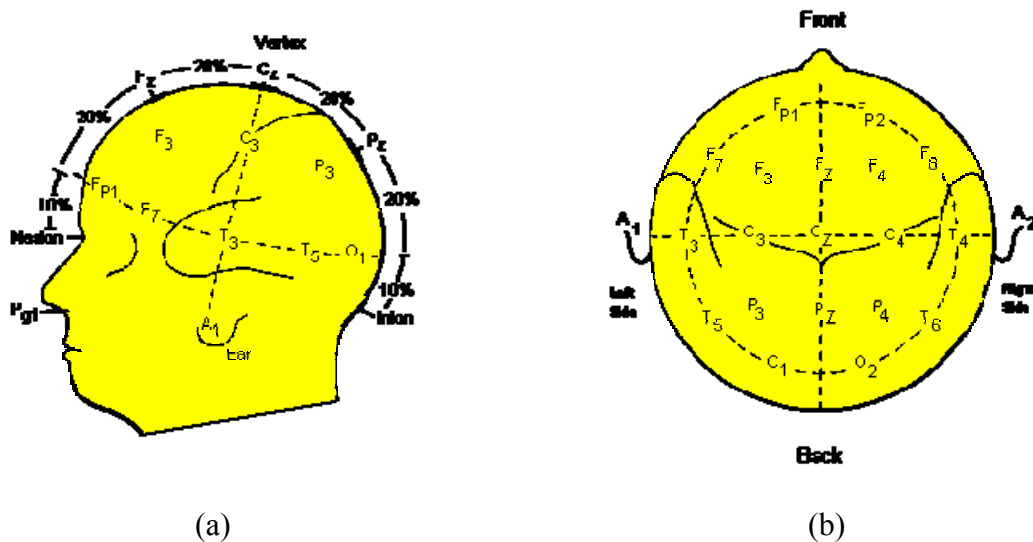


Fig. 2-5: The International 10-20 system of electrode placement. (a) A lateral view, (b) A top view [66].

2.4 Subject

It is known that the drowsiness often occurs during late nights, early morning and mid-afternoon. During these periods, alertness may easily diminish within one-hour monotonous working [7-8]. In drowsiness experiments, the subjects participated in the highway-driving simulation after lunch in the early afternoon.

All the subjects were instructed to keep the car at the center of the cruising lane by controlling a steering wheel. In all sessions, the subjects drive the car continuously for 60 minutes and were asked to try their best to stay alert. Participants then returned on different days to complete a second 60-minute driving session or more sessions if necessary. In opposition to the drowsiness experiments, for the kinaesthetic stimulus experiments, we arrange the experiment time in the morning or in the afternoon to keep the best condition for subjects. Each subject has to participate in two 30-minute sessions which replace the order of dynamic platform is motion and motionless of once experiment. In the same way, participants must return on different days to accumulate enough data to analyze. We collected EEG data from 16 subjects (ages from 20 to 35 year old) participating in the VR-based driving task. In drowsiness estimation experiment, we select participants who had two or more micro-sleeps checked by video recordings in both driving sessions for further analysis. Based on these criteria, five subjects were selected for further modeling and cross-session testing.

2.5 Spiked Dry Electrode

In recent years, the fabrication and characterization of Micro-Electro-Mechanical-Systems (MEMS) based silicon micro probe arrays, namely spiked dry electrodes, were explored for EEG measurement applications. A series of practical in-vivo tests had showed that the MEMS based spiked dry electrodes have more advantages and conveniences than the conventional standard electrodes. Comparing to the standard wet electrodes, the spiked dry electrodes can collect stronger signal intensity with a smaller device area, which means the design of related amplifier circuit can be simpler and easier. In addition, the spiked dry electrodes can be used without electrolytic gel, and they will not cause an uncomfortable feeling for the tested subject [67].

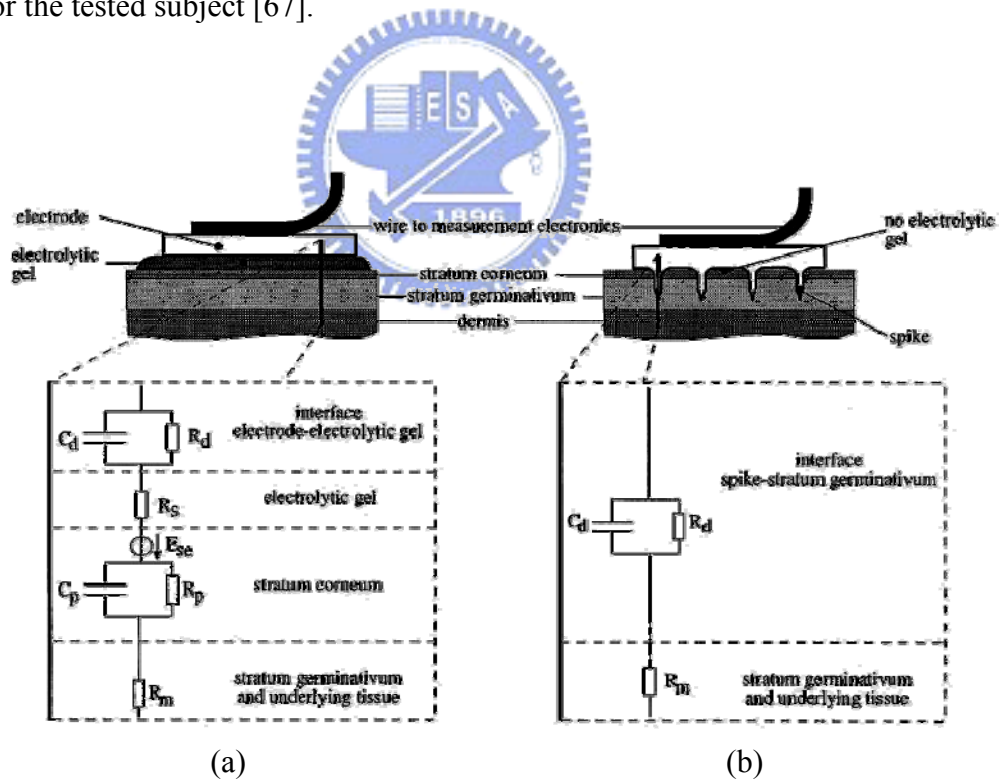


Fig 2-6: Corresponding equivalent circuit illustrated below shows that spiked dry electrodes can perform a low-impedance interface better than the standard electrodes. (a) Standard wet electrode, (b) Spiked dry electrode.

Reference: P. Griss, P. Enoksson, H. K.Tolvanen-Laakso, P. Merilainen, S. Ollmar (2001)

Biopotential electrode for EEG transforms the bio-signals from skin tissue to the amplifier circuit. Therefore, the most important characteristic of a biopotential electrode is low electrode-skin interface impedance to propagate signals without attenuation or production of noise. As the Fig. 2-6 indicates, the spiked dry electrode is designed to pierce the stratum corneum (SC) into the electrically conducting tissue layer of stratum germinativum (SG) in order to circumvent the high impedance characteristics of the SC.

In the Brain Research Center of the University System of Taiwan, the μ System & Control Lab led by Prof. J.C. Chiou had already developed the spiked dry electrodes. Three types of spiked dry electrodes varied in dimension including $4 \times 4 \text{ mm}^2$, $3 \times 3 \text{ mm}^2$ and $2 \times 2 \text{ mm}^2$ are successfully fabricated using MEMS technology. Each spiked dry electrode consists of 20×20 micro probes with $35 \mu\text{m}$ in diameter and $300 \mu\text{m}$ in height as shown in Fig. 2-7.

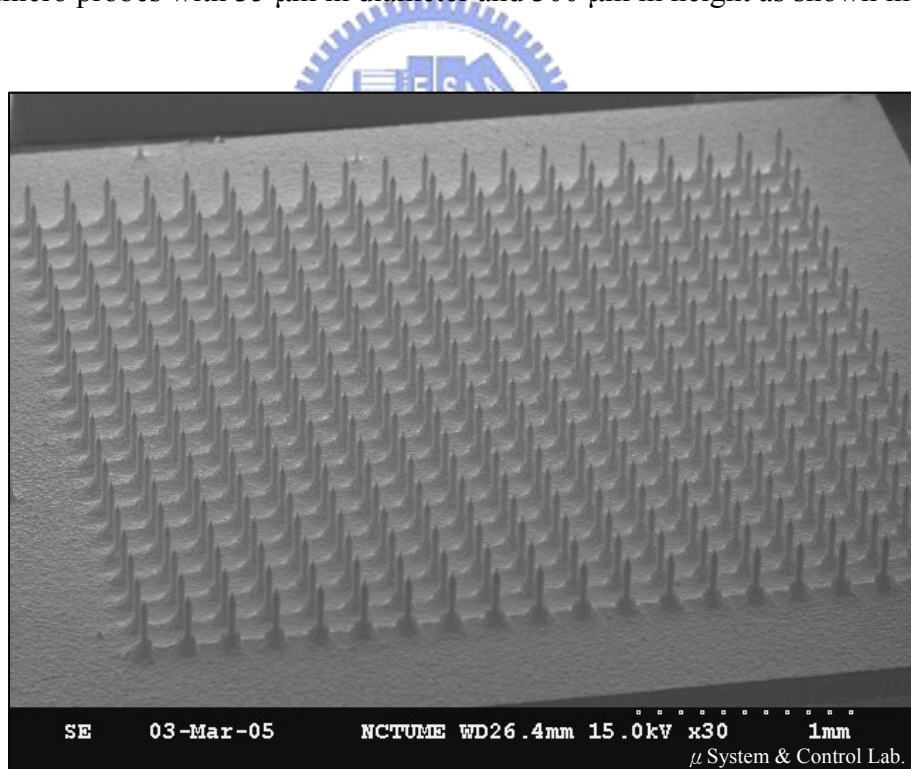


Fig. 2-7: Photographing of fabrication result of spiked dry electrodes using optical microscope.

III. Experimental Design

This study investigates the feasibility of using multi-channel EEG data to estimate and predict non-invasively the continuous fluctuations in human global level alertness in a realistic driving task. For this purpose, our concern is to carefully design a series of experiments for the scientific discovery and practical applications. Experimental designs are important because correct designs of experiments will distinctly acquire the expectable and incontrovertible results. Therefore, this chapter describes the design of each experiment in details and the flowchart is shown in Fig. 3-1.

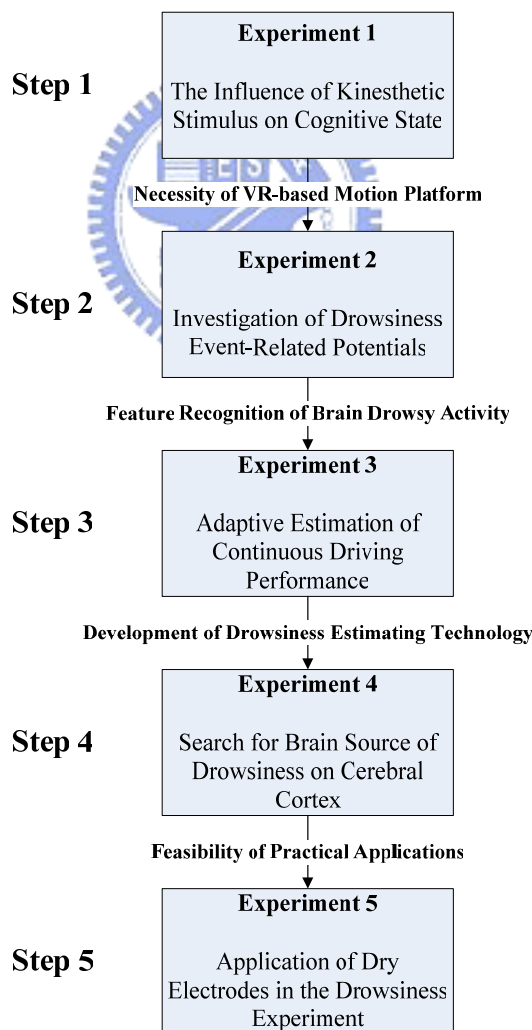


Fig. 3-1: The flowchart of designs and goals of all experiments.

3.1 The Influence of Kinesthetic Stimulus on Cognitive State

This topic intends to investigate the influence of kinesthetic stimulus on cognitive state and the purpose here is to justify the necessity of using VR-based motion platform. Through the movements of 6-DOF motion platform, this configuration provides drivers dynamic feeling with such as deceleration, acceleration, and deviation. We can investigate the cognitive states of the same driving actions with or without platform motion. For this fundamental research, we must simplify our concerned topic and reduce the other variations between the experiment and control. We develop a VR-based highway environment with a monotonic scene as shown in Fig. 3-2, because a complicated scene may bring unexpected visual stimulus. We keep the driving speed of simulation at 100 km/hr in order to avoid the stepping, that will cause large muscle activity on the throttle or brake. Similarly, the driving speed of simulation will automatically increase or decrease with the movements of motion platform if the traffic light is displayed on the screen.



Fig. 3-2: The view of the driving cabin forward at rear in VR-based highway scene.

In this research, each subject participated in two 30-minute sessions in one single day of experiment until enough EEG data for the ERP analysis were accumulated. The procedure of this experiment which we must comply with is to alternate two conditions, with and without platform movement. The motion and motionless will appear randomly to avoid expecting effect with a fixed order of two conditions. During the session, the VR-based scene and the car will be stopped, started and deviated according to the traffic lights in order to simulate the driving situations in the real world.

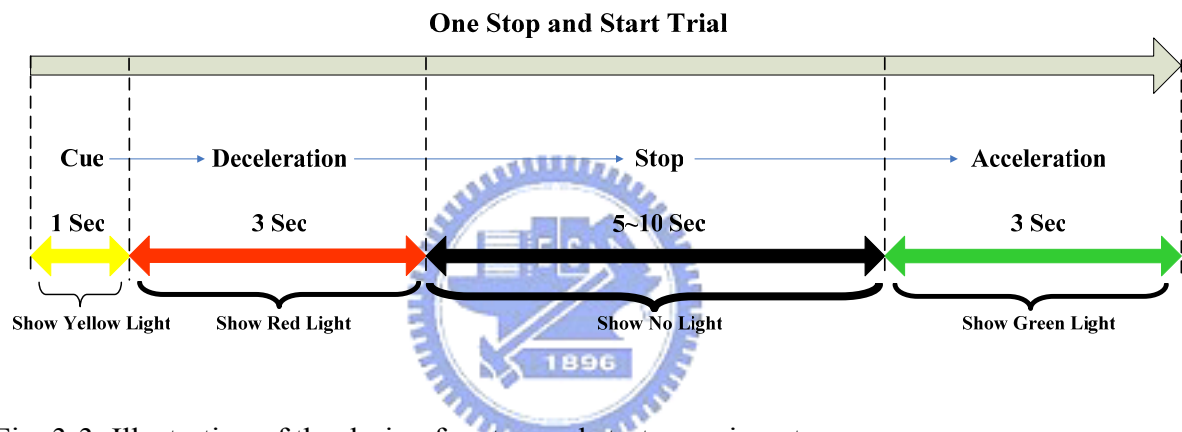


Fig. 3-3: Illustration of the design for stop and start experiments.

One trial in this experiment is explained as a combination of a stop and a start event with a 5 ~ 10 seconds time interval between two events. The stop and start events are maintained for 3 seconds with the displayed traffic light in red and green, respectively. Simultaneously, the movements of the platform, such as deceleration and acceleration, will depend on the corresponding events. In addition, the yellow light is displayed for 1 second before each trial so that the subject will not be shocked by the sudden deceleration of motion platform. The time interval between the trial and deviation event is 10 ~ 15 seconds. The time course of experiments is shown in Fig. 3-3.

3.2 Investigation of Drowsiness Event-Related Potentials

First of all, we have to find the relationship between the measured EEG signals and the subject's behavioral performance. One point should be taken as a quantified level of the subject's alertness while driving. Hence, we define the subject's driving performance index as the deviation between the center of the vehicle and the center of the cruising lane [43]. By examining the video recordings, the pilot experimental studies show that when the subject is drowsy, the driving performance will decrease and vice versa. The four lanes from left to right are separated by a median stripe in the VR-based scene. The distance from the left side of the road to the right side of the road is equally divided into 256 points for outputting digital signal from WTK program, and the width of each lane and the car is 60 units and 32 units, respectively. All the descriptions about the width are depicted in Fig. 3-4.

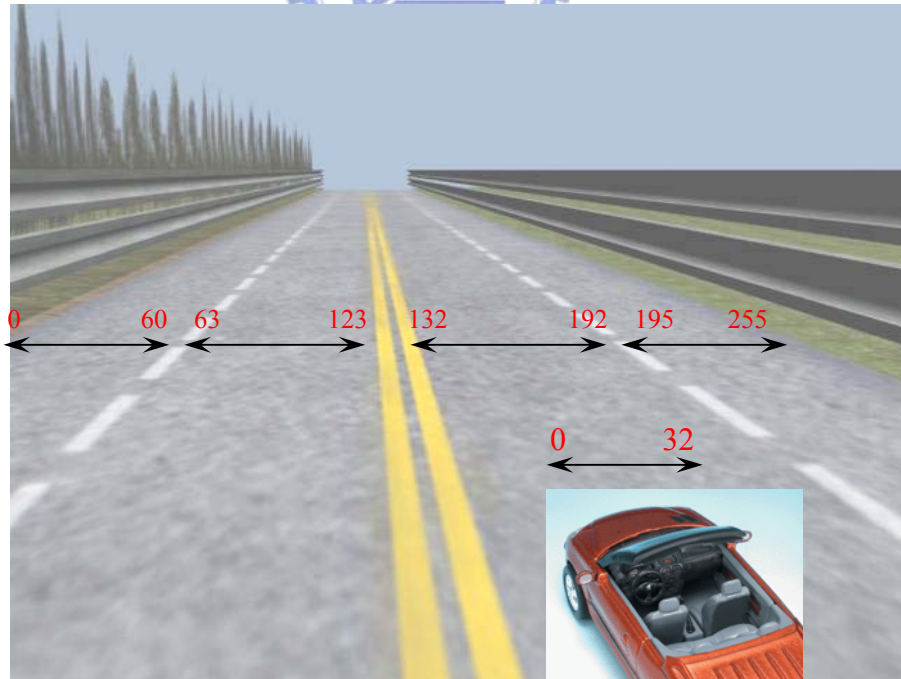
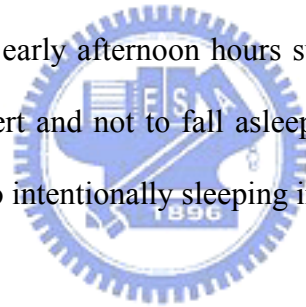


Fig. 3-4: The width of highway is equally divided into 256 units and the width of the car is 32 units.

The refresh rate of highway scene was set properly to emulate a car cruising at a fixed speed of 100 km/hr. The subject's performance is defined as the deviations between the center of the vehicle and the center of the cruising lane. The car is randomly drifted away from the center of the cruising lane to mimic the consequences of a non-ideal road surface. So the driver must maintain high attention to immediately correct the direction of vehicle in the cruising lane. When the driver is drowsy, the reaction time between the onset of deviation and steering wheel is increased. This event can be used for ERP analysis of different drowsiness states using 30-channel EEG signals. The reaction time is continuously and simultaneously measured by the WTK program and recorded in the physiological measurement system accompanying with EEG/EOG/ECG physiological signals. In this design, the subjects are asked to participate in the 60 minutes experiment twice for data accumulation. Although we fix the experiment time in the early afternoon hours such that drowsiness time often occurs, the drivers must try to stay alert and not to fall asleep. Otherwise the wrong cognitive state will be erroneously judged due to intentionally sleeping in driving.



3.3 Adaptive Estimation of Continuous Driving Performance

In addition to recognize the feature of brain activity in drowsiness, we also want to develop a drowsiness estimation system for driving. In differentiation to Experiment 2 of single-trial analysis, we deal with the continuous 30-channel EEG signals of long-term recordings. This design is similar to Experiment 2 because we use the same VR-based highway scene and the same length of experimental time. Therefore, the subject's performance is also defined as the deviations between the center of the vehicle and the center of the cruising lane. We select the participants who have two or more micro-sleeps checked by video recordings in both driving sessions for further analysis. The individual model which

estimates driving performance using the features will be established by the two sessions for training and testing respectively. Fig. 3-5 shows driving performance recorded in a 60-minute session of one subject.

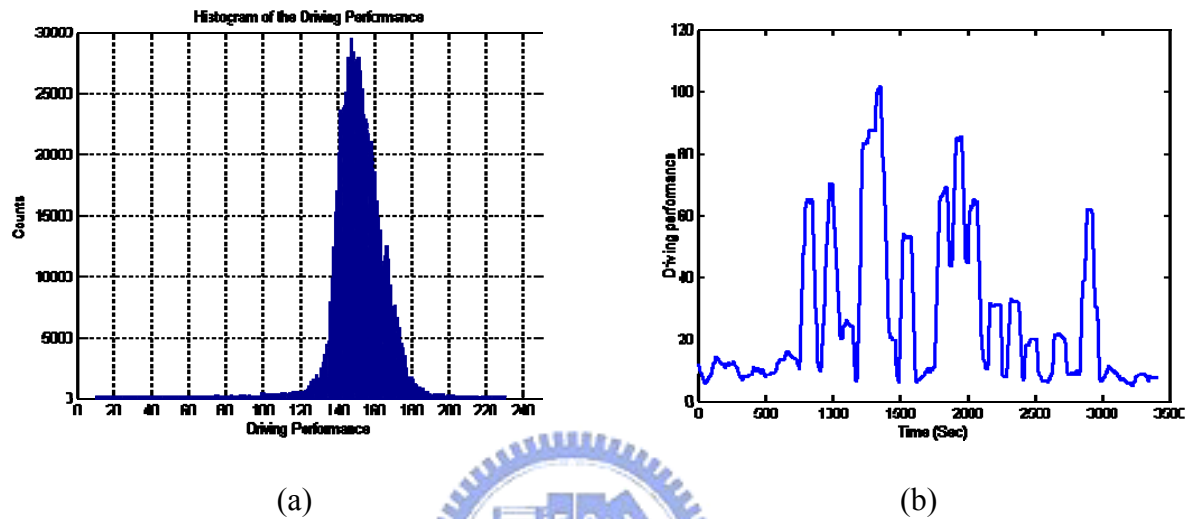


Fig. 3-5: The continuous driving performance of long-term recordings in the driving simulation. (a) The distribution of driving performance, (b) Moving averaged driving error in a 60-minute experiment with at least 2 drowsy periods.

3.4 Search for Brain Source of Drowsiness on Cerebral Cortex

After establishing the individual model to estimate driving performance, we will assess the feasibility of proposed method for practical applications. The main purpose of this experiment is to investigate the brain source of drowsiness. Hence we can use less EEG channels on relative region to perform satisfactory result for estimating driving performance. In this research, the estimation of driving performance will be evaluated to analyze the

number of EEG channels and the regions on the scalp. We expect to find out the universal brain source of drowsiness on cerebral cortex among our participants.

First we compare five results based on different number of EEG channels. These five conditions include 30, 20, 15, 10 and 6 EEG channels proportionally distributed on scalp by the International 10-20 system. We arbitrarily decide the locations of 6-channel EEG electrodes because they are unable to proportionally distribute in the International 10-20 system. Therefore, six most frequently used channels for common experiment are selected in this design. The detailed channel locations on scalp map we consider are shown as Fig. 3-6.

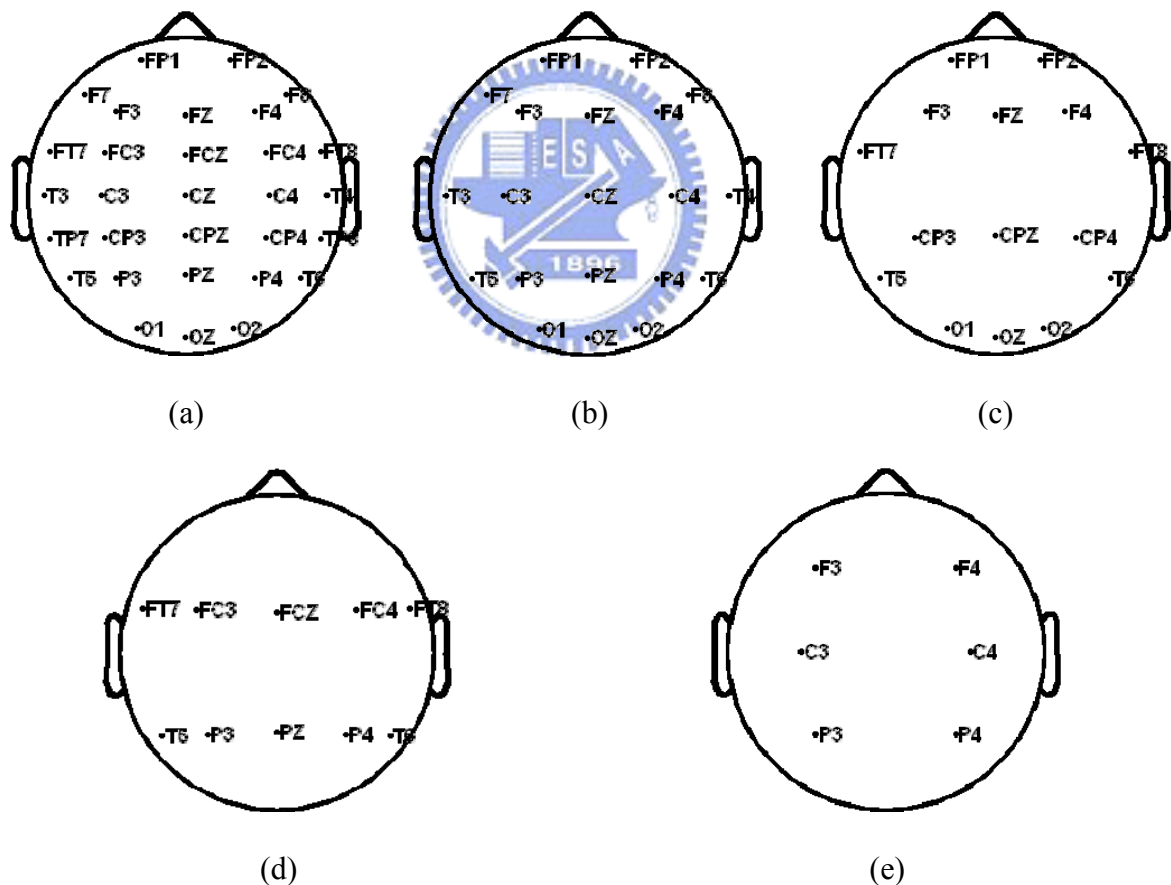


Fig. 3-6: Five conditions for different number of EEG channels. (a) 30 channels, (b) 20 channels, (c) 15 channels, (d) 10 channels, (e) 6 channels.

The Cz channel is the center of the International 10-20 system and the scalp is divided into four regions according to the position of Cz channel in this experiment. The frontal location is defined as the region from Cz to forehead as shown in Fig. 3-7 (a). The left and right temporal locations are defined as the regions from Cz to temples respectively as shown in Fig. 3-7 (b) (c). Finally, the parietal and occipital location is defined as the region including parietal and occipital bone as shown in Fig. 3-7 (d). Each region contains 7 electrodes for analysis.

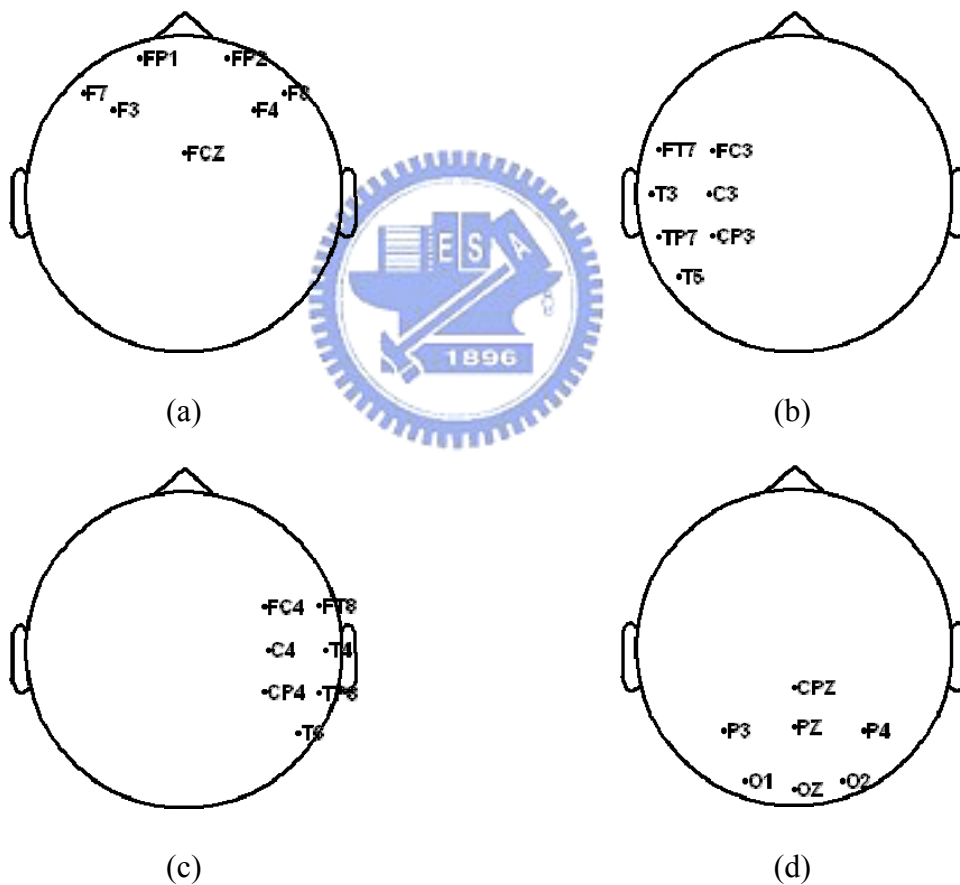
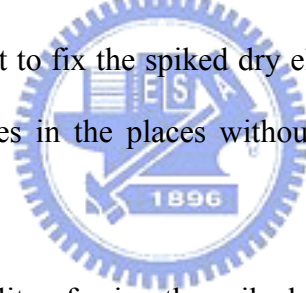


Fig. 3-7: Four clusters of electrodes on the scalp. (a) Frontal location, (b) Left temporal location, (c) Right temporal location, (d) Parietal and occipital location.

3.5 Application of Dry Electrodes in the Drowsiness Experiment

So far, we utilize a few channels from a region on the scalp to achieve a satisfactory result of estimating driving performance through a series of experiments. Although the estimation system has excellent performance in our experiments, it is difficult to apply the electrode cap with electrolytic gel in the realistic driving situations. The spiked dry electrode was designed in this experiment to replace the standard electrode to avoid using electrolytic gel. However, it still has difficulty in using the spiked dry electrodes at present. The first question is that the height of probes on the spiked dry electrodes, which are limited to the MEMS technology, is too short. The probes are difficult to contact stratum germinativum even stratum corneum because the thickness of human hair is usually about 80 μm . The hair elasticity also makes it difficult to fix the spiked dry electrode on the scalp. Therefore we try to fix the spiked dry electrodes in the places without hair in this experiment, such as the forehead.



In order to test the feasibility of using the spiked dry electrodes, we replace the standard electrodes on FP1 and FP2 channels with dry electrodes. We repeat the same experiment of drowsiness estimation in this design, but the only difference is that it includes two spiked dry electrodes as well as all EEG channels. The two EEG signals measured by the spiked dry electrodes will be used in our drowsiness estimation system in this experiment. We have adequate reason to believe that the cognitive state of drowsiness can be recognized in frontal region of the cerebral cortex. The result of estimation performance will verify the feasibility of practical application in the future.

IV.Data Analysis

Our study includes five topics of experiments as described in Chapter III. Two methodologies are used for data analysis. The first one is to deal with the single-trial EEG signals for ERP analysis in Experiment 1 and Experiment 2. The second one is to analyze the continuous EEG data of long-term recordings for the last three experiments. This chapter describes the data analysis procedure of the five experiments in terms of these two methodologies in details. The technology and algorithms applied in our experiments will also be presented in this chapter, including Independent Component Analysis (ICA), time-frequency spectral analysis, correlation analysis, adaptive feature selection mechanism (AFSM) and Self-cOnstructing Neuro-Fuzzy Inference Network (SONFIN).



4.1 Event-Related Potential (ERP) Analysis

Dawson first reported to record the evoked potentials (EP) from cerebral cortex by taking pictures and accumulation skill in 1947 [66]. Dawson initiated the new field of neuro-physiology by introducing the technology of averaging evoked potentials (AEP) in 1951. The AEP technology is extensively applied to many experiments due to the relative stimulus, so the AEP is gradually named event-related potentials (ERP) in recent years. The narrow definition of ERP is to present a specific region of perceptual systems and induce potential changes on the cerebral cortex when the stimulus appears or disappears. The board definition of ERP suggests the responses come from all neural system.

Generally, the ERP induced by the stimulus is $2 \sim 10 \mu\text{V}$, much less than ongoing potential of EEG amplitude, and it is hidden among the EEG signals. EEG signals are

composed of small signals and big noise so that the ERP is cannot to be directly measured and analyzed from EEG signal. In order to extract the ERP from EEG signal, the stimuli must be presented to the subject repeatedly. ERP is obtained by averaging EEG signals of accumulated single trials of the same condition. EEG signals across single trials are considered random and independent of the stimulus. However, it is assumed that the waveform and latency of ERP pattern are invariant to the same stimulus. After accumulating all ERP, the ERP increases proportionally to the number of trials and the EEG amplitude is the sum of adding according to random noise theorem. For example, if the number of trials for condition is n , the ERP will be n times the amplitude of original wave pattern and the EEG amplitude will only be \sqrt{n} times of the initial signal. Therefore, the signal to noise ratio (SNR) will be improved to \sqrt{n} multiples of the original ratio. ERP is the average of n trials of EEG epochs. Therefore, ERP sometimes can be named AEP and this is the basic theorem of extracting the ERP [68].

The ERP techniques are applied to Experiment 1 and Experiment 2 for analyzing events. We also use event-related spectral perturbation (ERSP) analysis in these experiments. In first experiment, we demonstrate the three events including stop, start and deviation events of VR-based driving simulation. The dynamic platform is either in moving or motionless conditions. For the stop and start events, the continuous EEG signals are extracted into several epochs, each of which contains the sampled EEG data from -1500 ms to 4000 ms with a light onset at 0 ms and the length of baseline is 500 ms foremost in each epoch. Similarly, the duration of the deviation event is 3000ms, ranging from -1000 ms to 2000 ms, with deviation onset at 0 ms. The baseline is computed from -1000 ms to 0 ms. Then we combine with the four events including the stop and start event in two conditions and use ICA algorithm to decompose 30-channel EEG signals into the 30 independent components. Simultaneously, we apply the ICA mixing matrix from above result to the deviation event and indicate reaction

time of each deviation event. Therefore we can compare with each component by ERP and ERSP analysis of these three events in the two conditions to justify the necessity of VR-based motion platform in driving simulation. The detailed flowchart of EEG data analysis is shown as Fig. 4-1.

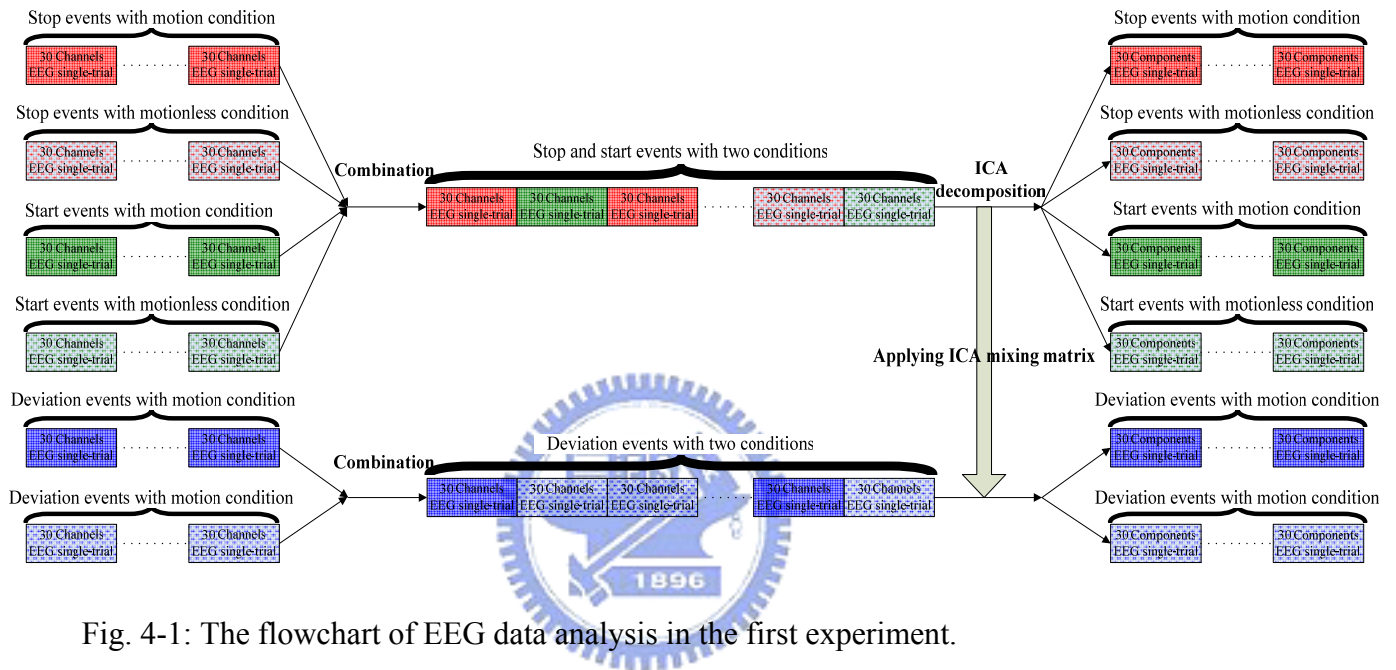


Fig. 4-1: The flowchart of EEG data analysis in the first experiment.

For Experiment 2, we study the ERP and ERSP of drowsiness single-trial in different cognitive states. From design point of view, the drowsiness event is similar to the deviation event of above experiment because the stimulus of these two events is equal. The continuous EEG signals are separated into several epochs where an epoch contains the sampled EEG data from -500 ms to 3500 ms with deviation onset at 0 ms and the baseline region of each epoch is before the onset. The duration of drowsiness event is longer than the deviation event because the driver may need more reaction time while he/she is drowsy. Then we combine with all drowsiness events of recordings from different day and use ICA algorithm to decompose 30-channel EEG signals into the 30 independent components. The reaction time of

each event is recorded for the analysis of drowsiness in different cognitive states. The reaction time of each event is sorted in ascending order and the sorted trials are equally divided into five groups, where each group has 20 percentages in order. Obviously, the first one group indicates that the driver is more alert than other groups while driving. Therefore we can compare with the five conditions of different cognitive states corresponding to the ERSP of drowsiness related component. The detailed flowchart of analysis is shown as Fig. 4-2.

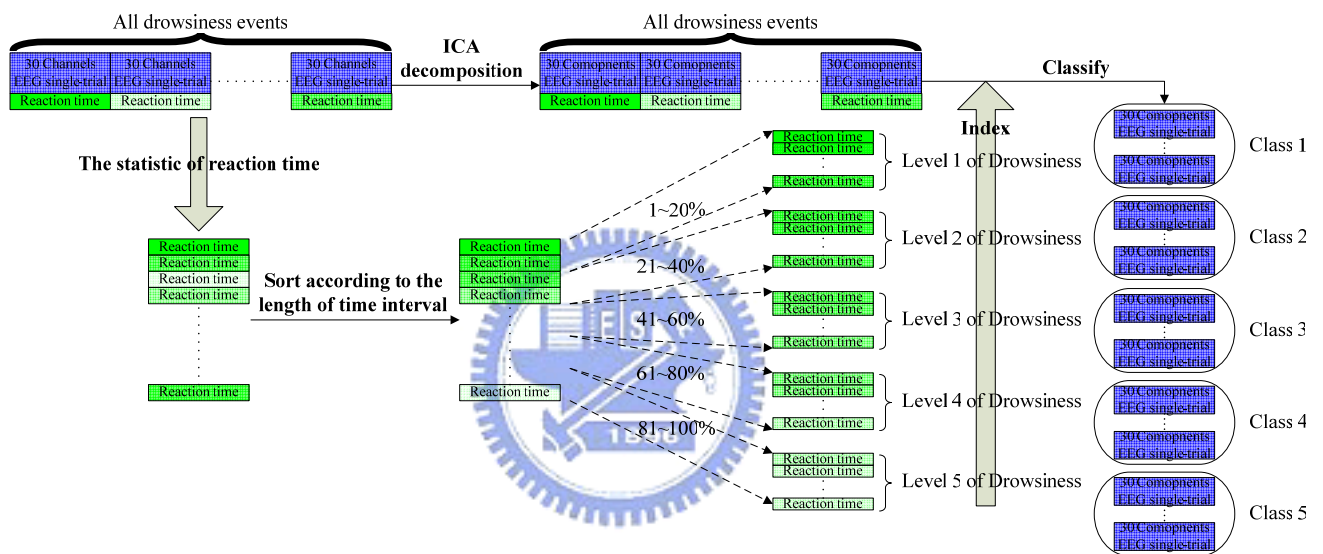


Fig. 4-2: The flowchart of analysis in Experiment 2.

4.2 Analysis of Continuous EEG Data

We attempt to apply the analysis from single-trial into continuous EEG signals for drowsiness for the last three experiments. By averaging accumulated single trials, the ERP analysis reduces noise and makes characteristic more visible in EEG signals. When dealing with the continuous EEG data, we must try to remove high-frequency noise by some

technology and the simplest way we used is moving average filter. In Experiment 3 we propose an adaptive alertness estimation methodology based on EEG, time-frequency spectral analysis, Independent Component Analysis and FNN models for continuously monitoring driver's drowsiness level with concurrent changes in the driving performance. Fig. 4-3 shows the flowchart of the proposed signal processing procedure.

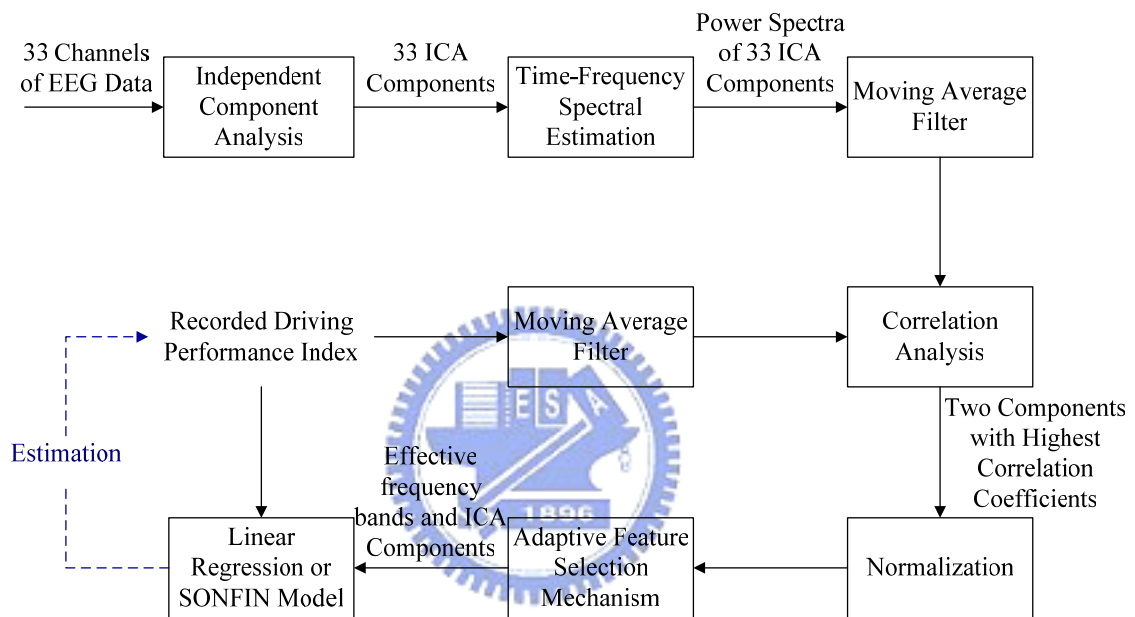


Fig. 4-3: The flowchart of data processing procedure for the drowsy estimation system.

In this experiment, participants who demonstrated waves of drowsiness containing two or more micro-sleep in both sessions were selected for training and testing, respectively. In the training process, the 33-channel EEG signals are first applied to train the ICA model. By applying ICA algorithm to the EEG recordings from the scalp, we attempt to achieve the twin goals: removing artifacts and possible source separation based on stabilities of ICA spatial weighting matrix and temporal independence between artifacts and EEG signals. The effectiveness for removing eye blinking and other artifacts by using ICA had been

demonstrated in many studies [52-59]. Secondly, we use time-frequency spectral analysis to transfer all 33 ICA components into log subband power spectrum with time.

Since the fluctuates of drowsiness level have cycle lengths longer than 4 minutes [27-28, 30], the spectral signals of 33 components and driving performance are smoothed by a causal 90-second square moving average filter advancing at 2-second steps to eliminate variance at cycle lengths shorter than 1~2 minutes. The correlation coefficients between the smoothed driving error and the subband power spectra of all ICA components at each frequency band form a correlation spectrum. The log subband power spectra of two ICA components with the highest correlation coefficient are further selected as features. Then we use the AFSM technology to select the log bandpower spectra of these two ICA components in some critical bands as the normalized input features to the linear regression or SONFIN model. Therefore the training data will establish the model to estimate the individual subject's driving performance.

The ICA weighting matrix, the EEG critical bands of the drowsy related source and the parameters of model in the training session were applied to estimate the individual subject's driving performance in the testing session. Finally, we use correlation analysis between the estimated and actual driving performance to evaluate the performance of model. For comparing with the result by ICA algorithm, the 33-channel EEG signals are directly used for our procedure without using ICA decomposition. We also repeatedly test that finding the most appropriate frequency bands for the best estimating result to prove the dependability of the AFSM technology. Then the performance of estimating results will be discussed by using linear regression or SONFIN to establish model. Detailed analyses are described in the following sub sections.

After we developed an adaptive drowsiness estimation system for driving, we find that this estimation system can get excellent results with only 2-channel EEG signals even with

one single channel. In Experiment 4, the estimation of driving performance will be evaluated to analyze the number of EEG channels and the regions on the scalp. For the discussion about the number of EEG channels, only the optimal frequency bands of the two EEG channels or ICA components with the highest correlation coefficient offered into our estimation system. Then we only use linear regression model to evaluate the estimating results of the five conditions. We expect to find the relationship between the estimated performance and the number of channels with ICA decomposition, and to determine the number of channels should used in our estimating system.

For the discussion about the regions on the scalp, we use the same way to evaluate the brain source of drowsiness on cerebral cortex. The only difference is that we use single channel in our estimating system for emphasizing the location of the four regions. By using a single channel or component with the highest estimating result in each of four regions, we expect to find the brain source of drowsiness on cerebral cortex.

Because it is difficult to apply electrode cap with electrolytic gel during realistic driving situations, the spiked dry electrodes will be a preferred solution. However, the spiked dry electrodes face the restriction to MEMS technology so that the electrodes may not be used to measure EEG signals from the regions we concerned. Hence we replace the standard electrodes on FP1 and FP2 channels with dry electrodes for testing the feasibility. By using the ICA technology, we expect to extract the features from FP1 and FP2 channels which might contain signals proposed from the brain source of drowsiness. We use two EEG signals measured from two dry electrodes for our drowsiness estimation system and compare it with the drowsiness estimation system that use the signals recorded by the standard electrodes in nearby regions. It demonstrates the feasibility of the drowsiness estimation system by using the spiked dry electrodes on the forehead according to the experimental results.

4.3 Independent Component Analysis (ICA)

The joint problems of electroencephalographic (EEG) source segregation, identification, and localization are very difficult since the EEG data collected from any point on the human scalp includes activity generated within a large brain area. The problem of determining brain electrical sources from potential patterns recorded on the scalp surface is mathematically underdetermined. Although the resistivity between the skull and brain is different, the spatial smearing of EEG data by volume conduction does not cause significant time delay and suggests that the ICA algorithm is suitable for performing blind source separation on EEG data. The ICA methods were extensively applied to blind source separation problem since 1990s [44-51]. In recent years, subsequent technical reports [52-59] demonstrated that ICA was a suitable solution to the problem of EEG source segregation, identification, and localization based on the following assumptions: (1) The conduction of the EEG sensors is instantaneous and linear such that the measured mixing signals are linear and the propagation delays are negligible. (2) The signal source of muscle activity, eye, and, cardiac signals are not time locked to the sources of EEG activity which is regarded as reflecting synaptic activity of cortical neurons [52-53].

In this thesis, we attempt to completely separate the twin problems of source identification and source localization by using a generally applicable ICA. Thus, the artifacts including the eye-movement (EOG), eye-blinking, heart-beating (EKG), muscle-movement (EMG), and line noises can be successfully separated from EEG activities. The ICA is a statistical “latent variables” model with generative form:

$$\mathbf{x}(t) = \mathbf{A}\mathbf{s}(t) \quad (1)$$

where \mathbf{A} is a linear transform called a mixing matrix and the s_i are statistically mutually independent. The ICA model describes how the observed data are generated by a process of

mixing the components s_i . The independent components s_i (often abbreviated as **ICs**) are latent variables, meaning that they cannot be directly observed. Also the mixing matrix \mathbf{A} is assumed to be unknown. All we observed are the random variables x_i , and we must estimate both the mixing matrix and the **IC**'s s_i using the x_i .

Therefore, given time series of the observed data $\mathbf{x}(t) = [x_1(t) \ x_2(t) \ \dots \ x_N(t)]^T$ in N -dimension, ICA will find a linear mapping \mathbf{W} such that the unmixed signals $\mathbf{u}(t)$ are statically independent.

$$\mathbf{u}(t) = \mathbf{W} \mathbf{x}(t). \quad (2)$$

Supposed the probability density function of the observations \mathbf{x} can be expressed as:

$$p(\mathbf{x}) = |\det(\mathbf{W})| p(\mathbf{u}), \quad (3)$$

the learning algorithm can be derived using the maximum likelihood formulation with the log-likelihood function derived as:

$$\mathbf{L}(\mathbf{u}, \mathbf{W}) = \log |\det(\mathbf{W})| + \sum_{i=1}^N \log p_i(u_i), \quad (4)$$

Thus, an effective learning algorithm using natural gradient to maximize the log-likelihood with respect to \mathbf{W} gives:

$$\Delta \mathbf{W} \propto \frac{\partial \mathbf{L}(\mathbf{u}, \mathbf{W})}{\partial \mathbf{W}} \mathbf{W}^T \mathbf{W} = [\mathbf{I} - \varphi(\mathbf{u}) \mathbf{u}^T] \mathbf{W}, \quad (5)$$

where the nonlinearity

$$\varphi(\mathbf{u}) = -\frac{\frac{\partial p(\mathbf{u})}{\partial \mathbf{u}}}{p(\mathbf{u})} = \left[-\frac{\frac{\partial p(u_1)}{\partial u_1}}{p(u_1)} \quad \dots \quad -\frac{\frac{\partial p(u_N)}{\partial u_N}}{p(u_N)} \right]^T, \quad (6)$$

and $\mathbf{W}^T \mathbf{W}$ rescales the gradient, simplifies the learning rule and speeds the convergence considerably. It is difficult to know a priori the parametric density function $p(\mathbf{u})$, which

plays an essential role in the learning process. If we choose to approximate the estimated probability density function with an Edgeworth expansion or Gram-Charlier expansion for generalizing the learning rule to sources with either sub- or super-Gaussian distributions, the nonlinearity $\varphi(\mathbf{u})$ can be derived as:

$$\varphi(\mathbf{u}) = \begin{cases} \mathbf{u} - \tanh(\mathbf{u}) & \text{for super - gaussian sources,} \\ \mathbf{u} + \tanh(\mathbf{u}) & \text{for sub - gaussian sources,} \end{cases} \quad (7)$$

Then,

$$\Delta W = \begin{cases} [\mathbf{I} - \tanh(\mathbf{u})\mathbf{u}^T - \mathbf{u}\mathbf{u}^T] \mathbf{W} & \text{super - gaussian,} \\ [\mathbf{I} + \tanh(\mathbf{u})\mathbf{u}^T - \mathbf{u}\mathbf{u}^T] \mathbf{W} & \text{sub - gaussian,} \end{cases} \quad (8)$$

Since there is no general definition for sub- and super-Gaussian sources, we choose $p(\mathbf{u}) = \frac{1}{2}(N(1,1) + N(-1,1))$ and $p(\mathbf{u}) = N(0,1)\text{sech}^2(\mathbf{u})$ for sub- and super-Gaussian, respectively, where $N(\mu, \sigma^2)$ is a normal distribution. The learning rules differ in the sign before the \tanh function and can be determined using a switching criterion as:

$$\Delta \mathbf{W} \propto [\mathbf{I} - \mathbf{K} \tanh(\mathbf{u})\mathbf{u}^T - \mathbf{u}\mathbf{u}^T] \mathbf{W}, \text{ where } \begin{cases} \kappa_i = 1 & \text{super - gaussian,} \\ \kappa_i = -1 & \text{sub - gaussian,} \end{cases} \quad (9)$$

where

$$\kappa_i = \text{sign}(E\{\text{sech}^2(u_i)\}E\{u_i^2\} - E\{\tanh(u_i)u_i\}), \quad (10)$$

represents the elements of N -dimensional diagonal matrix \mathbf{K} . After ICA training, we can obtain 33 ICA components $\mathbf{u}(t)$ decomposed from the measured 33-channel EEG data $\mathbf{x}(t)$.

$$\mathbf{x}(t) = \begin{bmatrix} x_1(t) \\ x_2(t) \\ \vdots \\ x_{33}(t) \end{bmatrix} = \mathbf{W}\mathbf{u}(t) = \begin{bmatrix} w_{1,1} \\ w_{2,1} \\ \vdots \\ w_{33,1} \end{bmatrix} u_1(t) + \begin{bmatrix} w_{1,2} \\ w_{2,2} \\ \vdots \\ w_{33,2} \end{bmatrix} u_2(t) + \cdots + \begin{bmatrix} w_{1,33} \\ w_{2,33} \\ \vdots \\ w_{33,33} \end{bmatrix} u_{33}(t). \quad (11)$$

Fig. 4-4 shows an example of the scalp topographies of ICA weighting matrix \mathbf{W} corresponding to each ICA component by projecting each $w_{i,j}$ onto the surface of the scalp, which provides spatial information about the contribution of each ICA component (brain source) to the EEG channels, e.g., eye activity was projected mainly to frontal sites, and the drowsiness-related potential is on the parietal lobe and occipital lobe, etc. We can observe that most artifacts and channel noises included in EEG recordings are effectively separated into independent components 1 and 4 as shown in Fig. 4-4 and independent components 5, 11, and 13 may be considered as effective “sources” related to drowsiness in the VR-based driving experiment.

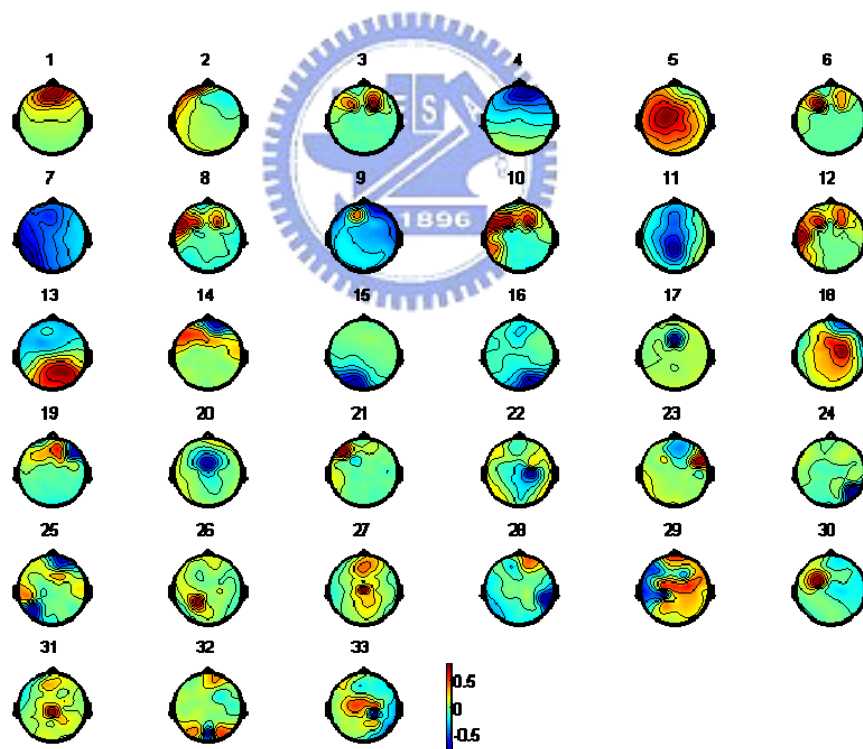


Fig. 4-4: Scalp topography of ICA weighting matrix \mathbf{W} by spreading each w_{ij} into the plane of the scalp corresponding to the j_{th} ICA components based on International 10-20 system.

4.4 Time-Frequency Spectral Analysis

Analysis of changes in spectral power and phase can characterize the perturbations in the oscillatory dynamics of ongoing EEG. Applying such measures to the activity time courses of separated independent component sources avoids confounds caused by miscancellation of positive and negative potentials from different sources to the recording electrodes, and by misallocation to the recording electrodes activity that originates in various and commonly distant cortical sources. The spectral analysis for each ICA component or EEG channel signal is shown in Fig 4-5.

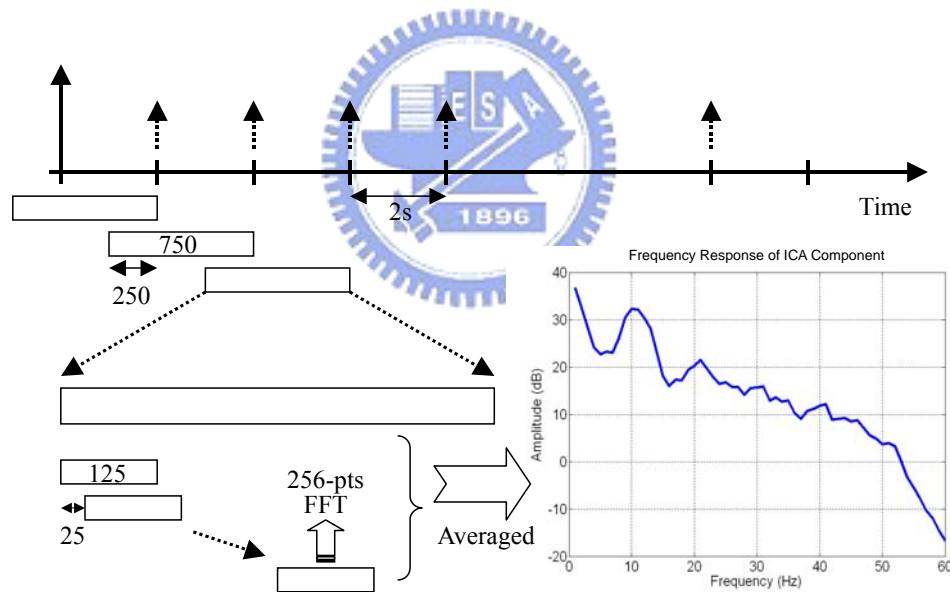


Fig. 4-5: Moving-averaged log power spectral analysis for i_{th} ICA component.

Detailed moving-averaged spectral analysis [69] of the ICA data was accomplished as follows: The ICA component $u_i(t)$ was first divided into several epochs using a 750-point

Hanning window with 250-point overlap, i.e., stepping in 2 seconds at sampling rate $\Omega_s = 250$ Hz.

$$p_m(t) = h(t)u_i(t + 500(m-1)), \quad (12)$$

where $t = 1, 2, \dots, 750$, m is the index of m_{th} epoch, and N -point Hanning window is

$$h(t) = \begin{cases} 0.54 - 0.46 \cos\left(\frac{2\pi t}{N-1}\right) & 0 \leq t \leq N-1 \\ 0 & \text{otherwise} \end{cases}, \quad (13)$$

Windowed 750-point epochs were sub-divided into several 125-point frames using Hanning windows again, with 25-point step size.

$$q_n(t) = h(t)p_m(t + 25(n-1)), \quad (14)$$

where $t = 1, 2, \dots, 125$, and n is the index of n_{th} frames. Each frame was extended to 256 points by zero-padding for a 256-point FFT.

$$v_n(k) = \sum_{t=0}^{N-1} q_n(t) e^{-j \frac{kt}{2\pi N}} \quad (15)$$

Where $N=255$, to normalize the expected multiplicative effects of sub cortical systems involved in wake-sleep regulation of ICA data amplitudes, ICA data spectra were further converted to a logarithmic scale for spectral calculation and driving performance estimation [70]. Then we averaged the bandpower corresponding to each frequency band in all the sub-windows to form a log bandpower spectrum.

$$\tilde{p}_m(k) = \frac{1}{N_t} \sum_{n=1}^{N_t} 10 \log_{10}(v_n(k)^2) \quad (16)$$

Thus, the time-frequency analysis of ICA component $u_i(t)$ of 1 ~ 60Hz stepping in 2 seconds can be expressed as $\tilde{p}_i(m, k)$, where m is the index of time-stepping, and k is the index of k_{th} frequency bands.

$$\mathbf{P}_i(n, k) = \frac{1}{M_p} \sum_{m=1}^{M_p} \tilde{p}_i(m + n - 1, k) \quad (17)$$

Finally, a median filtering using a moving averaged 90-second window was used to further minimize the presence of artifacts in the ICA/EEG signals.

4.5 Correlation Analysis

In order to find the relations between the brain activities and subject's driving performance, and to quantify the level of the subject's drowsiness, we computed the correlation coefficient between the time course of minute-scale fluctuations in driving error ($D_p(n)$) and the concurrent changes in the ICA spectrum of EEG signals by using the Pearson Correlation Coefficient defined as a statistical measure of the linear relationship between two random variables:

$$\text{CC}(i, k) = \frac{\sum_n (\mathbf{P}_i(n, k) - \bar{P}_i(k))(D_p(n) - \bar{D}_p)}{\sqrt{\sum_n (\mathbf{P}_i(n, k) - \bar{P}_i(k))^2} \sqrt{\sum_n (D_p(n) - \bar{D}_p)^2}}, \quad (18)$$

where $\bar{P}_i(k)$ and \bar{D}_p are the expected value of $P_i(n, k)$ and $D_p(n)$, respectively.

Therefore, the correlation coefficients between the driving performance and the ICA component i in the frequency band k can be expressed as a matrix:

$$CC(i,k) = \begin{bmatrix} c_{1,1} & c_{1,2} & \cdots & c_{1,60} \\ c_{2,1} & c_{2,2} & \cdots & c_{2,60} \\ \vdots & \vdots & \ddots & \vdots \\ c_{33,1} & c_{33,2} & \cdots & c_{33,60} \end{bmatrix} \quad (19)$$

Fig. 4-6 shows the results of correlation spectra of Subject 3 in 33 ICA components. The horizontal axis indexes frequency bands between 1 and 60 Hz and the vertical axis indexes the ICA components. The correlation spectra shows a strong evidence between fluctuations in ICA bandpower of frequency bands within 9 to 25 Hz and driving performance index with high positive correlations in ICA components 11 and 13. As driving error increases, so does ICA bandpower.

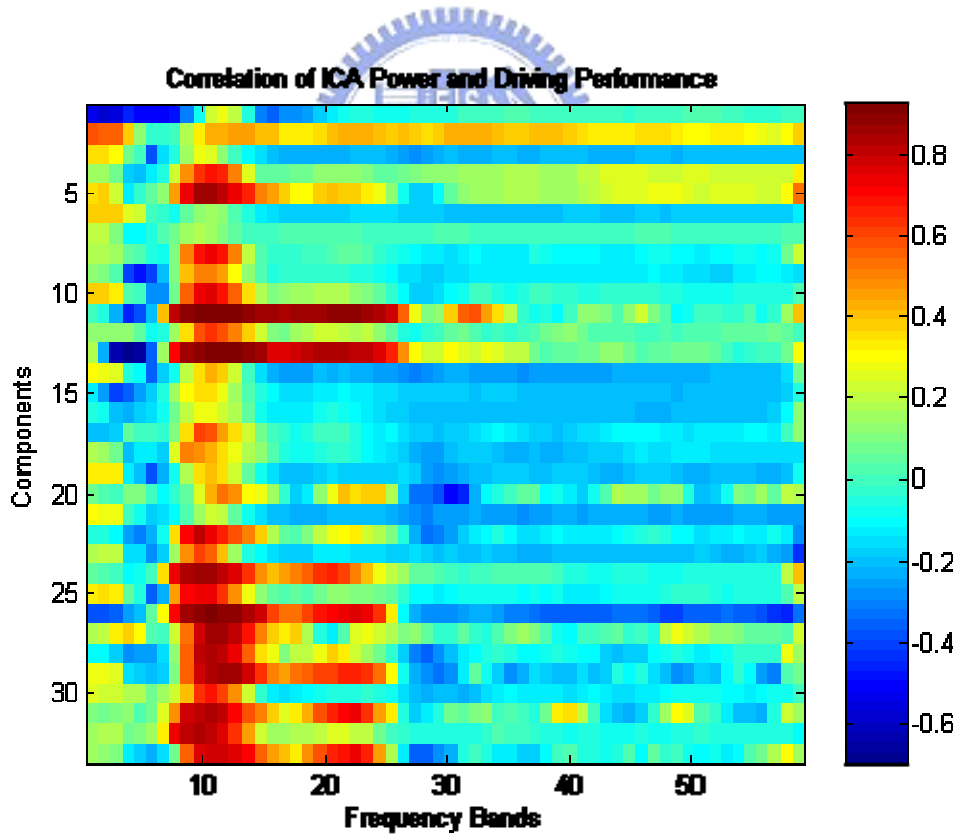


Fig. 4-6: Canonical correlation spectral matrix of subject 3. Note that the higher correlation coefficients appear at 9 ~ 25 Hz in ICA components 11 and 13, respectively.

4.6 Adaptive Feature Selection Mechanism

Signal features in many studies are extracted empirically and become a problem when applied for an on-line monitoring system. To solve this problem, an adaptive feature extracting mechanism is developed to extract useful frequency bands of representative ICA component selection according to the information of the correlation coefficients between log bandpower of ICA components and driving performance index. In this thesis, to extract the most representative ICA component and frequency bands, we first sort the correlation coefficients $CC(i,k)$ in frequency bands k for each component i in descending order by:

$$\mathbf{SC}(i,k) = \underset{k}{\text{sort}}(\mathbf{CC}(i,k)) = \left[\max_k(CC(i,k)) \cdots \min_k(CC(i,k)) \right], i = 1, 2, \dots, 33, \quad (20)$$

where the corresponding matrix indices $\mathbf{K}(i,k)$ is:

$$\mathbf{K}(i,k) = \arg \underset{k}{\text{sort}}(\mathbf{CC}(i,k)) = \left[\arg \max_k(CC(i,k)) \cdots \arg \min_k(CC(i,k)) \right], \quad (21)$$

where the first five frequency bands with the largest correlation coefficients of i_{th} component are expressed as $\mathbf{SC}(i,1) \sim \mathbf{SC}(i,5)$ with frequency band index recorded in $\mathbf{K}(i,k)$, $k=1 \sim 5$.

We then sort the $\mathbf{SC}(i,k)$ in descending order in the column direction to select the ICA components having the maximum value in the summations of the largest 5 correlation coefficients in frequency bands as:

$$\overline{\mathbf{SC}}(i) = \underset{i}{\text{sort}} \left(\frac{1}{5} \sum_{k=1}^5 \mathbf{SC}(i,k) \right), i = 1, 2, \dots, 33, \quad (22)$$

where the component indices in $\mathbf{K}(i,k)$ is also updated. Therefore, the first 2 ICA components with 5 largest correlation coefficients in the frequency bands can be derived as $\overline{\mathbf{SC}}(1)$ and $\overline{\mathbf{SC}}(2)$ with matrix index $\mathbf{K}(i,k)$, $i = 1 \sim 2$ and $k = 1 \sim 5$.

An example of the adaptive feature selection mechanism for subject 3 is given in Fig. 4-7.

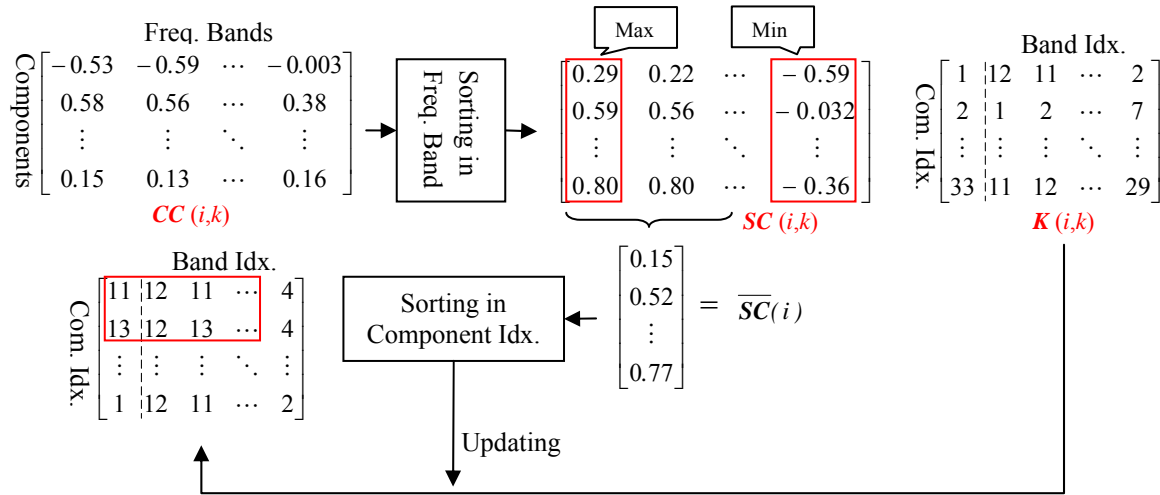


Fig. 4-7: Example of the adaptive feature selection mechanism for subject 3. Note that the band power of ICA components 11 and 13 at frequency bands 10 ~ 14 Hz are selected as input feature of the estimators.



4.7 Self-cOnstructing Neuro-Fuzzy Inference Network (SONFIN)

We developed a Self-cOnstructing Neural Fuzzy Inference Network called SONFIN shown in Fig. 4-8 and it is used for the drowsiness estimation in this thesis [71]. The SONFIN can always find its optimal structure and parameters automatically. Both the structure and parameter identification schemes are done simultaneously during on-line learning without any assignment of fuzzy rules in advance. The SONFIN can always construct itself with an economic network size, and the learning speed as well as the modeling ability is well appreciated. Comparing with other neural networks in different areas including control,

communication, and signal processing, the on-line learning capability of the SONFIN has been demonstrated.

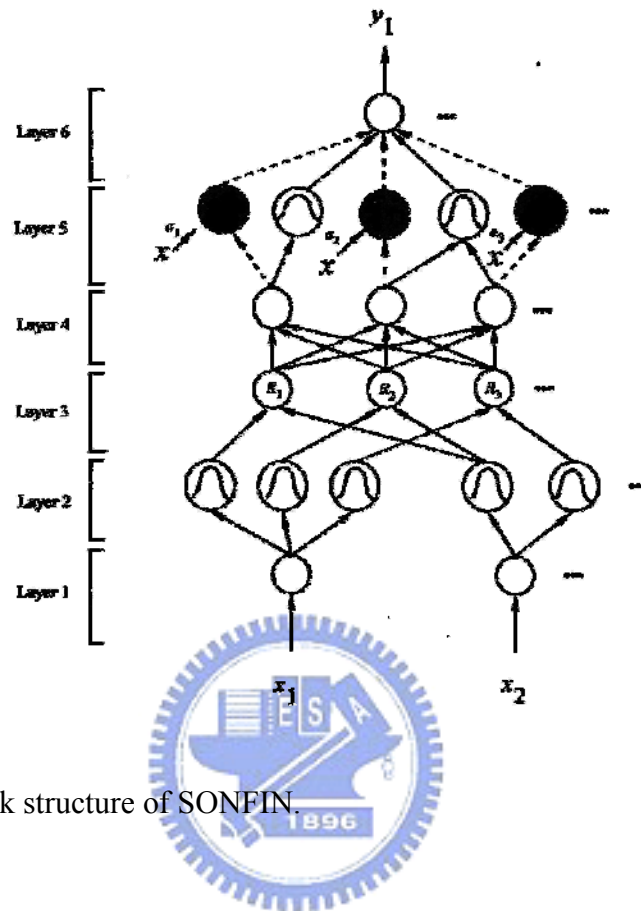


Fig. 4-8: The network structure of SONFIN.

This 6-layered network realizes a fuzzy model of the following form:

$$\begin{aligned}
 \text{Rule } i : \quad & \text{IF } x_1 \text{ is } A_{i1} \text{ and } \dots \text{ and } x_n \text{ is } A_{in} \\
 & \text{THEN } y \text{ is } m_{0i} + a_{j1}x_j + \dots,
 \end{aligned} \tag{23}$$

where A_{ij} is a fuzzy set, m_{0i} is the center of a symmetric membership function on y , and a_{ji} is a consequent parameter. Unlike the traditional TSK model where all the input variables are used in the output linear equation, only the significant ones are used in the SONFIN; i.e., some a_{jis} in the above fuzzy rules are zero.

Each node in Layer 1, which corresponds to one input variable, only transmits input values to the next layer directly. Each node in Layer 2 corresponds to one linguistic label

(small, large, etc.) of one of the input variables in Layer 1. A node in Layer 3 represents one fuzzy logic rule and performs precondition matching of a rule. The number of nodes in Layer 4 is equal to that in Layer 3, and the result (firing strength) calculated in Layer 3 is normalized in this layer. Layer 5 is called the consequent layer. Two types of nodes are used in this layer, and they are denoted as blank and shaded circles in Fig. 4-8, respectively. The node denoted by a blank circle (blank node) is the essential node representing a fuzzy set of the output variable. The shaded node is generated only when necessary. One of the inputs to a shaded node is the output delivered from Layer 4, and the other possible inputs (terms) are the selected significant input variables from Layer 1. Combining these two types of nodes in Layer 5, we obtain the whole function performed by this layer as the linear equation on the THEN part of the fuzzy logic rule in Eq. (23). Each node in Layer 6 corresponds to one output variable. The node integrates all the actions recommended by Layer 5 and acts as a defuzzifier to produce the final inferred output.

Two types of learning, structure and parameter learning are used concurrently for constructing the SONFIN. The structure learning includes both the precondition and consequent structure identification of a fuzzy if-then rule. Here the precondition structure identification corresponds to the input-space partitioning and can be formulated as a combinational optimization problem with the following two objectives: to minimize the number of rules generated and to minimize the number of fuzzy sets on the universe of discourse of each input variable. As to the consequent structure identification, the main task is to decide when to generate a new membership function for the output variable and which significant terms (input variables) should be added to the consequent part (a linear equation) when necessary. For the parameter learning based upon supervised learning algorithms, the parameters of the linear equations in the consequent parts are adjusted by either LMS or RLS algorithms and the parameters in the precondition part are adjusted by the back-propagation algorithm to minimize a given cost function.

The SONFIN can be used for normal operation at any time during the learning process without repeated training on the input-output patterns when on-line operation is performed. There are no rules (i.e., no nodes in the network except the input-output nodes) in the SONFIN initially. They are created dynamically as learning proceeds upon receiving on-line incoming training data by performing the following learning processes simultaneously: (1) input/output space partitioning; (2) construction of fuzzy rules; (3) optimal consequent structure identification; (4) parameter identification. In the above, learning processes (1), (2), and (3) belong to the structure learning phase and 4) belongs to the parameter learning phase.



V. Results and Discussions

The analysis procedures of the five experiments have been introduced in Chapter 4. In this chapter, the corresponding results of all experiments are discussed in details. One or few extension discussions are specified respecting to each experimental results. Moreover, the comparisons between the experiments are also given in this chapter.

5.1 The Influence of the VR-based Motion Platform on Cognitive States

In this section, we demonstrate the influence of kinesthetic stimulus on cognitive states. Firstly, we show the brain source of kinesthetic stimulus on cerebral cortex by the scalp topographies of the ICA components. Then we compare the results in two conditions, which the dynamic platform is moving and motionless, by the analysis of ERP and ERSP. The results of comparison indicate the necessity of VR-based motion platform for brain research in driving simulation

5.1.1 The Brain Source of Kinesthetic Stimulus on the Cerebral Cortex

First of all, we compare each component by ERP and ERSP analysis of the three events in the two conditions that the dynamic platform is moving and motionless. The scalp topographies of 30 ICA components obtained from Subject 1 is shown in Fig. 5-1 and two ICA components have different responses between the two conditions are shown in Fig. 5-2.

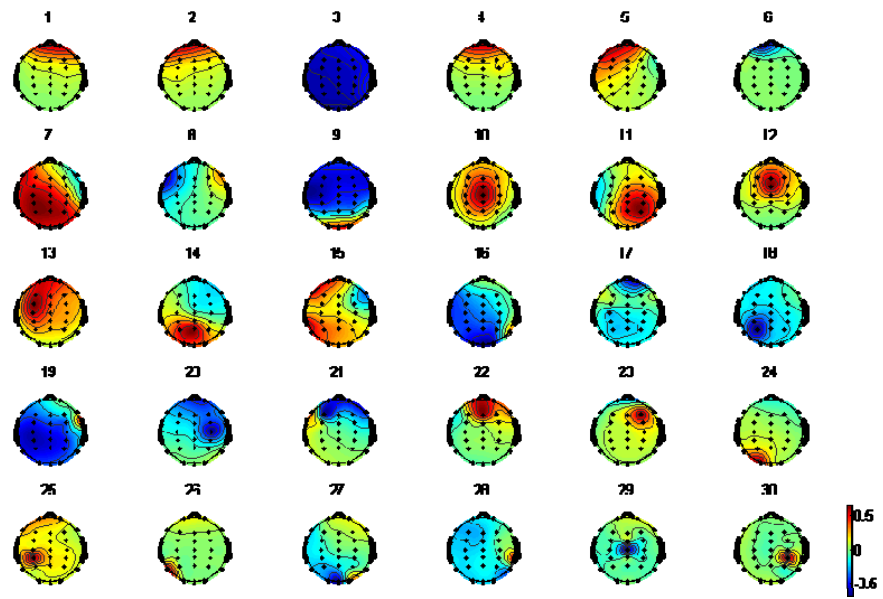


Fig. 5-1: The scalp topographies of all ICA components trained by EEG data from Subject 1.

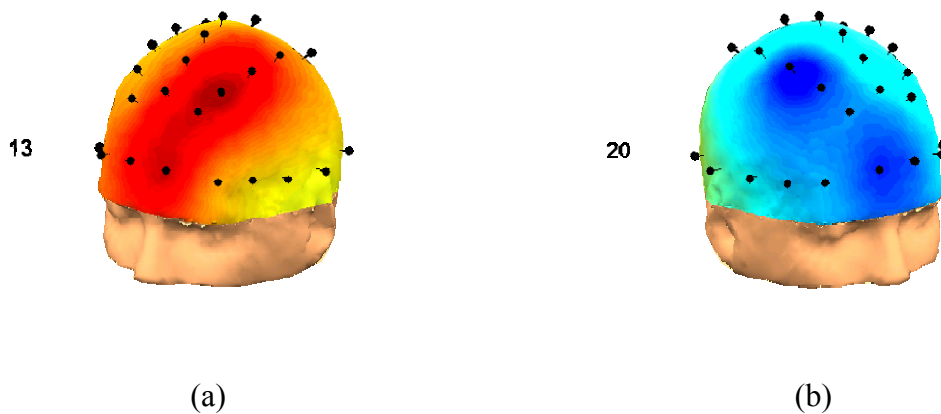


Fig. 5-2: Two ICA components have different responses between the two conditions of all events. (a) The source near FC3 location, (b) The source near FC4 location.

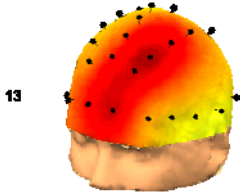
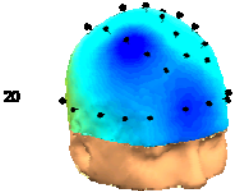
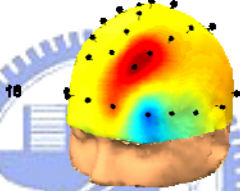
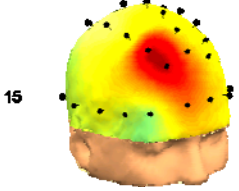
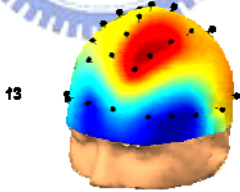
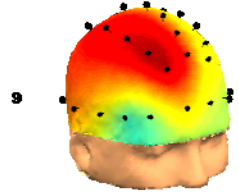
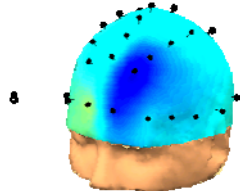
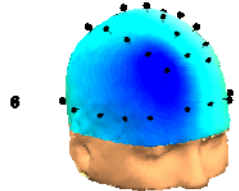
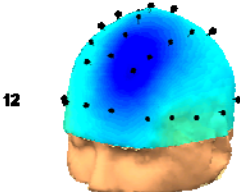
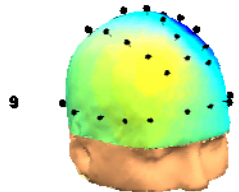
There is evidence in plenty to show that the vestibular system is related to kinesthetic perception of human body, and the brain can deal with the information of balance between optic scenes and kinesthetic perception [32]. This cognitive state will respond on the cerebral cortex and we can observe this phenomenon from EEG data. By the experiment design of the experiment group and control group, we can compare with each ICA component by ERP or ERSP analysis of two groups to determine the components related to kinesthetic stimulus. Beside we have excluded the difference between two groups due to the appearing order of experiments with the dynamic platform is moving and motionless.

All of the five participants of this experiment have exactly two ICA components related to kinesthetic stimulus and the results are presented in Table 5-1. The two scalp topographies of these ICA components are symmetrical on the left and right sides of all participants and the sources of these ICA components are near FC3 and FC4 channel locations, respectively. Especially, the vestibular system is just about under the sources we indicated on cerebral cortex. These two ICA components we selected are reasonable according to the results.

Table 5-1 indicates that the only two ICA components of all have the difference in the two conditions.

Table 5-1

The scalp topographies of two ICA components have different response in the two conditions.

ICA Components	Near FC3 Location	Near FC4 Location
Subject 1		
Subject 2		
Subject 3		
Subject 4		
Subject 5		

5.1.2 Necessity of VR-based Motion Platform

Then we select component 20 to demonstrate the results because the result of the other one component is similar. The ERP and ERSP analysis for stop event between the two conditions are shown in Fig. 5-3. We will begin with a sample observation for subject 1 as shown in Fig. 5-3 (a)(b). For driving stop event, the amplitude of ERP is a little smaller in the motion condition than the response in the motionless condition. The important point to note is the power spectra of ERP in two conditions as shown in Fig. 5-3 (c). When the dynamic platform is moving, the frequency near 10 Hz and its harmonic frequency will be obviously suppressed. The same results can be observed in driving start and driving deviation events as shown in Fig. 5-4 (c) and Fig. 5-5 (c).

Then we consider the ERSP of driving stop event in two conditions as shown in Fig. 5-3 (d)(e). One may notice that long-lasting suppression of near 10 Hz is conspicuous while the dynamic platform is in operation. The power spectra of driving stop event in two conditions are affected due to this phenomenon. There is other thing to note in driving stop event. When the vehicle has exactly stopped at the third second in the motionless condition, the perception of human is the most unbalanced corresponding to response of the ERSP analysis.

The influence of dynamic platform in driving start and driving deviation events are similar to the driving stop event as shown in Fig.5-4 and Fig. 5-5. The differences are the magnitude near 10 Hz and the amplitude of the response between the two conditions whether the ERP analysis or ERSP analysis for these two events. It is noted that in ERSP analysis of the driving start event as shown in Figs. 5-4 (d)(e), all frequency bands are suppressed accompanying the vehicle is accelerating while the dynamic platform is in operation. During the periods of acceleration, the driver may feel much centrifugal perception in the driving

cabin by the dynamic platform. The influence on cognitive state of kinesthetic stimulus can be also discussed in next experiment.

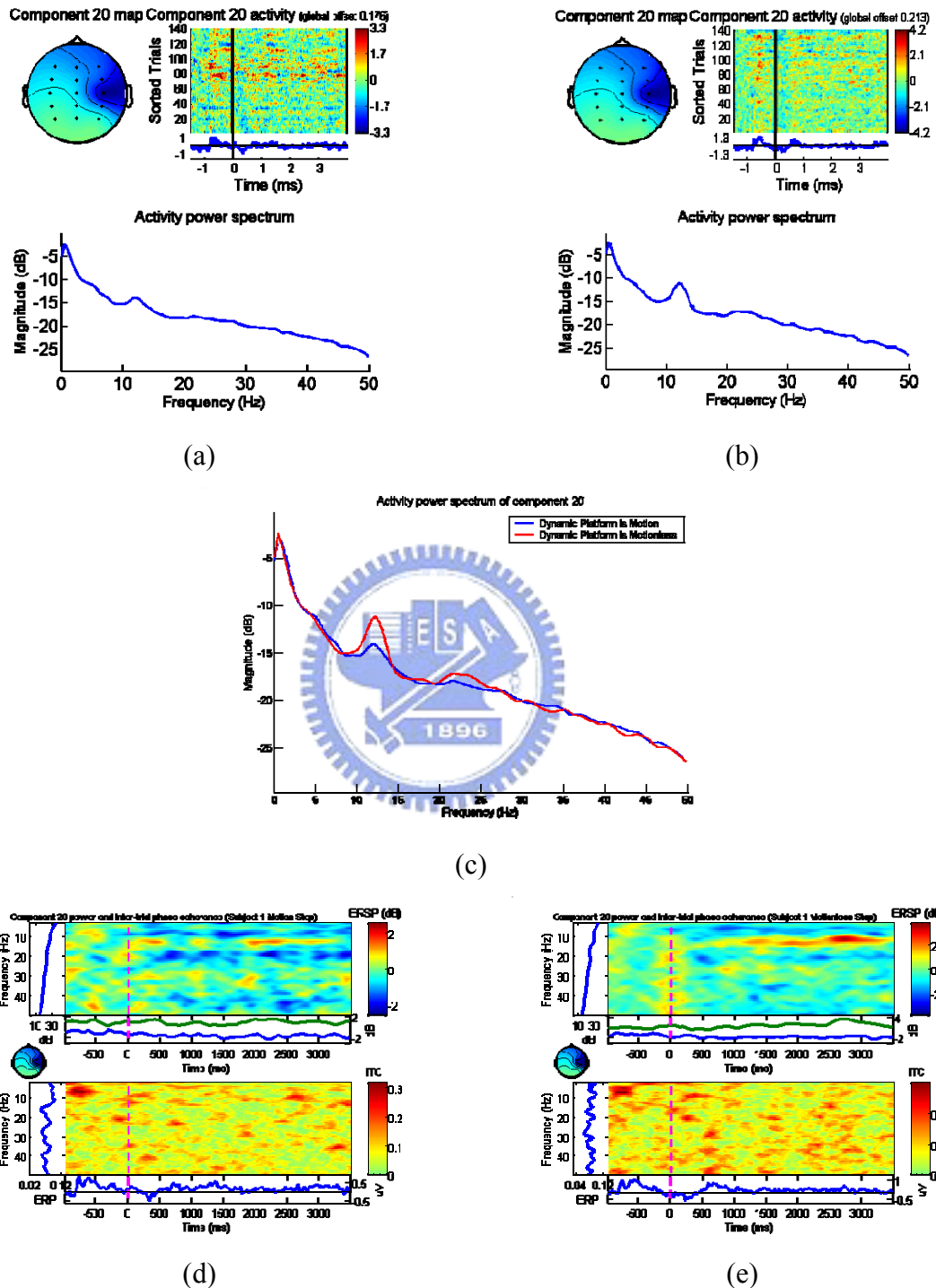
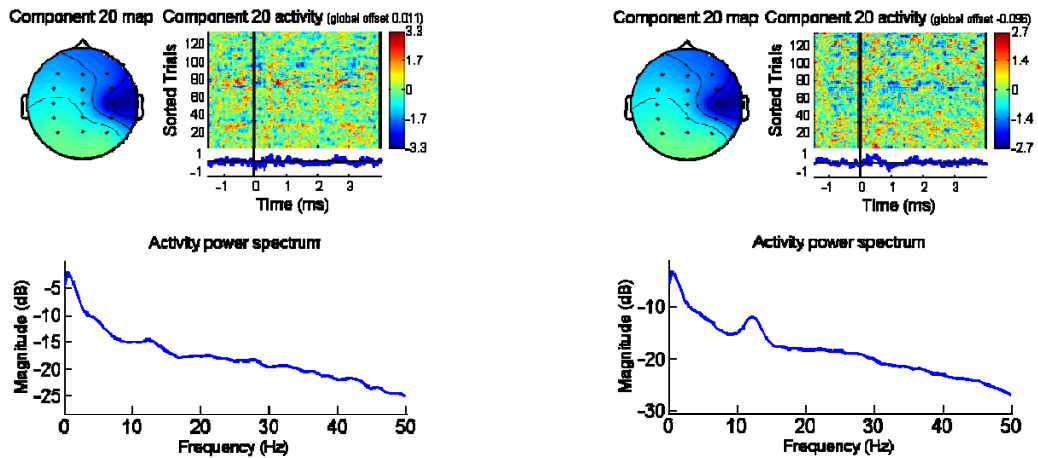
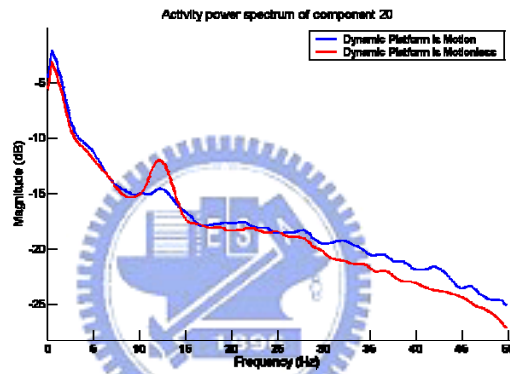


Fig. 5-3: The ERP and ERSP analyses of component 20 for stop event. (a) The ERP of motion condition, (b) The ERP of motionless condition, (c) Overplot power spectrum of two conditions, (d) The ERSP of motion condition, (e) The ERSP of motionless condition.

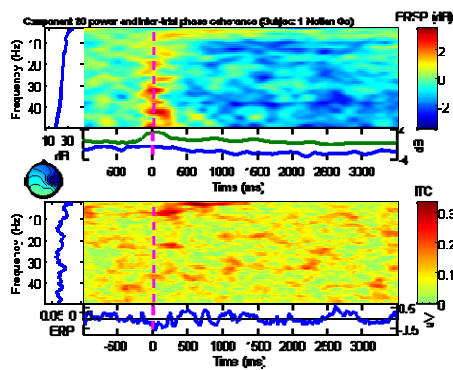


(a)

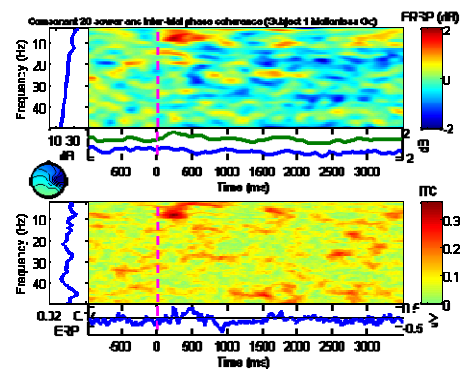
(b)



(c)

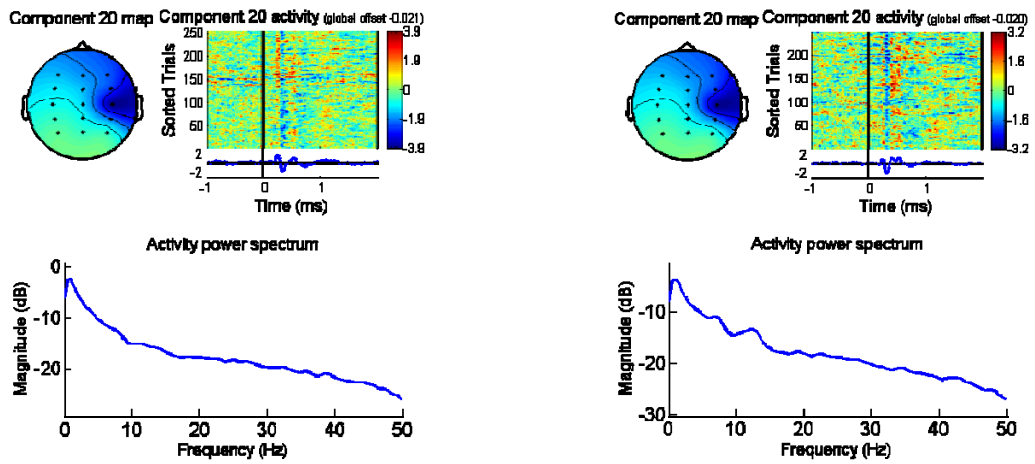


(d)



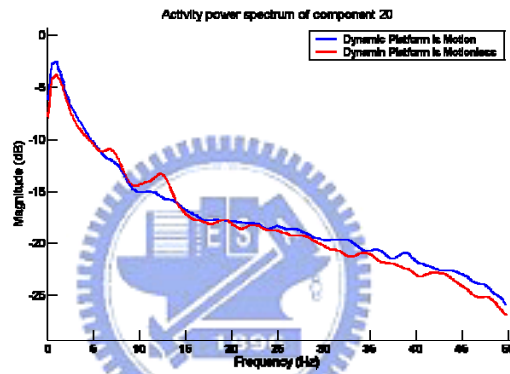
(e)

Fig. 5-4: The ERP and ERSP analyses of component 20 for start event. (a) The ERP of motion condition, (b) The ERP of motionless condition, (c) Overplot power spectrum of two conditions, (d) The ERSP of motion condition, (e) The ERSP of motionless condition.

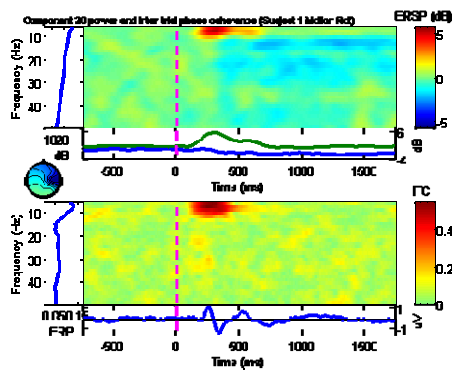


(a)

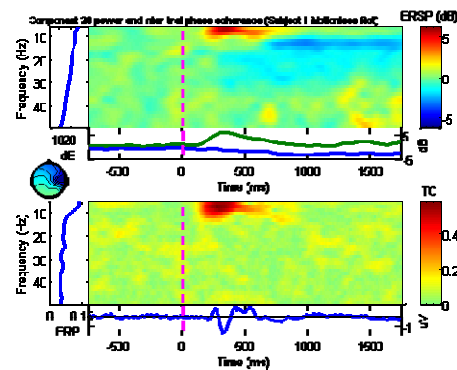
(b)



(c)



(d)



(e)

Fig. 5-5: The ERP and ERSP analyses of component 20 for deviation event. (a) The ERP of motion condition, (b) The ERP of motionless condition, (c) Overplot power spectrum of two conditions, (d) The ERSP of motion condition, (e) The ERSP of motionless condition.

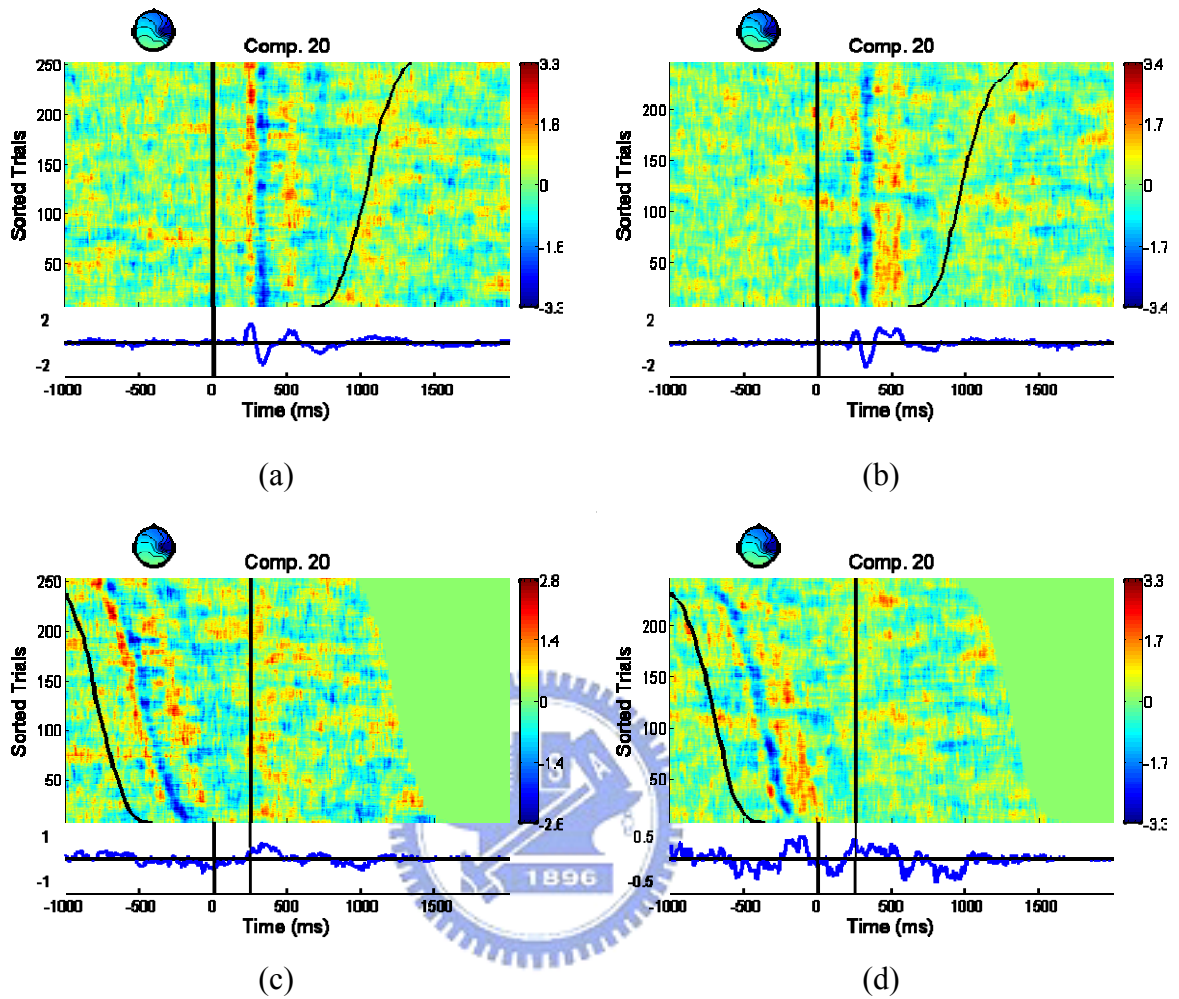


Fig. 5-6: The ERP analysis of component 20 for deviation event with reaction time. (a) The ERP with reaction time of motion condition, (b) The ERP with reaction time of motionless condition, (c) Aligning onset by reaction time from (a), (d) Aligning onset by reaction time from (b).

There is further evidence to suggest that the ICA components we concern about are related to the movement of the dynamic platform as shown in Fig. 5-6. The reaction time represents when the subject steers wheel to keep the vehicle in the cruising lane following the movement of dynamic platform. In Figs. 5-6 (a)(b), the black line at 0 ms is the onset of

deviation and the black curve with sorted trials means the reaction time. The onset of deviation and reaction time will company the movement of the dynamic platform if we consider the kinesthetic stimulus. When the dynamic platform is motion, the response of ERP with automatic vehicle deviation is larger and faster than the other condition. In Figs. 5-6 (c)(d), after aligning the onset of reaction time for two conditions, the response of steering wheel only occurs in motion condition. Therefore, it makes sure that the ICA components we concern about are related to the movement of the dynamic platform.

In addition to the results of Subject 1 in this experiment, the other four participants have similar results of the different responses between the two conditions and the most obvious difference is the spectral magnitude near 10 Hz.



5.2 The Brain Activity of Drowsiness in Different Cognitive States

In this section, we investigate the event-related potential of drowsiness in different cognitive states and we can recognize the features of brain drowsy activity for further analysis. Then we also discuss the influence of the dynamic motion platform on drowsiness in this section.

5.2.1 The Degree of Cognitive States in Drowsiness

Firstly, the trials are sorted according to the length of reaction time and equally divided into five groups as the index for further analysis. Each group has 20 percentages of trials in order and an example of Subject 4 is shown in Fig. 5-7. Then we select one component which is related to drowsiness for analysis as shown in Fig. 5-8.

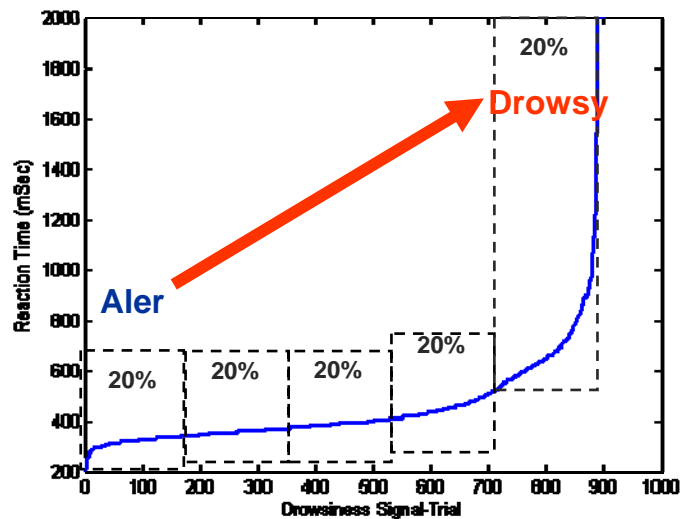


Fig. 5-7: The trials are sorted according to reaction time and equally divided into five groups of subject 4.

Fig. 5-7 provides a start-point to observe the reaction time of all single-trials in this experiment. When the driver is drowsy, the reaction time between the onset of deviation and steering wheel is increasing. Because the onset of deviation is random and unanticipated in each drowsiness single-trial, it has sufficient demonstration to show the reaction time can be the index for the degree of drowsiness. By equally dividing all single-trials into five groups, we can discuss five degrees of cognitive states in drowsiness prior to falling into micro-sleep at NREM. We may indicate by Fig. 5-8 what the responses of cognitive states will follow the reaction time and occur before the onset of reaction time and behind the onset of reaction time.

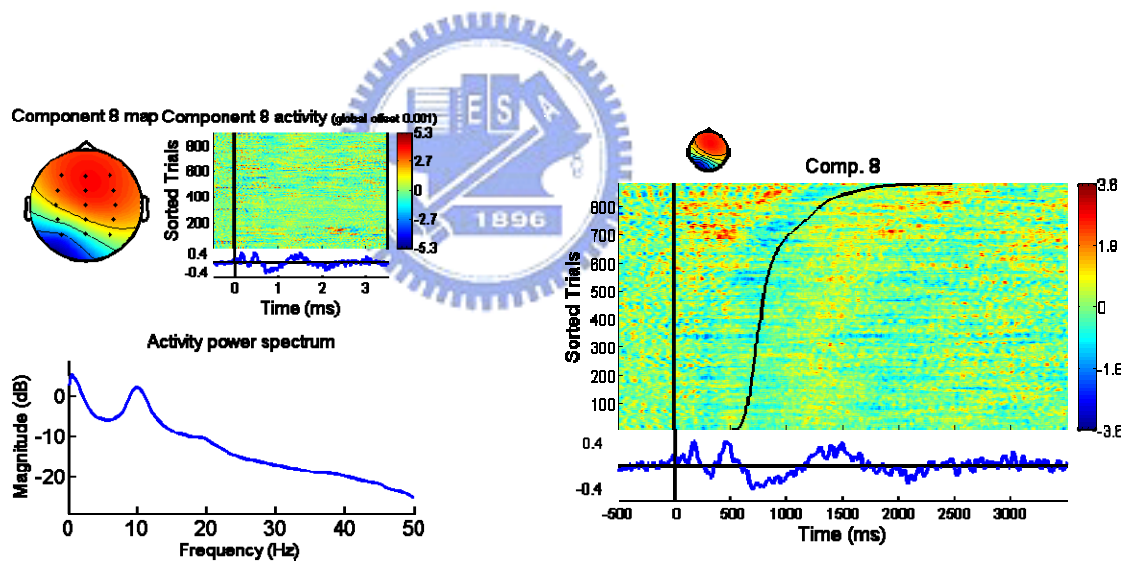


Fig. 5-8: One component is related to drowsiness and the ERP analysis with all single-trials.

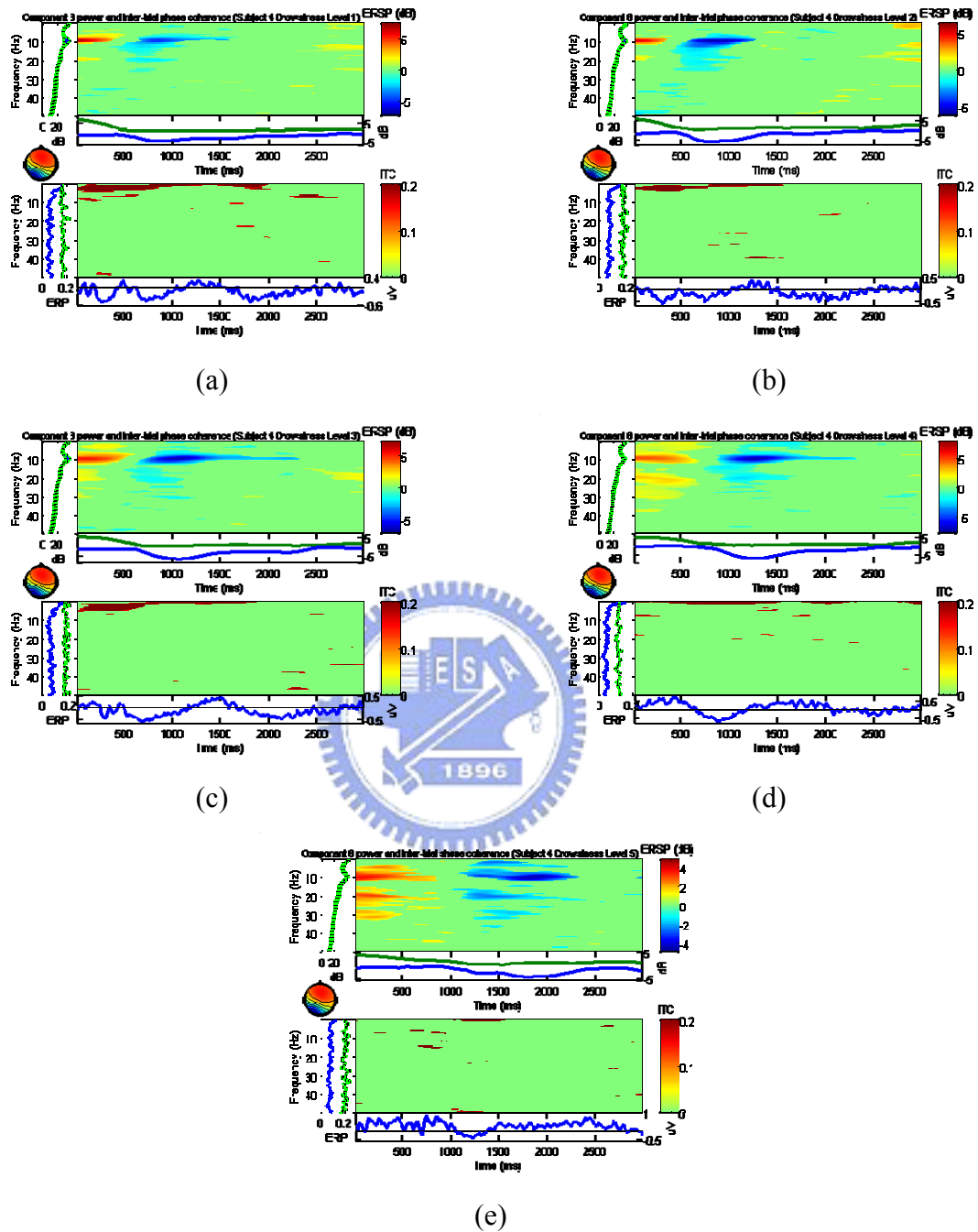


Fig. 5-9: The results of ERSP analysis in five different cognitive states. (a) Drowsiness level from 1 ~ 20 %, (b) Drowsiness level from 21 ~ 40 %, (c) Drowsiness level from 41 ~ 60 %, (d) Drowsiness level from 61 ~ 80 %, (e) Drowsiness level from 81 ~ 100 %.

Fig. 5-9 is a series of five diagrams illustrating the different cognitive states in five degrees of drowsiness. We can imply the approximate reaction time of ERSP analysis by Fig. 5-7 in all conditions. In the first stage of the five degrees as shown in Fig. 5-9 (a), it means the driver is more alert than other stages and the reaction time is shorter than the other degrees while driving. The reaction time of the first stage is about 300 ms and the amplitude of time-frequency spectrum enhances 5 dB near 10 Hz against power spectrum of baseline before the onset of reaction time. Then the amplitude of time-frequency spectrum reduces 3 ~ 5 dB near 10 Hz against power spectrum of baseline after the onset of reaction time. The results of ERSP analysis in the second stage as shown in Fig. 5-9 (b) are similar to the results in the first stage because the reaction times of these two conditions are much closed.

In the third stage of the five degrees as shown in Fig. 5-9 (c), the enhancement of power spectrum near 10 Hz has duration with 500 ms due to the reaction time is slightly longer than the first two conditions. And the amplitude of time-frequency spectrum is reduced and it lasts about 1500 ms after the onset of reaction time. In the fourth stage of the five degrees as shown in Fig. 5-9 (d), the reaction time becomes a little later to previous conditions. Similar to the results in the third stage, the time-frequency spectrum of harmonic frequency in 10 Hz has the same response before and after the onset of the reaction time. Finally, in the last stage of the five degrees as shown in Fig. 5-9 (e), the reaction time is the latest of all conditions and the response of enhancement and reduction in 10Hz and harmonic frequency is more obvious than the results in the fourth stage. The importance of the phenomenon in the five stages cannot be overemphasized. Although the driver is micro-drowsy and not fall into sleeping in driving, the feature of the magnitude in 10 Hz will change with the different drowsiness level.

5.2.2 The Dynamic Platform Influences Drowsiness ERP

Now, we consider the results of above procedure if the dynamic platform is motionless and it is shown in Fig. 5-10.

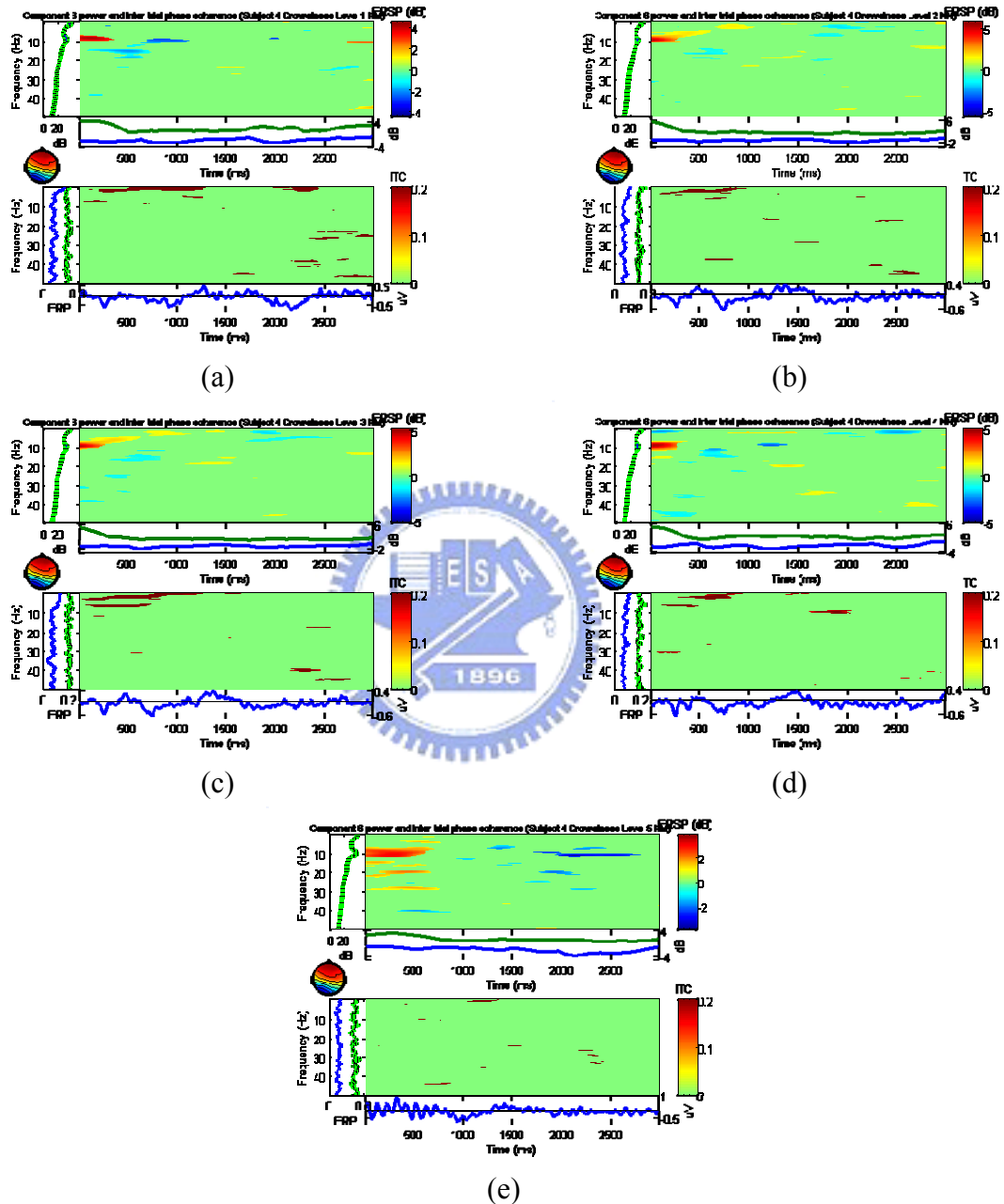


Fig. 5-10: The results of ERSP analysis in five different cognitive states if the dynamic platform is motionless. (a) Drowsiness level from 1 ~ 20 %, (b) Drowsiness level from 21 ~ 40 %, (c) Drowsiness level from 41 ~ 60 %, (d) Drowsiness level from 61 ~ 80 %, (e) Drowsiness level from 81 ~ 100 %.

Here we can demonstrate the dynamic platform influencing the results of drowsiness ERP. The results of Experiment 1 produce evidence for the response of power spectrum near 10 Hz by kinesthetic stimulus. As shown in Fig. 5-9, the feature of drowsiness single-trial in different cognitive states is also the power spectrum near 10 Hz. Fig. 5-10 tells us the influence of dynamic simulator on drowsiness experiment.

First of all, we compare with the two conditions of dynamic platform is motion and motionlessness for drowsiness experiment at the same time. The reaction times of the Fig. 5-9 and Fig. 5-10 in the five degrees of drowsiness are almost equal. Then the durations of the response before the onset of the reaction time are similar in the five degrees. However, the spectral magnitude responses near 10 Hz in the motionless condition enhances less than the results in the motion condition for all degrees of drowsiness. In addition, the suppression response of 10 Hz after the onset of the reaction time almost disappears in the motionless condition. Therefore, the dynamic platform is necessary for the study of drowsiness experiments in the real world.



5.3 The Performance of Adaptive Drowsiness Estimation

We discuss the performance of the proposed adaptive drowsiness estimation of continuous driving in this section. First we demonstrate the dominant ICA components and EEG channels for drowsiness. Then we compare the results of estimating performance by using ICA components or EEG channels, selectivity experts or AFSM method feeding to linear regression model or SONFIN model. Finally, we also discuss the optimal length of the moving average windows for drowsiness experiments.

5.3.1 Relationship between the ICA/EEG Power Spectrum and Drowsiness

First of all, we compare the correlation between log subband power spectra and driving performance for each frequency bands and individual ICA components to find the adaptive subbands and localization of electrodes according to the scalp topographies of ICA weighting matrices. Then we also show the correlation analysis results by using EEG channel signals. The two correlation coefficient spectra of Subject 3 are shown in Fig. 5-11.

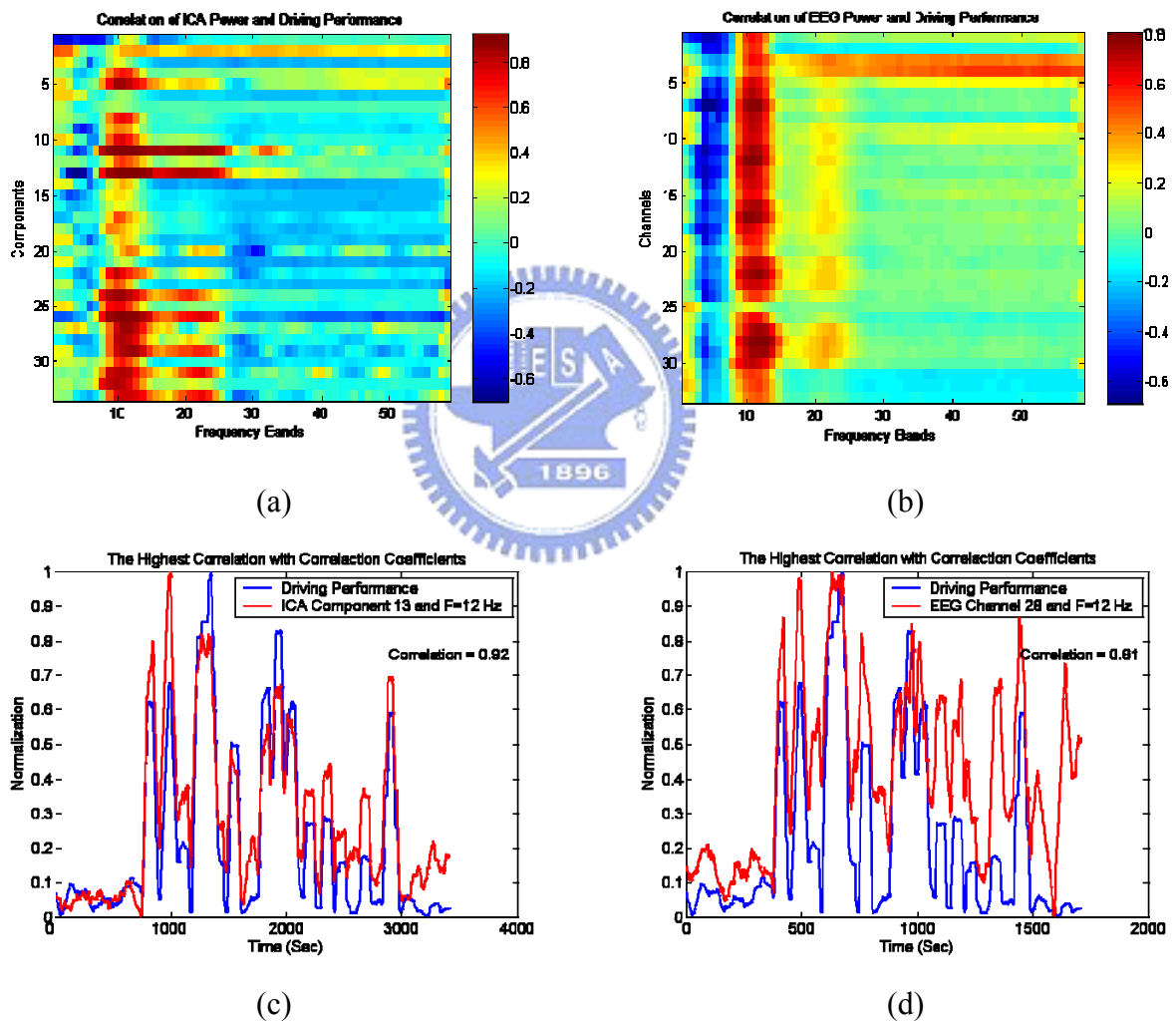


Fig. 5-11: The results of correlation coefficient analysis for Subject 3. (a) The correlation coefficient spectra of ICA components, (b) The correlation coefficient spectra of EEG channels, (c) The ICA component with highest correlation with the driving performance, (d) The EEG channel with highest correlation with the driving performance.

The scalp topographies of all ICA components trained by EEG data of Subject 3 have been shown in Fig. 4-4. Hence, we will select two ICA components and two EEG channels which have the highest correlation coefficient with the driving performance index as the features for adaptive drowsiness estimation as shown in Fig. 5-11.

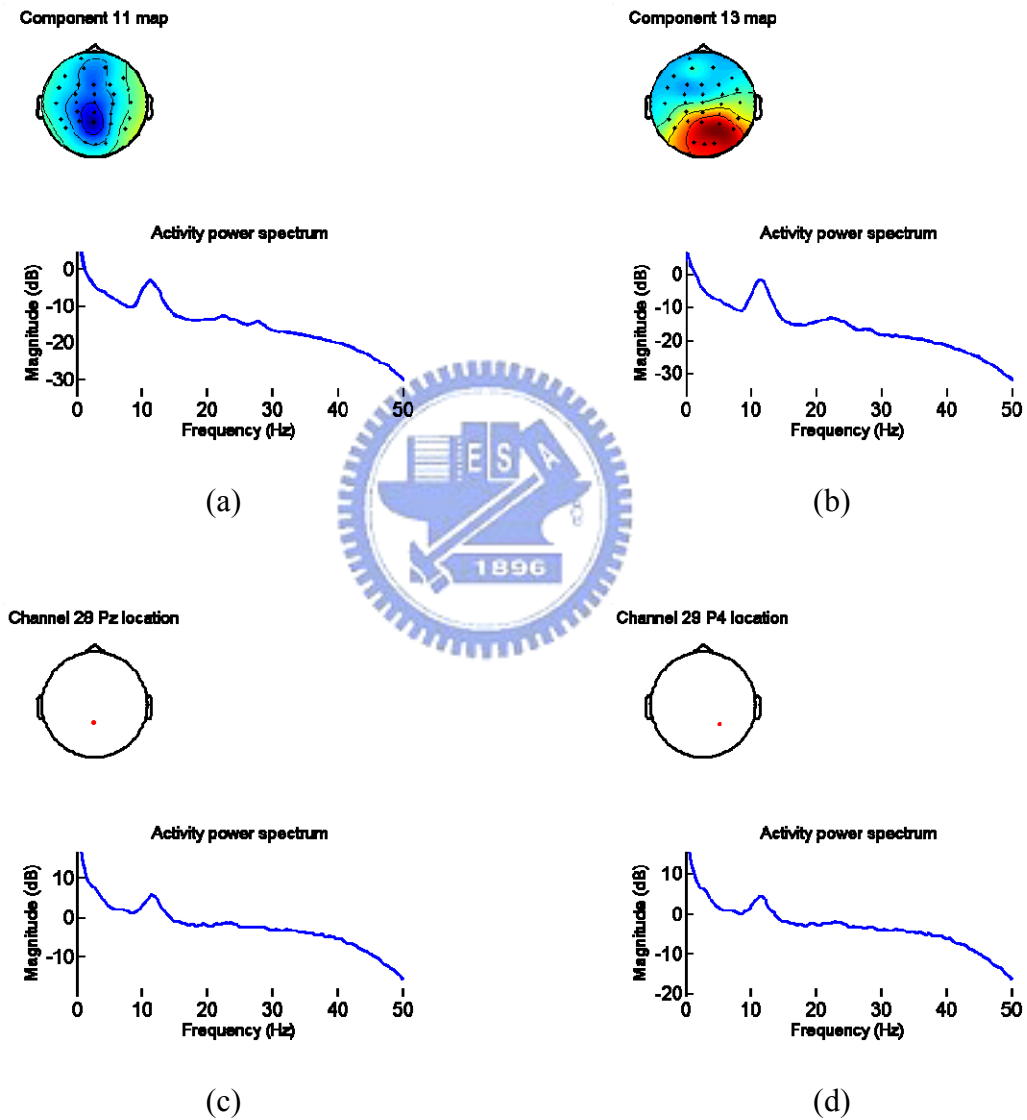


Fig. 5-12: Two ICA components and two EEG channels with the highest correlation coefficient with the driving performance index. (a) ICA Component 11, (b) ICA Component 13, (c) EEG Pz channel, (d) EEG P4 channel.

After ICA training and time-frequency analysis for each ICA component and EEG channel, we compute the spectral correlation coefficients between the ICA/EEG log subband power spectrum and the driving performance index. Fig. 5-11 (a)(b) shows the correlation spectra of Subject 3 in 33 ICA components and 33 EEG channels, respectively. The horizontal axis indexes frequency bands between 1 ~ 60 Hz and the vertical axis indexes the EEG channels or ICA components. In Fig. 5-11 (a), the correlation spectra show a strong evidence between fluctuations in EEG bandpower of frequency bands within 10 ~ 14 Hz and driving performance with high positive correlations in most EEG channels. The driving deviation increases with the EEG bandpower as shown in Fig. 5-11 (c). We also investigate these relationships by plotting the correlation coefficients between bandpower of 33 ICA components and driving performance. A similar monotonic relationship exists in a wide frequency bands, especially the frequency bands from 9 to 25 Hz in ICA components 11 and 13 achieve a high positive correlation with the driving deviation as shown in Fig. 5-11 (b).



5.3.2 The Dominant ICA Components and EEG Channels for Drowsiness

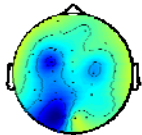
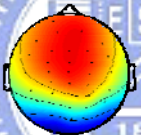
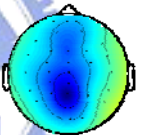
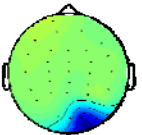
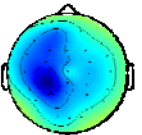
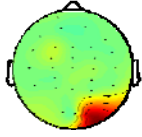
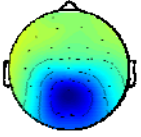
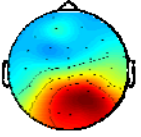
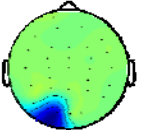
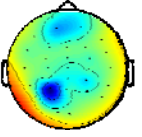
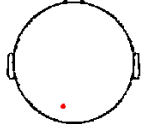
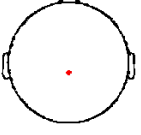
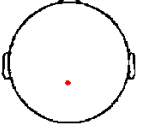
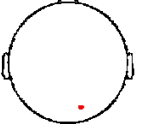
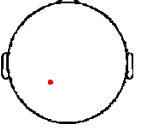
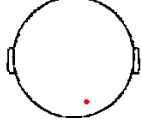
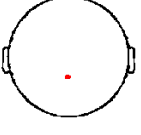
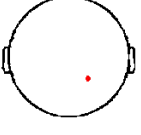
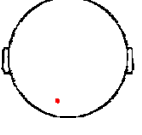
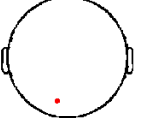
Fig. 5-12 show the spatial distributions in scalp topography weighting matrices W for dominant ICA component 11 that is centered near Pz channel location and ICA component 13 that is centered near P4 channel location of the Subject 3. The two EEG signals of Pz and P4 channels locations are selected for further analysis because these EEG signals have the highest correlation coefficients among all EEG channels according to Table 5-2, the sources of two ICA components, which we selected with the highest correlation coefficients, are near the two EEG channels locations selected by the same procedure of the five participants. The correlations are particularly strong at central and posterior areas, which are similar to the results of previous studies in the driving experiments [19,21,25]. The relatively high

correlation coefficients of near α -band (8 ~ 13 Hz) with driving performance suggests that α -band frequencies may be suitable for drowsiness estimation, where the subject's cognitive state might fall into stage one of the NREM.

Table 5-2 summarizes the scalp topographies of the two ICA components and two EEG channels we used for adaptive drowsiness system of the five participants.

Table 5-2

Two ICA components and two EEG channels of the five participants with the highest correlation coefficients with the driving deviation are selected for adaptive drowsiness estimation.

	Subject 1	Subject 2	Subject 3	Subject 4	Subject 5
ICA Components	Component 17 map 	Component 6 map 	Component 11 map 	Component 6 map 	Component 22 map 
	Component 26 map 	Component 17 map 	Component 15 map 	Component 8 map 	Component 26 map 
EEG Channels	Channel 21 O1 location 	Channel 22 CPz location 	Channel 28 Fz location 	Channel 25 O2 location 	Channel 27 F8 location 
	Channel 23 O2 location 	Channel 26 Fz location 	Channel 20 P4 location 	Channel 21 O1 location 	Channel 21 O1 location 

5.3.3 Selection of Frequency Bands Based on Spectral Correlation and AFSM

For subject 3, the correlation coefficients between different frequency bands from 8 to 15 Hz of the ICA components 11 or 13 and the driving performance in different experimental sessions are shown in Table 5-3. The results of estimating system show that the optimal frequency bands of Subject 3 are from 10 to 14 Hz of the ICA component 11 and 13.

Table 5-3

The correlation coefficients between the log subband power spectra and the driving performance of Subject 3 corresponding to the different frequency bands from 8 to 15 Hz of the ICA component 11 and 13 in the training and testing sessions that uses the same ICA weighting matrix obtained from the training session.

Frequency		8Hz	9 Hz	10 Hz	11 Hz	12 Hz	13 Hz	14 Hz	15 Hz
Com 11	Training Session	0.82	0.89	0.92	0.92	0.92	0.92	0.89	0.87
	Testing Session	0.78	0.90	0.93	0.93	0.93	0.94	0.94	0.91
Com 13	Training Session	0.77	0.88	0.90	0.91	0.92	0.91	0.90	0.86
	Testing Session	0.76	0.89	0.91	0.92	0.93	0.92	0.92	0.89

In this section, we use the correlation coefficients to find the optimal frequency bands and localizations of electrodes according to the scalp topographies of ICA weighting matrices. Previous studies [27-31] showed that it is not applicable to use full EEG frequency bands to accurately estimate individual changes in vigilance and performance. Because the artifacts and individual variability in the EEG dynamics accompanying loss of alertness even the information about alertness may be distributed over the entire EEG spectrum. Table 5-3 shows the correlation coefficients between different frequency bands of the two ICA components and driving performance of Subject 3 in training and testing sessions. The results

show the better frequency bands of ICA components 11 and 13 are from 10 to 14 Hz with the correlation rate up to 0.94. Table 5-4 lists the correlation results for both sessions using the optimal frequency bands within 10~14 Hz in single ICA component of Subject 3. The results show that the frequency bands from 10 to 14 Hz of ICA components 11 and 13 have the highest correlation coefficients than the other components.

Table 5-4

The correlation coefficients between log subband power spectra and the driving performance of subject 3 using the optimal frequency bands (from 10 to 14 Hz) corresponding to single component.

ICA Component	11	13	26	24	5	31	29	32	27
Training Session	0.92	0.91	0.88	0.82	0.80	0.78	0.78	0.77	0.76
ICA Component	11	13	26	5	33	24	28	29	31
Testing Session	0.93	0.92	0.89	0.84	0.83	0.82	0.82	0.82	0.79

Table 5-5 shows the frequency bands of the five participants which are selected by manual method and AFSM technology, respectively. The frequency bands selected by manual method are called the optimal frequency bands in this experiment. The optimal frequency bands means repeatedly testing to find the most appropriate frequency bands for the best estimating result. For Subject 3, the manual method and the AFSM technology determine the same frequency bands.

The frequency bands of the five participants are selected according to the two ICA components for both the manual methods and the AFSM technology. It is noted that these two methods also select the same frequency bands by using the EEG channels for the five participants.

Table 5-5

The frequency bands for the two ICA components in Table 5-2 selected by manual method and the AFSM technology corresponding to different subjects.

Frequency Bands	Subject 1	Subject 2	Subject 3	Subject 4	Subject 5
Manual Selection	5 ~ 8 Hz	8 ~ 13 Hz	10 ~ 14 Hz	4 ~ 7 Hz	8 ~ 13 Hz
AFSM Technique	4 ~ 8 Hz	8 ~ 12 Hz	10 ~ 14 Hz	5 ~ 9 Hz	9 ~ 13 Hz

Table 5-5 shows the optimal frequency bands ranges corresponding to different subjects according to the higher correlation coefficients and repeated testing [72]. And it also shows the frequency bands selected by the AFSM technique of all subjects. It shows that the better frequency bands are not necessarily the same for different subjects. The frequency bands selected by manual method and the AFSM technique are almost the same but slightly different for different subject. Hence, the results of driving error estimation by using the frequency bands selected by manual method and AFSM technique will be similar.

5.3.4 Drowsiness Estimation based on ICA Components or EEG Channels

Fig. 5-13 shows the actual and estimated driving performance index of training and testing sessions with respect to Subject 3 using the optimal frequency bands selected manually combined with linear regression model. It can be found that the estimated driving performance matches well with the actual driving performance index with correlation coefficient $r = 0.93$ in the training and $r = 0.92$ in the testing by using two ICA components of subject 3.

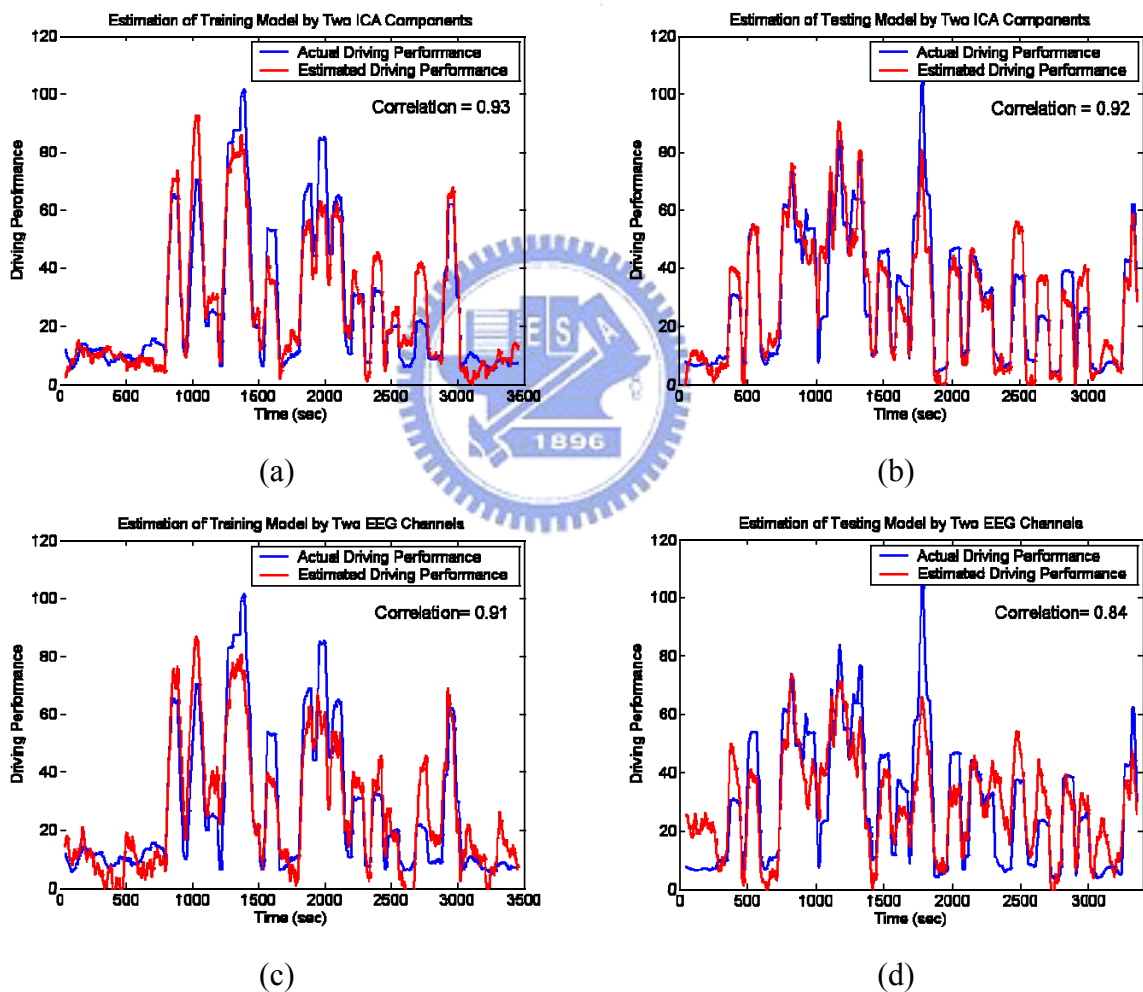


Fig. 5-13: Driving performance estimation of Subject 3 using linear regression model with the optimal frequency bands selected manually. (a) Result of training session by using ICA components, (b) Result of testing session by using ICA components, (c) Result of training session by using EEG channels, (d) Result of testing session by using EEG channels.

In this study, we use a least-square linear regression model to estimate the subject's driving performance based on the information obtained from the time-frequency power spectra analysis of ICA components or EEG channels. We used only two ICA components that performed the highest correlation between the ICA subband power spectrum and the driving performance such that the most artifacts can be removed and the available information of drowsiness estimation is extracted. Fig. 5-13 (a)(b) plots the estimated and actual driving performance of training and testing sessions for Subject 3. The linear regression model is trained with one session and tested against a separated session. As we can see, the estimated driving performance matched well with the actual driving performance with correlation coefficient $r=0.93$ in the training and $r=0.92$ in the testing.

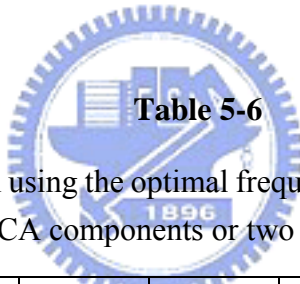


Table 5-6

Driving performance estimation using the optimal frequency bands and linear regression model of the five participants by two ICA components or two EEG channels.

Performance of Results		Subject 1	Subject 2	Subject 3	Subject 4	Subject 5	Average
ICA Components	Trainin	92 %	91 %	93 %	89 %	90 %	91 %
	Testing	91 %	89 %	92 %	86 %	80 %	87.6 %
EEG Channels	Trainin	88 %	90 %	91 %	87 %	94 %	90 %
	Testing	78 %	86 %	84 %	84 %	73 %	81 %

Table 5-6 shows the statistics across ten sessions for five selected subjects. The mean correlation coefficient between actual driving performance time series and within training session estimation is 0.91 ± 0.016 , whereas the mean correlation coefficient between actual driving performance and cross testing session estimation is 0.876 ± 0.048 . These results suggest that continuous ICA-based driving performance estimation using a small number of

frequency bands is feasible, and can give accurate information about minute-to-minute changes in operator's alertness.

The driving performance estimation of Subject 3 based on a linear regression model with frequency bands 10~14 Hz of EEG channels Pz and P4 as inputs features are shown in Fig. 5-13 (c)(d). The correlation coefficient between estimated and actual driving performance is $r = 0.91$ in the training session and $r = 0.84$ in the testing session, which is just a little lower than those using corresponding ICA components. The mean correlation coefficient between actual driving performance time series and within training session estimation is 0.90 ± 0.027 , whereas the mean correlation coefficient between actual driving performance and cross testing session estimation is 0.81 ± 0.054 .



5.3.5 Driving Performance Estimation based on AFSM and SONFIN

To verify the correctness and effectiveness of the AFSM method, the optimal frequency bands of the ICA components in these critical bands were feed as the input features of the linear regression models. We also used the Self-cOnstructing Neuro-Fuzzy Inference Network (SONFIN) [71] model to estimate and predict the individual driver's driving performance by taking the advantages of fuzzy reasoning, learning abilities, and flexibility of fuzzy neural networks. By the SONFIN technology, we expect to compensate the results of driving performance estimation by using the AFSM method for further application in the realistic driving environment in opposition to using the optimal frequency bands selected manually and linear regression model.

Table 5-7 shows the comparison results of driving performance estimation. Although the results of performance based on AFSM methods using linear regression models are somewhat lower than those selected manually, the adaptive feature selection mechanism has the advantages of saving time and cost when the whole system is applied for on-line alertness monitoring.

Table 5-7

Driving performance estimation using the frequency bands selected by manual method and the AFSM technology based on two dominant ICA components as input features of the linear regression model and SONFIN models for five subjects.

Performance of Results			Subject 1	Subject 2	Subject 3	Subject 4	Subject 5	Average
Linear Regression Model	Manual Selection	Training	92 %	91 %	93 %	89 %	90 %	91 %
		Testing	91 %	89 %	92 %	86 %	80 %	87.6 %
	AFSM Technology	Training	92 %	91 %	93 %	82 %	90 %	89.6 %
		Testing	91 %	88 %	92 %	78 %	80 %	85.8 %
SONFIN Model	Manual Selection	Training	94 %	93 %	97 %	93 %	94 %	94.2 %
		Testing	93 %	87 %	94 %	88 %	83 %	89 %
	AFSM Technology	Training	92 %	92 %	96 %	87 %	91 %	91.6 %
		Testing	91 %	89 %	94 %	83 %	85 %	88.4 %

Table 5-7 also shows the estimating results based on AFSM methods combined with SONFIN. Compared to the results using linear regression models with manual method, using fuzzy neural network models can achieve higher estimating results and can compensate slightly by using AFSM technique. Therefore, these results suggest that continuous EEG-based driving performance estimation using a small number of frequency bands is

combined with both linear models and fuzzy neural models, and can give accurate information changes in operator's alertness.

5.3.6 Performance Comparison Using Different Moving-Average Window

Length

The correlation coefficients between two time series of the driving performance and EEG log bandpower spectrum from 9 ~ 15 Hz in Pz channel using moving average with different window for Subject 3 is shown in Fig. 5-13. It shows that the 90-second moving average windows can perform the maximum correlation coefficient for continuous drowsiness analysis.

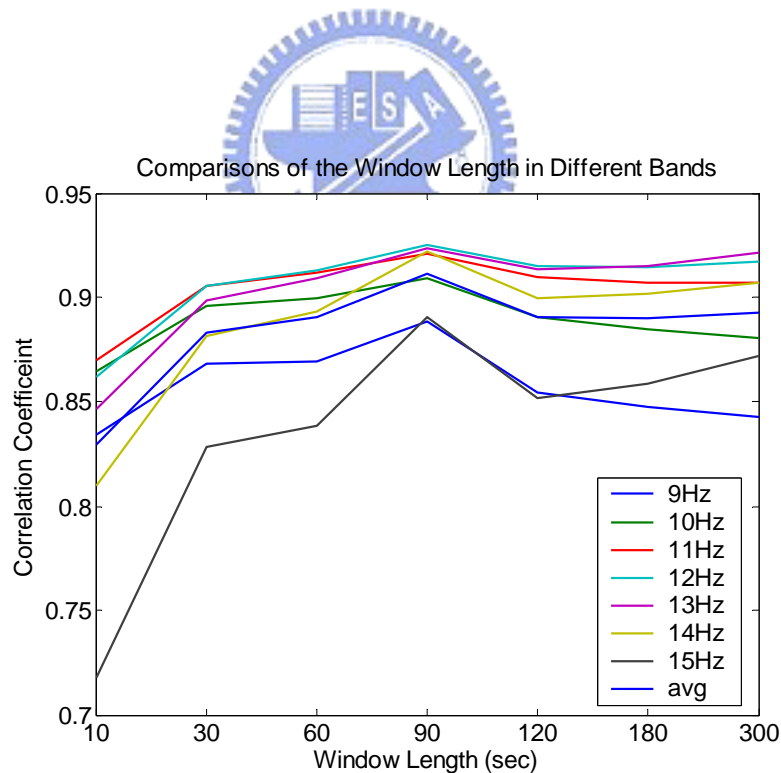


Fig. 5-14: Correlation coefficients between the driving performance and EEG log power spectrum from 9 ~ 15 Hz in Pz channel of subject 3 by using different moving averaged windows lengths.

5.4 The Brain Source of Drowsiness on the Cerebral Cortex

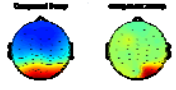
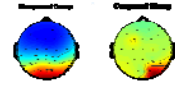
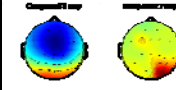
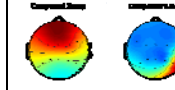
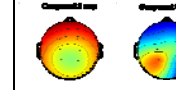





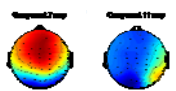
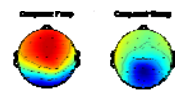
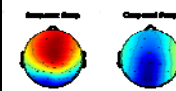
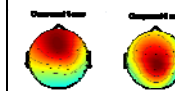
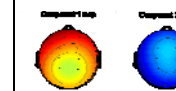




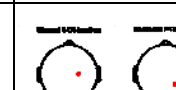
In this session, the estimation of driving performance will be evaluated to analyze the number of EEG channels and the regions on the scalp. The experimental results also show the brain source of drowsiness on the cerebral cortex.

5.4.1 Comparison with Using Different Number of EEG Channels

The driving performance estimation by the optimal frequency bands of two ICA components and EEG channels obtained using different number of EEG channels are shown in Table 5-8.

Table 5-8

Comparison of driving performance estimation obtained from different number EEG channels by using the optimal frequency bands of two EEG channels or ICA components as the features of linear regression model for the five participants.

Five Conditions		30 channels	20 channels	15 channels	10 channels	6 channels
Subject 1	Two ICA Components					
	Performance	89 %	87 %	88 %	86 %	82 %
	Two EEG Channels					
	Performance	81 %	81 %	81 %	79 %	73 %
Subject 2	Two ICA Components					
	Performance	90 %	90 %	89 %	90 %	89 %
	Two EEG Channels					
	Performance	88 %	88 %	91 %	88 %	84 %

Five Conditions		30 channels	20 channels	15 channels	10 channels	6 channels
Subject 3	Two ICA Components					
	Performance	92 %	91 %	89 %	91 %	91 %
	Two EEG Channels					
	Performance	84 %	84 %	87 %	84 %	85 %
Subject 4	Two ICA Components					
	Performance	88 %	88 %	87 %	84 %	88 %
	Two EEG Channels					
	Performance	84 %	84 %	84 %	83 %	84 %
Subject 5	Two ICA Components					
	Performance	77 %	76 %	72 %	74 %	72 %
	Two EEG Channels					
	Performance	72 %	72 %	72 %	70 %	70 %

It can be found that the performance of drowsiness estimation decreases if less number of EEG channels were used. It is reasonable because the more EEG channels we used, the more information we extract. Hence we can observe the estimating results of the five participants in the final condition, which we only use six EEG channels, the performance is slightly reduction to the results in the first condition. For using six EEG channels of all

participants, the mean performance is 84.4 ± 7.7 % by ICA components and the mean performance is 79.2 ± 7.1 % by EEG channels.

For example, we can compare with the estimating results of different tracking methods by using two ICA components and EEG channels for subject 1 as shown in Fig. 5-15.

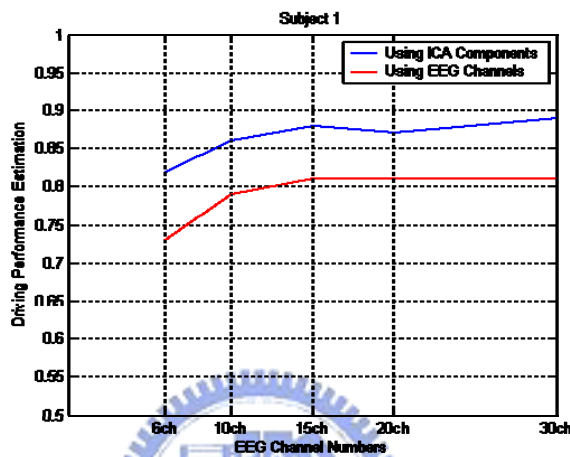


Fig. 5-15: Comparison of estimating results by using ICA components and EEG channels.

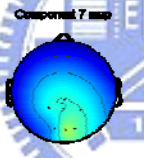
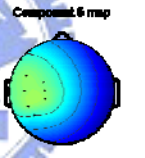
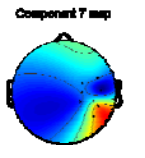

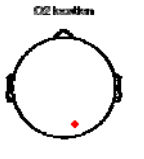

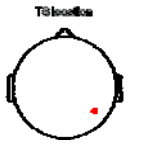
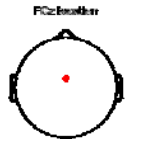

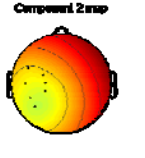


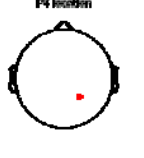
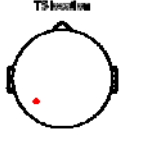
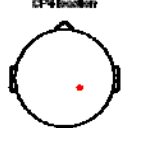
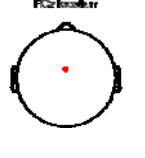
For each subject, the sources of the ICA components are near the channel locations of EEG signals regardless of the number of EEG channels we used. Even we only have six EEG channels signals, this six EEG channels can still collect much information propagated from any source to the channels locations. Through ICA decomposition, we can also get desired ICA components by using six EEG channels. However, the less information from EEG signals we collect the fewer artifacts will be removed by ICA technology. For all participants, the more EEG channels we used, the advantage of ICA-based approach is more obvious. Therefore, only using six EEG channels can achieve high estimating results for reducing the calculation in the real-time applications.

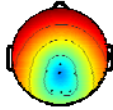






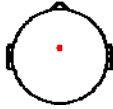
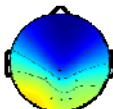

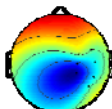




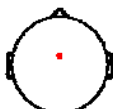


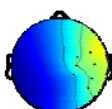


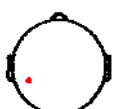
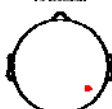
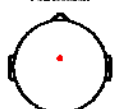
5.4.2 Comparison of Using Different Region of EEG Channels

The comparison of driving performance estimation using two EEG channels located at the four different regions by the optimal frequency bands combined with linear regression model for the five participants are shown in Table 5-9.

Table 5-9

Comparison of driving performance estimation using two EEG channels of the four different regions.

Four Regions on the Scalp		Parietal and Occipital	Left Temporal	Right Temporal	Frontal
Subject 1	One ICA Component				
	Performance	90 %	93 %	84 %	73 %
	One EEG Channel				
	Performance	86 %	74 %	82 %	38 %
Subject 2	One ICA Components				
	Performance	90 %	93 %	94 %	92 %
	One EEG Channels				
	Performance	92 %	88 %	91 %	93 %

Four Regions on the Scalp		Parietal and Occipital	Left Temporal	Right Temporal	Frontal
Subject 3	One ICA Components	Component 6 map 	Component 2 map 	Component 1 map 	Component 4 map 
	Performance	91 %	88 %	88 %	88 %
	One EEG Channels	F4 location 	CP3 location 	T9 location 	FCz location 
	Performance	86 %	83 %	84 %	89 %
Subject 4	One ICA Components	Component 5 map 	Component 3 map 	Component 4 map 	Component 4 map 
	Performance	86 %	80 %	82 %	79 %
	One EEG Channels	O2 location 	T8 location 	T8 location 	FCz location 
	Performance	84 %	78 %	74 %	82 %
Subject 5	One ICA Components	Component 2 map 	Component 1 map 	Component 5 map 	Component 4 map 
	Performance	77 %	80 %	63 %	69 %
	One EEG Channels	O1 location 	TP7 location 	T9 location 	FCz location 
	Performance	82 %	72 %	69 %	68 %

According to Table 5-8, the sources of all ICA components and locations of all EEG channels we selected for estimating drowsiness are near parietal and occipital regions on cerebral cortex. In this session, we want to find out the universal brain source of drowsiness

on cerebral cortex among our participants. By using one ICA component or one EEG channel of different regions on cerebral cortex, we can explore the better regions for drowsiness experiments according to the performance of estimating drowsiness.

Table 5-9 help us to understand the brain source of drowsiness on cerebral cortex of all participants. First, we consider about the parietal and occipital regions of the five subjects. There is no doubt about the EEG channels we selected are on the parietal and occipital regions on cerebral cortex. And the sources of ICA components we used indicate the same regions particularly near Pz and Oz channel locations.

Secondly, we discuss the left and right temporal regions of the five subjects. For selecting the EEG channels, the locations of the selected channels approach to parietal regions on cerebral cortex. For selecting the ICA components, the scalp topographies of all indicate the sources also approach to parietal regions on cerebral cortex. Through ICA weighting matrices W , the sources of spatial distributions in scalp topography may extend to the occipital regions on cerebral cortex. Therefore, the performance of estimating results is still excellent by using signals measured from temporal regions on cerebral cortex due to we can collect the source signals propagated from the parietal and occipital regions to the temporal regions through ICA decomposition.

Finally, for frontal region on cerebral cortex, it is clear that the FCz channel is selected for the five subjects by using EEG channel signals. Because of this channel is the nearest location to the parietal and occipital regions on cerebral cortex. Broadly speaking, the performance of drowsiness estimation is acceptable by only using FCz channel signals. Although the estimated result of using EEG channel at FCz is poor for subject 1, the result can be improved to be passable through ICA technique. The scalp topographies of ICA components indicate the sources of spatial distributions approach to occipital regions on cerebral cortex. The results of study using EEG channels on the frontal region for drowsiness

estimation are very important for further study of using the spiked dry electrodes. According to about discussion, we may conclude that the brain sources of drowsiness the parietal and occipital regions on cerebral cortex.

5.5 Actual Application of the Spiked Dry Electrodes

In this session, we first examine the performance of the spiked dry electrodes developed by the μ System & Control Lab, in the Brain Research Center of the University System of Taiwan. Fig. 5-16 shows electrode-skin-electrode impedance (ESEI) of three types the spiked dry electrodes is lower than the standard wet electrodes.

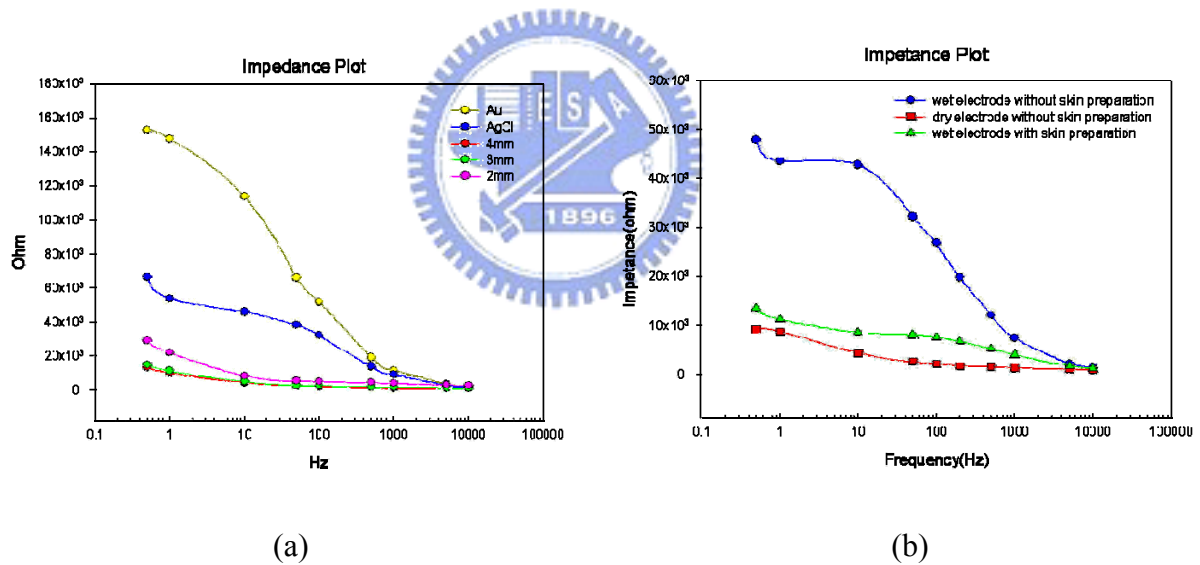


Fig. 5-16: The ESEI comparison between dry electrodes and wet electrode with/without skin preparation. (a) Without skin preparation, (b) With/without skin preparation

μ System and Control Lab, Brain Research Center of the University System of Taiwan

Then, the 32-channel EEG signals of Subject 2 measured by 2 spiked dry electrodes and 30 standard electrodes are decomposed into 32 ICA components. The scalp topographies of these ICA components for Subject 2 are shown in Fig. 5-17.

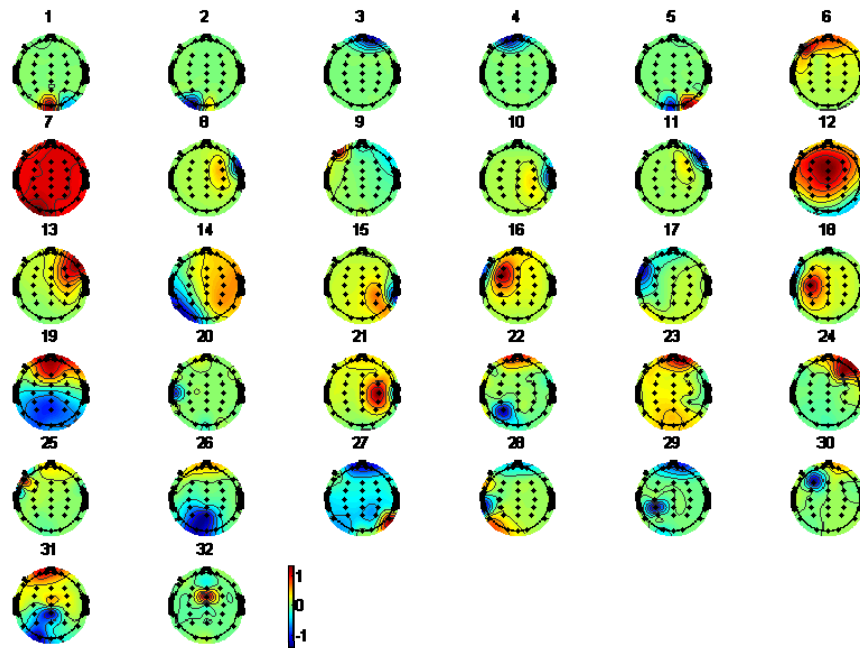
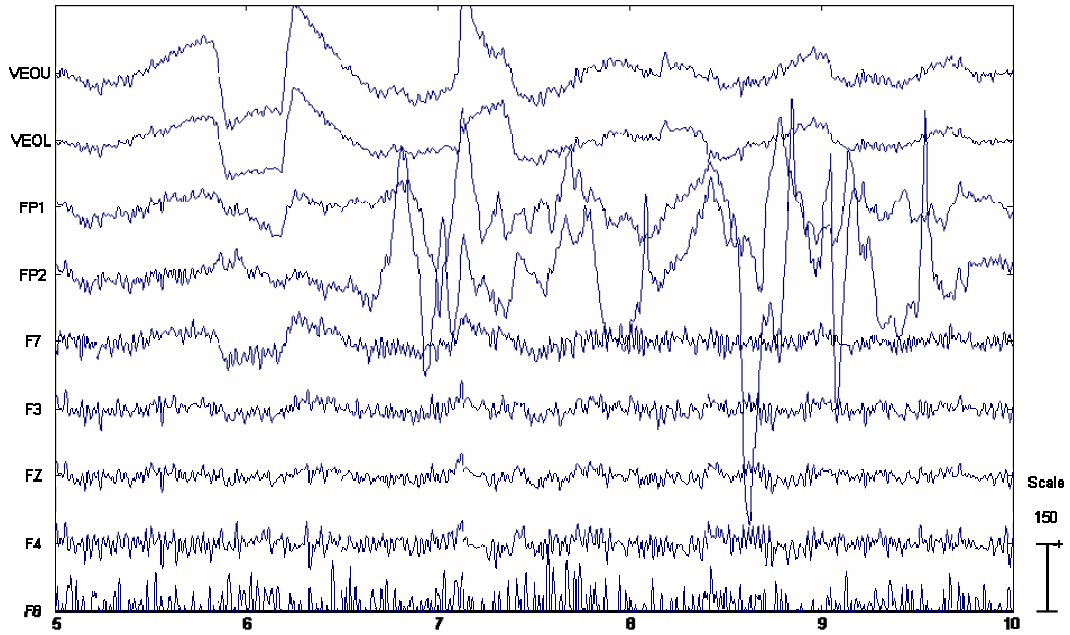


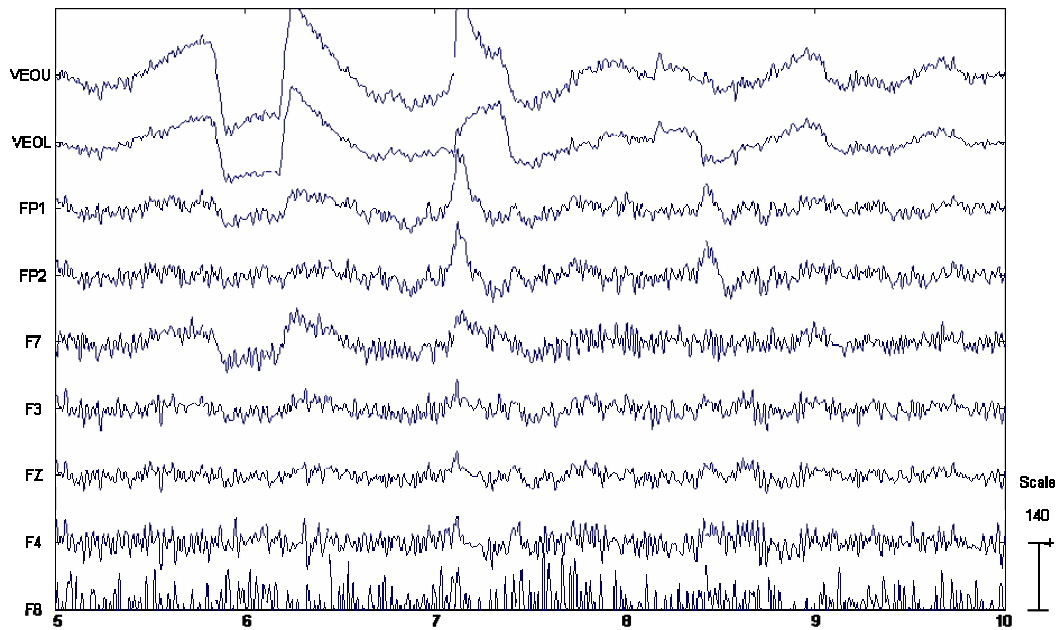
Fig. 5-17: The scalp topographies of all ICA components trained by EEG data of Subject 2 using 2 spiked dry electrodes and 30 wet electrodes.



The first question of using the spiked dry electrodes is the height of probes limited by the MEMS technology. The second question is the movement without using the electrolytic gel. Fig. 5-18 (a) shows the EEG signals measured by the spiked dry electrodes on FP1 and FP2 channels with moving activity noise. This problem can be solved by the ICA decomposition technique. For example, the ICA components 3 and 4 of Subject 2 in Fig. 5-19 can be regarded as the noise component of movement artifacts. In order to using the EEG signals measured by the spiked dry electrodes into drowsiness estimated system, we remove these components from the measured EEG signals and the resultant EEG signals are shown in Fig. 5-18 (b).



(a)



(b)

Fig. 5-18: The raw EEG data are measured by placing the spiked dry electrodes at FP1 and FP2 channels using the standard electrodes for the others channels of Subject 2. (a) The EEG signals of FP1 and FP2 channels with movement artifacts, (b) The EEG signals after ICA-based artifact removal.

Similarly, we remove the other noise components from 1 to 11 for further analysis. Fig. 5-19 shows the resultant EEG signals at FP1 and FP2 channels after removing the ICA components from 1 to 11.

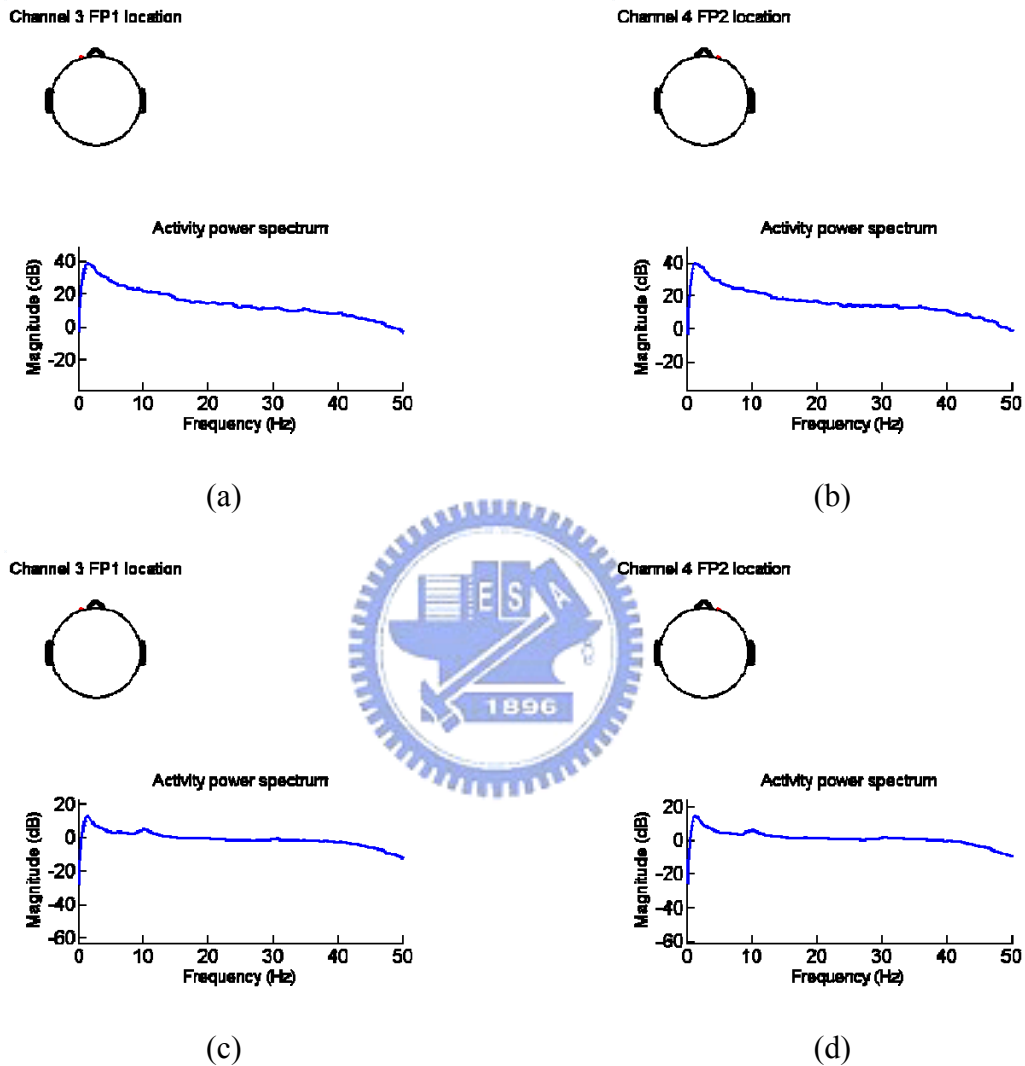


Fig. 5-19: The EEG signals measured by using the spiked dry electrodes before/after artifacts removal using ICA decomposition technology. (a) and (b) EEG power spectra signals of FP1 and FP2 channels before removing all noise components, (c) and (d) EEG power spectra of FP1 and FP2 channels after removing all noise components.

Comparing Fig. 5-19 (a)(b) and (c)(d), it can be observed the small peak near 10 Hz of power spectrum appears after removing noise components by ICA technique. The features

propagated from the source on the parietal and occipital regions can be applied to the following drowsiness estimation.

The correlation coefficients between log subband power spectra and driving performance for each frequency of all EEG channels after noise components removal is shown in Fig. 5-20. It is obvious that the correlation spectra shows a strong evidence between fluctuations in EEG bandpower of frequency bands within 8 ~ 13 Hz and driving performance with high positive correlations in most EEG channels including FP1 and FP2 channels.

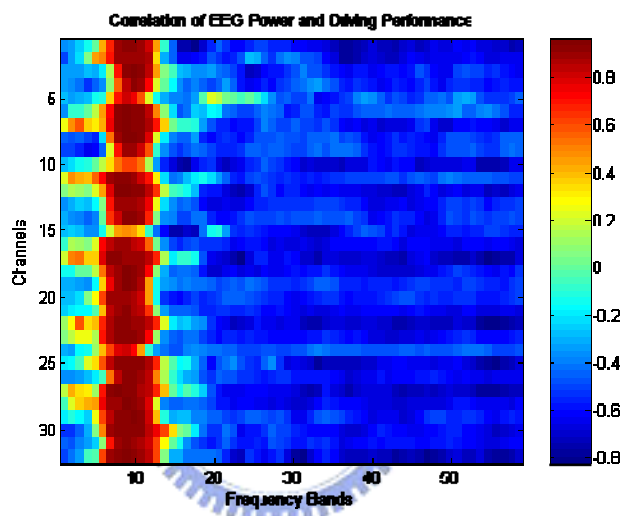


Fig. 5-20: Correlation coefficients spectra of all EEG channels after removing all noise components.

The experimental results show in Table 5-10 demonstrate that it is feasible to using two EEG signals at frontal region acquired by dry electrodes for drowsiness estimation.

Table 5-10

Driving performance estimation of subject 2 by using two spiked dry electrodes.

	Performance of Results
Training Session	73 %
Testing Session	70 %

VI. Conclusions

In this thesis, we propose an EEG-based drowsiness estimation technology based on independent component analysis, time-frequency spectral analysis, correlation analysis and the fuzzy neural network model to continuously and indirectly estimate fluctuations of human alertness level in the VR-based dynamic driving environment. The VR-based dynamic motion platform combined with the EEG measurement system is an innovation in brain and cognitive engineering researches. Our study provides good evidence to show that the VR-based dynamic motion platform is required for the study of human cognitive state in the real world. The kinesthetic stimuli obviously influence the cognitive states and it can be observed by analyzing the EEG signals. Using ICA decomposition technique, we also demonstrate the brain sources related to kinesthetic stimulus are symmetrical on the both sides near FC3 and FC4 channel locations on scalp, respectively.

Secondly, we also compare the EEG changes related to different drowsiness levels in the dynamic and static environment. The experimental results show that the EEG power spectrum near α -band will change accompanying different drowsiness level. This is an important observation for the EEG-based drowsiness estimation. In addition, the dynamic motion platform obviously influences the cognitive states of drowsiness.

Thirdly, we demonstrate a close relationship between fluctuations in driving performance and the log subband power ICA and EEG spectrum. This relationship appears stable within individuals across sessions, but is somewhat variable between subjects. We also proposed a novel AFSM to solve the sorting problem of ICA components and to extract useful frequency bands based on the correlation analysis. The averaged accuracies of training and testing session for the five participants can achieve high to 92 % and 88%, respectively by using the AFSM technique combined with the fuzzy neural networks.

We also observed that the brain sources of drowsiness locate in the brain parietal and occipital regions by analyzing the correlation of EEG signals on different regions and the drivers' drowsiness index. For practical applications, we are the pioneers involving the spiked dry electrodes into the drowsiness estimation system. The experimental results show that it is feasible to put the spiked dry electrodes on the frontal region combined with ICA technique to estimate drivers' drowsiness level.

In the future, we can design more driving tasks to discuss the influence of kinesthetic stimulus on EEG dynamic changes. We can develop the EEG-based drowsiness estimation technology for the dynamic driving environment. It will be different from the method proposed in this thesis, since we have discovered that the drivers' EEG α -band responses as different the dynamic platform is moving or motionless. We can also use the spiked dry electrodes array placed on frontal region combined with ICA technique to replace the scalp cap for practical application.



Reference

- [1] URL: <http://www.drowsydriving.org/>
- [2] URL: <http://www.nhtsa.dot.gov/>
- [3] URL: <http://www.sleepfoundation.org/>
- [4] URL: <http://www.aaafoundation.org/>
- [5] L. Y. Chang and F. Mannering, "Analysis of injury severity and vehicle occupancy in truck-non-truck-involved accidents," *Accident Analysis and Prevention*, 31: 579-592, 1999.
- [6] L. P. Kostyniuk, F. M. Streff, and J. Zakarajsek , "Identifying unsafe driver actions that lead to fatal car-truck crashes," *AAA Foundation for Traffic Safety*, 2002.
- [7] J. Hendrix, "Fatal crash rates for tractor-trailers by time of day," *Proceedings of the International Truck and Bus Safety Research and Policy Symposium*, 237-250, 2002.
- [8] H. Ueno, M., Kaneda, and M. Tsukino," Development of drowsiness detection system," *Proceedings of the 1994 Vehicle Navigation and Information Systems Conference*, Vol. 31, pp.15–20, Sep. 1994.
- [9] G. Hamouda, and F. F. Saccomanno, "Neural network model for truck driver fatigue accident detection," *Proceedings of the 1995 Electrical and Computer Engineering Canadian Conference*, Vol. 1, pp. 362-365, Sep. 1995.
- [10] M. Eriksson, and N. P. Papaniktopoulos, "Eye-tracking for detection of driver fatigue," *Proceedings of the 1997 IEEE Conference on Intelligent Transportation System*, pp. 314–319, Nov. 1997.
- [11] R. Grace, A. Guzman, J. Staszewski, B. A. Peters, M. Mallis, and D. F. Dinges, "The Carnegie Mellon TruckSim: a tool to improve driving safety," *Proceedings of the 1998 IEEE 17th Conference on Digital Avionics Systems*, Vol. 2, pp. I35/1 - I35/831, Nov. 1998.
- [12] R. Grace, V. E. Byrne, D. M. Bierman, J. M. Legrand, D. Gricourt, B. K. Davis, J. J.Staszewski, and B. Carnahan, " A drowsy driver detection system for heavy vehicles," *Proceedings of the 1998 the 17th AIAA/IEEE/SAE Conference on Digital Avionics Systems*, Vol.162, pp. I36/1-I36/8, Nov. 1998.
- [13] C. A. Perez, A. Palma, C. A. Holzmann, and C. Pena, "Face and eye tracking algorithm based on digital image processing," *Proceedings of the 2001 IEEE International Conference on Systems, Man, and Cybernetics*, Vol. 2, pp.1178-1183, Oct. 2001.
- [14] T. Pilutti, and G. Ulsoy, "Identification of driver state for lane-keeping tasks," *IEEE Trans. Syst, Man, Cybern., Part A: Systems and Humans*, Vol. 29, pp. 486-502, Sep. 1999.
- [15] J. C. Popieul, P. Simon, P. Loslever, "Using driver's head movements evolution as a

- drowsiness indicator,” *Proceedings of the 2003 IEEE International Intelligent Vehicles Symposium*, pp. 616–621, Jun. 2003.
- [16] J. Qiang, Z. Zhiwei, P. Lan, “Real-time nonintrusive monitoring and prediction of driver fatigue,” *IEEE Transactions on Vehicular Technology*, Vol. 53, Issue: 4, pp.1052– 068, Jul.2004.
- [17] R. S. Huang, C. J. Kuo, L. L. Tsai, and O. T. C. Chen, ”EEG pattern recognition-arousal states detection and classification,” *Proceedings of the 1996 IEEE Conference on Neural Networks*, Vol. 2, pp. 641-646, Jun. 1996.
- [18] A. Vuckovic, V. Radivojevic, A. C. N. Chen, and D. Popovic, “Automatic recognition of alertness and drowsiness from EEG by an artificial neural network,” *Medical Engineering and Physics* Vol. 24, pp. 349-360, Jun. 2002.
- [19] S. Roberts, I. Rezek, R. Everson, H. Stone, S. Wilson, and C. Alford, ”Automated assessment of vigilance using committees of radial basis function analysers,” *IEEE Science Measurement and Technology*, Vol. 147 , pp. 333–338, Nov. 2000.
- [20] K. B. Khalifa, M. H. Bedoui, R. Raytchev, and M. Dogui, ”A portable device for alertness detection,” *Proceedings of 2000 1st Annual International IEEE-EMBS Special Topic Conference on Microtechnologies in Medicine and Biology*, pp. 584–586, Oct. 2000.
- [21] B. J. Wilson, and T. D. Bracewell, ”Alertness monitor using neural networks for EEG analysis,” *Proceedings of the 2000 IEEE Signal Processing Society Workshop on Neural Networks for Signal Processing X*, Vol. 2, pp.814-820, Dec. 2000.
- [22] J. Santamaria and K. Chiappa, “The EEG of drowsiness in normal adults,” *J. Clin. Neurophysiol*, Vol. 4, no. 4, pp. 327-382, 1987.
- [23] Rechtschaffen, A., Kales, A. (Eds.): “A manual of standardized terminology in techniques and scoring system for sleep stages of human subjects,” BIS/BRI, UCLA, Los Angeles, CA, 1968.
- [24] R. B. Berry, (Series Editors:) S. A. Sahn, and J. E. Heffner, “Sleep medicine pearls,” Hanley and Belfus Inc., Philadelphia, 1999.
- [25] P. Parikh, and E. Micheli-Tzanakou, “Detecting drowsiness while driving using wavelet transform,” *Proceedings of the IEEE 30th Annual Northeast on Bioengineering Conference*, pp. 79-80, Apr. 2004.
- [26] H. Park, “Automated sleep stage analysis using hybrid rule-based and case-based reasoning,” Ph. D. Dissertation, Seoul National University, Aug. 2000.
- [27] T. P. Jung, S. Makeig, M. Stensmo, and T. J. Sejnowski, “Estimating alertness from the EEG power spectrum,” *IEEE Trans. Biomed Eng*, 44(1), 60-69, 1997.
- [28] S. Makeig and T. P. Jung, “Tonic, phasic and transient EEG correlates of auditory awareness in drowsiness,” *Cogn. Brain Res.* 4, 15-25, 1996.
- [29] M. Treisman, “Temporal rhythms and cerebral rhythms in Timing and Time Perception,” J. Gibbon and L. Allan. Eds. New York: Academic, Vol. 423, pp. 542-565, 1984.

- [30] S. Makeig and M. Inlow, "Lapses in alertness: Coherence of fluctuations in performance and EEG spectrum," *Electroencephalogr. Clin. Neurophysiol.*, Vol. 86, pp. 23-35, 1993.
- [31] J. Beatty, A. Greenberg, W. P. Deibler, and J. O'Hanlon, "Operant control of occipital theta rhythm affects performance, in a radar monitoring task, " *Science*, Vol. 183, pp. 871-873, 1974.
- [32] Andras Kemeny and Francesco Panerai "Evaluating perception in driving simulation experiments," *TRENDS in Cognitive Sciences*, Vol.7, No.1, Jan. 2003
- [33] Berthoz, A. "The Brain's Sense of Movement," Harvard University Press, 2000
- [34] Goldberg, J.M. and Fernandez, C. "Responses of peripheral vestibular neurons to angular and linear acceleration in the squirrel monkey". *Acta Otolaryngol.* 80, 101–110, 1975
- [35] Seidmann, S.H. et al. "Tilt perception during dynamic linear acceleration," *Exp. Brain Res.* 119, 307–314, 1998
- [36] Merfeld, D.M. et al. "Humans use internal models to estimate gravity and linear acceleration," *Nature* 398, 615–618, 1999
- [37] Berthoz, A. et al. "Spatial memory of body linear displacement: what is being stored," *Science* 269, 95–98, 1995
- [38] Wexler, M. et al. "The stationarity hypothesis: an allocentric criterion in visual perception," *Vis. Res.* 41, 3023–3037, 2001
- [39] Wierville, W.W. et al. "Driver steering reaction time to abrupt onset crosswind, as measured in a moving-base driving simulator," *Hum. Factors* 25, 103–116, 1983
- [40] Reymond, G. et al. "Role of lateral acceleration in curve driving: driver model and experiments on a real vehicle and a driving simulator," *Hum. Factors* 43, 483–495, 2001
- [41] Page, N.G. and Gresty, M.A. "Motorist's vestibular disorientation syndrome," *J. Neurol. Neurosurg. Psychiatry* 48, 729–735, 1985
- [42] Groen, E.L. et al. "Influence of body roll on visually induced sensation of self-tilt and rotation," *Perception* 28, 287–297, 1999
- [43] P. Philip, J. Taillard, et al. "Effect of fatigue on performance measured by a driving simulator in automobile drivers," *Journal of Psychosomatic Research* 55, pp. 197-200, 2003
- [44] C. Jutten and J. Herault, "Blind Separation of Sources I. An Adaptive Algorithm Based on Neuromimetic Architecture," *Signal Process*, Vol. 24, pp. 1-10, 1991.
- [45] J. F. Cardoso, and A. Souloumiac, "Blind beamforming for non Gaussian signals," *IEEE Proceedings-F 140*, Vol. 6, pp. 362-370, 1993.
- [46] P. Comon, "Independent component analysis — A new concept," *Signal Processing*, pp. 287–314, Vol. 36, 1994.
- [47] A. J. Bell and T. J. Sejnowski, "An information-maximization approach to blind separation and blind deconvolution," *Neural Computation*, Vol. 7, pp. 1129–1159, 1995.
- [48] J. F. Cardoso, and B. Laheld, "Equivariant adaptive source separation," *IEEE Transactions on Signal Processing*, Vol. 45, pp. 434–444, 1996.

- [49] D. T. Pham, "Blind separation of instantaneous mixture of sources via an independent component analysis," *IEEE Transactions on Signal Processing*, Vol. 44, pp. 2768–2779, 1997.
- [50] M. Girolami, "An alternative perspective on adaptive independent component analysis," *Neural Computation*, Vol. 10, pp. 2103–2114, 1998.
- [51] T. W. Lee, M. Girolami, and T. J. Sejnowski, "Independent component analysis using an extended infomax algorithm for mixed sub-Gaussian and super-Gaussian sources," *Neural Computation*, Vol. 11, pp. 606–633, 1999.
- [52] S. Makeig, A. J. Bell, T. P. Jung, and T. J. Sejnowski, "Independent component analysis of Electroencephalographic data," *Advances in Neural Information Processing Systems* 8, 145-151, 1996.
- [53] T. P. Jung, C. Humphries, T. W. Lee, S. Makeig, M. J. McKeown, V. Iragui, and T. J. Sejnowski, "Extended ICA removes artifacts from electroencephalographic recordings," *Advances in Neural Information Processing Systems* 10:894-900, 1998.
- [54] T. P. Jung, S. Makeig, C. Humphries, T. W. Lee, M. J. McKeown, V. Iragui, T. J. Sejnowski, "Removing electroencephalographic artifacts by blind source separation," *Psychophysiology*, Vol. 37, pp. 163-78, 2000.
- [55] T. P. Jung, S. Makeig, W. Westerfield, J. Townsend, E. Courchesne, and T. J. Sejnowski, "Analysis and visualization of single-trial event-related potentials," *Human Brain Mapping*, 14(3), pp. 166-85, 2001.
- [56] A. Yamazaki, T. Tajima, and K. Matsuoka, "Convulsive independent component analysis of EEG data," *Annual Conference on SICE*, Vol. 2, pp. 1227 – 1231, Aug. 2003.
- [57] A. Meyer-Base, D. Auer, A. Wismueller, "Topographic independent component analysis for fMRI signal detection," *Proceedings of the International Joint Conference on Neural Networks* Vol.1, pp. 601 – 605, July 2003.
- [58] M. Naganawa, Y. Kimura, K. Ishii, K. Oda, K. Ishiwata, and A. Matani, "Extraction of a plasma time-activity curve from dynamic brain pet images based on independent component analysis," *IEEE Transactions on Biomedical Engineering*, Vol. 52, pp. 201 – 210, Feb. 2005.
- [59] R. Liao, J. L. Krolik, and M. J. McKeown, "An information-theoretic criterion for intrasubject alignment of FMRI time series: motion corrected independent component analysis," *IEEE Transactions on Medical Imaging*, Vol. 24, pp. 29 – 44, Jan. 2005.
- [60] WorldToolKit *Reference Manual*, Release 7, SENSE8 Corporation, Mill Valley, USA., 1997.
- [61] Stewart, D. "A platform with six degrees of freedom," *Proc. Instn Mech. Engr*, 180, 371–386, 1965
- [62] Liu, K., Fitzgerald, J. M. and Lewis, F. L. "Kinematic analysis of a Stewart platform manipulator," *IEEE Trans. Ind. Electronics*, 40(2), 282–293, 1993
- [63] Kim, J., Park, F. C., Ryu, S. J., Kim, J., Hwang, J. C. and Iurascu, C. C. "Design and

- analysis of a redundantly actuated parallel mechanism for rapid machining,” *IEEE Trans. Robotics and Automn*, 17(4), 423–434, 2001
- [64] C. T. Lin, J. Y. Lin and Y. C. Lin, “A neural fuzzy inference network for the motion analyses of Stewart platform,” *Int. J. Fuzzy Systems*, 2002, 4(2), 704–714.
- [65] C. F. Hsu, C. T. Lin, T. Y. Huang and K. Y. Young, “Development of multipurpose virtual-reality dynamic simulator with a force-reflection joystick,” *J. Systems and Control Engineering*, Vol. 209, 2005
- [66] UW Computing & Communications
URL: <http://faculty.washington.edu/chudler/1020.html>
- [67] P. Griss, P. Enoksson, H. K.Tolvanen-Laakso, P. Merilainen, S. Ollmar, “Micromachined electrodes for biopotential measurements,” *Journal of Microelectromechanical Systems*,” Vol. 10, No. 1, March 2001.
- [68] Hillyard S A, Kutas M, “Electrophysiology of cognitive processing,” *Annual Review of Psychology*, 34, 33-61, 1983
- [69] A. Papoulis, “Minimum bias windows for high resolution spectral estimation,” *IEEE Trans. Inform. Theory*, Vol. IT-19, pp. 9-12, 1973.
- [70] M. Steriade, “Central core modulation of spontaneous oscillations and sensory transmission in thalamocortical systems,” *Current Opinion in Neurobiol.*, Vol. 3, no. 4, pp. 619-625, 1993.
- [71] C. F. Juang and C. T. Lin, “An On-line Self-Constructing Neural Fuzzy Inference Network and Its Applications,” *IEEE Trans. On Fuzzy Systems*, Vol.6, No.1, pp.12-32, 1998
- [72] C.T. Lin, S. F. Liang, W.H. Chao, Y.J. Chen, and T. P. Jung, “EEG-based Drowsiness Estimation for Safety Driving Using Independent Component Analysis,” will be published in *IEEE Transactions on Circuit and System*, 2005